Filtered Multi-Carrier Modulations for Industrial Wireless Communications based on Cognitive Radio

Aitor Lizeaga Goikoetxea

Mondragon Unibertsitaea
Electronics and Computer Science Department

October 10th, 2017

Filtered Multi-Carrier Modulations for Industrial Wireless Communications based on Cognitive Radio

Aitor Lizeaga Goikoetxea

Supervisors:

Dr. Mikel Mendicute
Dr. Iñaki Val

Submitted for the degree of Doctor of Philosophy
at Mondragon Unibertsitatea

Committee:
Chair: Dr. Stephan Weiss (University of Strathclyde)
Member: Dr. Iker Sobrón (EHU-UPV)
Member: Dr. Idoia Jiménez (Ormazabal Protection & Automation)
Member: Dr. Maitane Barrenechea (Mondragon Unibertsitatea)
Secretary: Dr. Egoitz Arruti (Mondragon Unibertsitatea)

October 10th, 2017

Acknowledgments

First and foremost, I wish to thank my thesis supervisors, Mikel Mendicute and Iñaki Val. I am grateful for their guidance, support, valuable advices and all their contributions to this doctoral thesis.

I also would like to thank the Engineering Faculty of Mondragon Unibertsitatea and specially the Electronics and Computer Science Department, for giving me the chance of carrying out this doctoral thesis. Thanks also to the Basque Government for its support through the projects TIPOTRANS and CIIRCOS; and to the Spanish Ministry of Economy and Competitiveness for its support through the project COWITRACC.

A mi madre y a Alfonso mi más profundo agradecimiento por todo. Por toda vuestra ayuda y apoyo, por el amparo que siempre me habéis brindado y por la total confianza que en todo momento me habéis mostrado. Posiblemente nunca pueda agradecéroslo lo suficiente.

Nire emazte eta bizikide den Garaziri, nire eskerrik minena bide honetan eman dizkidazun laguntza eta babes neurtezinengatik; bai nire eginbeharrak arinduaz eta, bereziki, alor animiko eta afektiboan. Mila esker!

Azkenik, eskerrik asko bihotzez nire doktoregai kide izandako Idoia, Iñaki, Maite, Aritz, Joxe, Unai, Enaitz, Alain, Mikel, Aitor, Ane eta Daniri zuen laguntza guztiagatik eta elkarrekin pasa ditugun une itzelengatik. Kide bikainak zarete!

Originality statement

I declare that I am the sole author of this work. I understand that my work may be available to the public, either at the university library or in electronic format.

Laburpena

Doktoretza-tesi honetako helburu nagusia, hari gabeko komunikazio industrialetarako fidagarritasun maila onargarria eman dezakeen maila fisikoko modulazio bat aurkitzea da. Eremu industrialetako radio bidezko kanaletan ematen diren komunikazioetarako baldintza bereziki aurkakoak direla eta, helburu hori lortzea benetako erronkatzat jo liteke. Gainera, modulazio horrek "Radio Cognitiva" deritzoten teknikekin bateragarria izan beharra dauka, hauek hari gabeko komunikazioen fidagarritasuna hobetzeko gaitasuna baitute.

Bibliografian oinarrituz, gaur egungo baliabideekin hari gabeko komunikazio industrial kasu ugariri konponbidea emateko aukera badela ondoriozta genezake, baina ez kasu guztiei ordea. Hari gabeko kanalen egoera bereziki aurkakoa denerako eta komunikazio sistemek denbora muga bereziki zorrotzak bete behar dituztenerako, ezta erantzun nahikoa ona eman lezakeen hari gabeko komunikazio sistema industrialik bibliografia zientifikoan.

Hori dela eta, doktoretza tesi honetan, "Radio Cognitiva" delakoa eta 5G-rako aurreikusita dauden filtro bankuetan oinarrituriko modulazio multigarraiatzaileak bezalako teknologia hasiberrietara jotzen dugu, aurrez aipaturiko arazoari konponbide berriak bilatu nahian. Bibliografian dauden filtro bankuetan oinarrituriko modulazio multi-garraiatzaileak aztertu eta ondoren beraien egokitasuna ebaluatzen dugu, kanal dispertsiboen aurkako sendotasuna eta "Radio Cognitiva" teknikekin izan lezaketen bateragarritasuna irizpide hartuz.

Ebaluaketa horretan oinarrituz, doktoretza-tesi honetan "Radio Cognitiva" teknikekin bateragarria den WCP-COQAM proposatzen dugu modulazio industrial gisa. Modulazio teknika berau erakusteaz gain, bibliografian eskuragarri ez dauden WCP-COQAM-rentzat sinkronizazio eta kanal estimazio teknikak ere aurkezten ditugu.

Resumen

El objetivo principal de esta tesis doctoral consiste en encontrar una modulación de capa física capaz de proporcionar robustez y fiabilidad suficientes a sistemas de comunicaciones inalámbricas industriales. Esto supone un desafío, dadas las adversas condiciones del canal inalámbrico propias de entornos industriales. Además, dicha modulación deberá presentar una alta compatibilidad con las técnicas de Radio Cognitiva, debido al potencial de éstas para mejorar la fiabilidad de las comunicaciones inalámbricas.

Basándonos en la bibliografía, concluímos que las soluciones presentes en el estado del arte actual cubren una amplia variedad de escenarios dentro de las comunicaciones inalámbricas industriales, pero no todas. Para los escenarios con canales altamente dispersivos y requerimientos de tiempo especialmente estrictos, no existe ninguna solución en la industria ni dentro de la bibliografía científica.

En esta tesis doctoral nos centramos en tecnologías incipientes como la Radio Cognitiva y las modulaciones multi-portadora con bancos de filtros para 5G para tratar de buscar nuevas soluciones al problema anteriormente descrito. Por lo tanto, analizamos algunas de las técnicas multi-portadora con bancos de filtros presentes en la bibliografía científica y las evaluamos basándonos en su robustez frente a canales altamente dispersivos y su compatibilidad con la Radio Cognitiva.

Basándonos en dicha evaluación, proponemos WCP-COQAM como posible candidata a modulación industrial compatible con Radio Cognitiva. Además de la propia técnica de modulación, presentamos métodos de sincronización y estimación de canal para la misma que no se encuentran presentes en el estado del arte.

Abstract

The main goal of this doctoral thesis is to find a physical layer modulation able to provide high enough robustness and reliability levels for wireless industrial communications systems. Considering the harsh wireless channel conditions of industrial environments, that goal implies a considerable challenge. Besides, this modulation should be highly compatible with Cognitive Radio techniques, due to their potential to improve the reliability of wireless communications.

Based on the bibliography, we conclude that the existent solutions in the current state of the art cover a wide range of wireless industrial communications scenarios, but not all of them. There is no solution, neither in the industry nor in the scientific bibliography, for those scenarios involving highly dispersive wireless channels and particularly stringent timeliness requirements.

In this doctoral thesis, we focus on upcoming technologies such as Cognitive Radio and multi-carrier modulations based on filter banks for 5G, in order to search new solutions for the aforementioned problem. Therefore, we analyse some of the multi-carrier modulations based on filter banks of the scientific bibliography and we evaluate them in terms of robustness against highly dispersive channels and in terms of compatibility with Cognitive Radio.

In this doctoral thesis we propose the modulation WCP-COQAM as possible candidate for industrial wireless modulation and compatible with Cognitive Radio. In addition to the modulation technique itself, we also introduce some synchronization and channel estimation techniques which are not present in the state of the art.

Contents

List of Figures

List of Tables

Acronyms

3GPP	3rd Generation Partnership Project
5G	5th Generation
ABB	Asea Brown Boveri
AFB	Analysis Filter Bank
AFH	Adaptive Frequency Hopping
AL	Application Layer
AoA	Angle of Arrival
AoD	Angle of Departure
AP	Auxiliary Pilot
AS	Angular Spread
ASK	Amplitude Shift Keying
AWGN	Additive White Gaussian Noise
BER	Bit Error Rate
BI	Beacon Interval
BLT	Balian-Low Theorem
BO	Beacon Order
BPSK	Binary Phase-Shift Keying
CAP	Contention Access Period
CFO	Carrier Frequency Offset

CFP	Contention-Free Period
COQAM	Circular Offset Quadrature Amplitude Modulation
CP	Cyclic Prefix
CR	Cognitive Radio
CSI	Channel State Information
CSMA	Carrier Sense Multiple Access
CSMA-CA	Carrier Sense Multiple Access - Collision Avoidance
CMTC	Critical Machine-Type Communication
DFT	Discrete Fourier Transform
DSSS	Direct Sequence Spread Spectrum
EMBB	Enhanced Mobile Broadband
FA	Factory Automation
FBMC	Filter Bank Multi-Carrier
FBMC-COQAM	Filter Bank Multi-Carrier - Circular Offset Quadrature Amplitude Modulation
FBMC-OQAM	Filter Bank Multi-Carrier - Offset Quadrature Amplitude Modulation
FDD	Frequency Division Duplex
FDE	Frequency Domain Equalization
FDMA	Frequency Division Multiple Access
FEC	Forward Error Correction
FFT	Fast Fourier Transform
FH	Frequency Hopping
FHSS	Frequency Hopping Spread Spectrum
FMC	Filtered Multi-Carrier

FMT	Filtered Multi Tone
FP7	7th Framework Programme
FPGA	Field Programmable Gate Array
FS	Frequency Spreading
FS-FBMC	Frequency Shift - FBMC
GFDM	Generalized Frequency Division Multiplexing
GFDM-OQAM	Generalized Frequency Division Multiplexing - Offset Quadrature Amplitude Modulation
GI	Guard Interval
GTS	Guaranteed Time Slot
HART	Highway Addressable Remote Transducer Protocol
HR	High Resolution
HR-FDE	High Resolution-Frequency Domain Equalization
ICI	Inter-Carrier Interference
IEC	International Electrotechnical Commission
IEEE	Institute of Electrical and Electronics Engineers
IFFT	Inverse Fast Fourier Transform
ISA	International Society of Automation
ISI	Inter-Symbol Interference
ISM	Industrial, Scientific and Medical
ITU	International Telecommunication Union
IWSAN	Industrial Wireless Sensor and Actuator Network
LOS	Line Of Sight
LR	Low Resolution
LR-FDE	Low Resolution-Frequency Domain Equalization

LTE	Long Term Evolution
MAC	Medium Access Control
MBB	Mobile Broadband
MCM	Multi-Carrier Modulation
MIMO	Multiple Input Multiple Output
MMTC	Massive Machine-Type Communication
MSE	Mean Square Error
NLOS	Non Line Of Sight
NM	Network Manager
NR	New Radio
OFDM	Orthogonal Frequency Division Multiplexing
OOB	Out Of Band
OQAM	Offset Quadrature Amplitude Modulation
OQPSK	Offset Quadrature Phase-Shift Keying
PA	Process Automation
PAN	Personal Area Network
PAPR	Peak to Average Power Ratio
PDP	Power Delay Profile
PHY	Physical
PLR	Packet Loss Rate
PNO	Profibus and Profinet user organization
PPN	Polypahse Network
PSD	Power Spectral Density
QAM	Quadrature Amplitude Modulation

QoS	Quality of Service
RFI	Radio Frequency Interference
RMS	Root Mean Square
RRC	Root Raised Cosine
RT	Real-Time
SCO	Synchronous Connection Oriented
SD	Superframe Duration
SDR	Software Defined Radio
SE	Spectral Efficiency
SFB	Synthesis Filter Bank
SIA	Shenyang Institute of Automation
SISO	Single Input Single Output
SNR	Signal to Noise Ratio
SO	Superframe Order
STO	Symbol Time Offset
TDMA	Time Division Multiple Access
TEDS	Telecommunication Equipment Distribution Service
TFL	Time-Frequency Localization
UFMC	Universal Filtered Multi-Carrier
URLL	Ultra-Reliability and Low-Latency
URLLC	Ultra-Reliable and Low-Latency Communications
UWB	Ultra Wide Band
WCP-COQAM	Windowed Cyclic Prefix-Circular Offset Quadrature Amplitude Modulation
WI	Window Interval

WIA-PA	Wireless Networks for Industrial Automation - Process Automation
WIA-FA	Wireless Networks for Industrial Automation - Factory Automation
WISA	Wireless Interface for Sensors and Actuators
WLAN	Wireless Local Area Network
WMAN	Wireless Metropolitan Area Network
WPAN	Wireless Personal Area Network
WWAN	Wireless Wide Area Network
WSAN	Wireless Sensor and Actuator Network
WSAN-FA	Wireless Sensor and Actuator Network for Factory Automation
ZF	Zero-Forcing
α**S**	Alpha Stable

Chapter 1

Introduction

In this chapter we explain the context in which this thesis has been carried out. First of all, the main problems which motivate this research are introduced; secondly, the aims and scope of the research are defined and the objectives of this thesis are detailed. Then, the methodology followed to get these objectives is described; and last, we present the outline of this doctoral thesis report.

1.1 Motivation

Wireless communication technologies play an important role in our daily life. This fact seems to be obvious considering the amount and the diversity of wireless devices available: mobile phones, Wi-Fi routers, remote controls, television, radio, etc.

The key of wireless communications' success lies on two principal factors: user's convenience and cost reduction. That is because users can do without any cable and development, establishment and maintenance are cheaper in wireless systems than in wired ones. There is an increasing interest in wireless communications for industrial applications in the market nowadays. Wireless communications between the devices within an industrial plant would provide more flexibility concerning physical distribution and deployment, allowing to reach otherwise inaccessible points such as rotatory elements or particularly difficult to reach cavities. Besides, they would reduce costs derived from the establishment and maintenance of wiring.

However, establishment of wireless communications in industrial environments carries some challenges, among which the most remarkable one is achieving sufficiently robust communications. Wireless communications are more vulnerable than wired ones, due to Radio Frequency Interference (RFI) and channel phenomenons such as scattering, path loss, fading and shadowing. Besides, reliability and robustness requirements in industrial wireless networks are more stringent

than the ones in common WLANs at home or offices. The reason for this is that channel conditions in industrial environments are particularly hostile comparing to homes, offices or other similar environments. The large and numerous metallic machines, the electromagnetic fields inducted by high electrical currents, increased temperatures, vibrations, etc. enlarge the RFI and the aforementioned channel phenomenons, making industrial wireless channels specially hostile. For this reason, robustness and reliability are two of the main challenges in the deployment of industrial wireless communications.

In addition to the aforementioned harsh environmental conditions, there is another remarkable inconvenient regarding the deployment of wireless communications in industrial automation scenarios, an it is related to the data traffic characteristics of industrial communications. Several industrial automation applications are characterized by their stringent requirements in terms of synchronism, timeliness and latency. Reaching the narrow time margins required by some critical industrial applications, such as closed-loop control systems, demands certain throughput and capacity from a wireless communication system, and that might suppose a challenge. Considering the timeliness and latency issues and the harsh environmental and channel conditions described until now, there is no wireless communication standard which provides sufficient reliability and robustness in the current state of the art.

The relevance of reliability and robustness in industrial wireless communications comes from the very nature of those production processes which are carried out within industrial plants. Most of those processes work on real-time, so that any loss or delay in data reception and processing may lead to production process failure. This is specially relevant if we consider mission critical applications, in which such failures may cause non affordable losses or even jeopardize staff safety. Avoiding this sort of potentially hazardous situations is the main reason why communications in automation processes must be robust and highly reliable.

1.2 Scope of the research

The main goal of this doctoral thesis consists on finding a Physical (PHY) layer modulation technique able to provide high enough robustness and reliability levels for wireless communications in industrial automation applications. In addition to the robustness property, this modulation should also be compatible with Cognitive Radio (CR) techniques, due to their potential to improve the reliability of wireless communications in frequency bands with high occupation. In this sense, CR gets special relevance because the industrial wireless communications addressed in this thesis are supposed to work in the free and highly occupied Industrial, Scientific and Medical (ISM) bands. However, before continuing with the aims of this thesis,

we must specify some concepts and contextualise the research work we introduce in this work.

Wireless industrial communications are a very wide concept and they comprise a great variety of research areas: Wireless Sensor and Actuator Networks (WSANs), topologies and devices deployment; Medium Access Control (MAC) layer techniques and protocols; PHY layer modulations, channel estimation, synchronization, coding and other techniques; characterization of industrial scenarios; etc. These are some research areas that wireless industrial communications involve, remarkable due to their presence and number of related works in the bibliography.

To begin with, industrial environments may differ significantly one from another, in terms of physical characteristics, such as size, space distribution or equipment and its deployment; and also in terms of production activity. From the point of view of wireless communications these factors have certain implications. Thus, depending on the physical properties of the industrial scenario the wireless channels in it will present different characteristics, while depending on the production activity, industrial applications and requirements will be different. Regarding industrial automation classification two main classes are identified: Factory Automation (FA) and Process Automation (PA). PA typically refers to chemical industry scenarios such as oil refineries, petrochemical, paper and pulp factories, etc. On the other hand, FA refers to production lines with numerous and intense mechanical elements and activity. From the point of view of wireless communications both scenarios present very different requirements. PA applications do not carry a major challenge in terms of latency and timeliness and state of the art solutions already address them. On the contrary, current state of the art solutions are not capable of addressing the stringent real-time requirements of FA applications along with the harsh environmental conditions of such scenarios.

Plenty of technologies and techniques address the issue of wireless industrial communications in scenarios where requirements and channel conditions are moderately challenging. Industrial Wireless Sensor and Actuator Network (IWSAN) technologies based on conventional MAC protocols and standard PHY layer modulations cover many of these industrial applications. However, for more stringent and harsh environmental conditions of FA applications, new technologies and techniques must be contemplated.

In this sense, emerging technologies such as CR and Filtered Multi-Carrier (FMC) modulations, such as the ones used in 5th Generation (5G), might be promising solutions. A CR communication system consists on knowing certain information about its environment and actuating depending on it. Thus, in variable environments, such as industrial wireless channels, MAC techniques based on CR are expected to provide higher throughput and robustness due its adaptability. A FMC modulation, on the other hand, consist on a Multi-Carrier Mod-

ulation (MCM) system whose sub-carriers are filtered in order to provide lower Out Of Band (OOB) radiation. Thus, these FMC modulations provide narrower sub-carriers and more efficient spectrum usage than the conventional Orthogonal Frequency Division Multiplexing (OFDM).

It is worth mentioning that this doctoral thesis is part of a collaborative research project between the Signal Theory and Communications research group of the Electronic and Computer Science department of Mondragon Unibertsitatea and IK4-Ikerlan. It has been partly supported by the projects CIIRCOS and COWITRACC of the Basque Government and the Spanish Ministry of Economy and Competitiveness, respectively. This whole research project comprises two main different but related parts: one part is this doctoral thesis and focuses on PHY layer modulations for wireless industrial communications; the second is formed by the doctoral thesis of Pedro Manuel Rodríguez, which focuses on MAC protocols based on CR techniques [1–4].

1.3 Objectives of the thesis

In this context, we focus on researching FMC modulations for FA scenarios. Regarding FMC modulations, on the one hand, their restrained spectrum might provide higher flexibility in frequency domain and a greater compatibility with CR systems than OFDM; on the other hand, since they are MCM techniques as OFDM, they might share robustness against the multipath characteristic of wireless industrial channels. We analyse the FMC modulation techniques Filter Bank Multi-Carrier - Offset Quadrature Amplitude Modulation (FBMC-OQAM), Generalized Frequency Division Multiplexing - Offset Quadrature Amplitude Modulation (GFDM-OQAM) and Windowed Cyclic Prefix-Circular Offset Quadrature Amplitude Modulation (WCP-COQAM) and we evaluate their suitability for wireless industrial communications in terms of robustness, CR compatibility and timeliness.

Considering all the aforementioned, we have defined the following main goals for this doctoral thesis:

- To evaluate the aforementioned FMC modulation techniques in terms of robustness, CR compatibility and timeliness, and choose the most suitable one for FA applications.

- To propose time-frequency synchronization and channel estimation techniques for the previously chosen FMC modulation system, in order to address characteristic impairments of actual communication systems and provide more realistic simulations, results and conclusions.

1.4 Hypotheses

In this doctoral thesis we analysed several modulation schemes; related techniques such as synchronization and channel estimation; and channel characterization models of the sate of the art. Based on the preliminary results we obtained from the analysis and evaluation of some of the FMC modulations and their related techniques, we state the following hypotheses:

- FBMC-OQAM cannot match the performance of block-wise FMC modulations with Cyclic Prefix (CP) extension in terms of Bit Error Rate (BER) and Spectral Efficiency (SE), under highly dispersive channel conditions and FA timeliness requirements.
- Block-wise FMC modulations with CP extension can match the performance of OFDM in terms of BER, under equal channel conditions and assuming equal Guard Interval (GI).
- Pilot-aided channel estimation based on High Resolution-Frequency Domain Equalization (HR-FDE) for WCP-COQAM outperforms the pilot-aided channel estimation based on Low Resolution-Frequency Domain Equalization (LR-FDE) for FBMC-OQAM and Generalized Frequency Division Multiplexing (GFDM) explained in the bibliography, under time varying and highly dispersive channel conditions.

1.5 Methodology

In order to get the main results and contributions of this thesis, we try to prove the hypotheses stated above. The research strategy we follow for this task consists on computer simulations run in Matlab. By means of these simulations we evaluate and compare the performance of OFDM, FBMC-OQAM, GFDM-OQAM and WCP-COQAM in terms of BER against E_b/N_0 ratio. On the other hand, we evaluate the time-frequency synchronization and channel estimation techniques that we propose in this thesis in terms of Mean Square Error (MSE) against E_b/N_0 ratio. In order to calculate these error rates we run Monte Carlo iterations, which are configured so that we provide confidence intervals between 1 and 2 orders (10 - 10^2) below the error rate given at a confidence level of 99.9%.

Considering the special relevance of the environment and the context this thesis focuses on, i.e. wireless communications in industrial scenarios, characterization of such environments in the aforementioned simulations has been a vital issue during this research. In order to characterize the corresponding channel conditions we employ the native Rayleigh fading channel object in Matlab. We get the configuration

parameters for this Matlab channel object, such as the Power Delay Profile (PDP) and the Doppler spectrum, from different wireless channel and industrial wireless characterization models in the bibliography. Although there is not any standard industrial wireless channel model, we pick the parameters so that the whole model behaves as close to an actual industrial channel model as possible. During the simulations, we employ the same channel model to run a whole cycle of Monte Carlo iterations but different channel realization at each iteration.

More specific considerations about simulation criteria are explained in their corresponding sections along with their respective results.

1.6 Outline

Next, we enumerate the chapters introduced in this doctoral thesis report and we give a brief description of them:

- **Chapter 2, Background and related work:** In Chapter 2 we take into consideration several aspects and research fields related to our investigation. Before introducing the main contributions of this doctoral thesis, we provide a general analysis of the state of the art and some theoretical background related to the work introduced in this thesis.

- **Chapter 3, Evaluation of WCP-COQAM, GFDM-OQAM and FBMC-OQAM for Industrial Wireless Communications with Cognitive Radio:** In Chapter 3 we analyse the following FMC modulations in depth: FBMC-OQAM, GFDM-OQAM and WCP-COQAM. Besides, according to the ultra-reliability and low latency requirements of industrial communications, we simulate the aforementioned modulations in low-band transmissions through large indoor spaces and severe multipath channels, emulating industrial halls. Based on these results, we aim at providing a notion about the suitability of FMC modulation schemes for industrial wireless communications based on CR.

- **Chapter 4, CFO and STO synchronization and channel estimation techniques for WCP-COQAM:** In Chapter 4 we address the issues of Carrier Frequency Offset (CFO) and Symbol Time Offset (STO) synchronization and time varying channel estimation for WCP-COQAM. We analyse CFO and STO synchronization techniques for GFDM and OFDM available in the bibliography and we adapt them in order to propose synchronization techniques for WCP-COQAM. The simulation results we present here show that the proposed synchronization techniques can be suitable solutions for the CFO and STO in WCP-COQAM systems. Additionally, we also propose

a robust and low-latency pilot-based channel estimation technique for short WCP-COQAM transmissions. The simulation results we present here show that the channel estimation technique we introduce provides significantly higher robustness against time-variant and highly frequency selective channels than the solutions from the bibliography. Furthermore, we also show the overall performance of WCP-COQAM under more realistic conditions, due to the simulation of actual impairments such as time-frequency offset and channel estimation.

- **Chapter 5, Conclusions and future work:** In Chapter 5 we state the conclusions we obtained from the whole research carried out during this doctoral thesis. We also state the scientific contributions we made during the development of this doctoral thesis. Finally, we make an analysis on the works and research that might derive from the results and contributions provided in this doctoral thesis.

Chapter 2

Background and related work

In this chapter we take into consideration several aspects and research fields related to our investigation. Before introducing the main contributions of this doctoral thesis, in this chapter we provide a general analysis of the state of the art and some theoretical background related to the work introduced in this thesis.

First of all, we start defining the characteristics of industrial wireless scenarios and the requirements that wireless communications must fulfil in industrial automation applications. Next, we analyse the existing state of the art solutions for wireless industrial communications and the requirements they can and cannot fulfil. In addition to the already existing wireless industrial communications, we analyse what the 5th Generation (5G) of communications is expected to contribute to wireless industrial communications and we also introduce the background of the fundamental modulation techniques which are expected to form the 5G standards. Last, we introduce some basics about CR paradigm and analyse its benefits for wireless industrial communications. To conclude the chapter, we introduce a discussion about the analysis of the state of the art and we state its scarcities concerning the scope of our investigation.

2.1 Wireless communications requirements in industrial environments

Industrial environments significantly differ from the well-known office and home environments. Besides the challenges on technologies and systems due to harsh environmental conditions, such as increased temperatures or vibrations, they are remarkably different in terms of wireless systems deployment. Mainly with respect to two aspects: the industrial traffic characteristics and the industrial wireless channel. Moreover, these problems make harder for wireless communications to cope with the already stringent requirements in timeliness and reliability of

industrial applications.

When characterizing industrial wireless scenarios, it is worth bearing in mind that each industrial environment may present very specific wireless channel characteristics. Hence, there is no generic industrial wireless channel model available in the bibliography. In this section the typical requirements for industrial communication applications are analysed.

The major challenge for currently employed industrial wireless communication systems are the high requirements of industrial automation applications regarding latency, synchronism and reliability [5]. The capability of a communication system to match all these requirements will make it suitable or not for such applications. These requirements differ considerably depending on the kind of industrial application, so that timeliness and real-time parameters can vary from less than tens of milliseconds up to hundreds of milliseconds from one application to another [6]. In this section, the requirements for two kinds of industrial automation environments are defined: Process Automation (PA) and Factory Automation (FA). PA typically refers to chemical industry scenarios such as oil refineries, petrochemical, paper and pulp factories, etc. On the other hand, FA refers to production lines with numerous and intense mechanical elements and activity.

2.1.1 Communication requirements in Process Automation

Although there is some overlap of wireless communications applications between PA and FA, they are considerably different environments. The specifications targeting industrial PA tend to have more tolerance for network latency than what is needed for FA. Most applications in PA are representatives of the class of soft real-time. Existing WSAN in typical PA spaces, such as oil refineries, usually employ communication protocols with low data rates, up to 250 kbps range [7]. Moreover, non-critical closed-loop applications have a latency requirement that can be as low as 100 milliseconds but open-loop controls are tolerant of latencies above 1 second [8].

The aforementioned requirements do not carry a major challenge in terms of latency and timeliness. This fact, along with the relatively low throughput requirement, can suppose a good chance for a wireless communication system to fulfil the reliability requirements for industrial PA applications. Current state of the art already provide solutions for this kind of PA scenarios. There exist several WSAN standards, such as WirelessHART, ISA 100.11a and Wireless Networks for Industrial Automation - Process Automation (WIA-PA), which are widely extended in the industry [9].

2.1.2 Communication requirements in Factory Automation

The current state of the art solutions for wireless automation do not consider closed-loop control applications, a class of field level applications which present particularly hard challenges on the real-time behaviour of their associated communication system [10,11]. When classifying FA applications with respect to their real-time characteristics, closed-loop control applications belong to the class of hard real-time, i.e. given temporal deadlines have to be strictly met, or isochronous real-time, i.e. hard real-time plus additional constraints on the jitter.

Table 2.1 enumerates characteristic use cases of field level applications and some of their requirements. Both the requirements for manufacturing cell application (which comprises, for instance, the control of robot arms) and for sensor-actuator application are fulfilled with state of the art narrowband wireless systems such as Bluetooth, Wireless Interface for Sensors and Actuators (WISA) or Wireless Sensor and Actuator Network for Factory Automation (WSAN-FA) [12]. In contrast, closed-loop control applications [13] require shorter transmission delays (in the order of 100 μs device-to-device transmission times) as well as higher data rates. In other words, the aforementioned wireless technologies present significant limitations for closed-loop control applications due to their challenging requirements as listed in Table 2.1.

Table 2.1: Parameter of field level application examples [6]

Application example	Payload [Bytes]	Cycle time [ms]	Jitter [μs]
Manufacturing cell	< 16	50	500
Sensor-actuator	< 20	n.s.	n.s.
Closed-loop control	low	n.s.	20
- Machine tools	50	0.5	1
- Printing machines	30	2	5
- Packaging machines	15	5	20

Besides, it is worth bearing in mind that all given use cases of Table 2.1 require Packet Loss Rate (PLR) $< 10^{-9}$ on application level, which is mandatory for field level applications in FA. Therefore, in addition to real-time requirements, reliability, high degree of synchronism and high availability in time and space, represent the other major challenges for wireless industrial communication systems.

2.2 Industrial environment characterization

In industrial environments, the noise that communication devices suffer can be significant due to the high operating temperatures, strong vibrations and excessive electromagnetic noise caused by large coils, motors, etc. Interferences from other wireless systems transmitting on the same frequency band might also be present. Moreover, the signal might be exposed to heavy multipath propagation caused by multiple reflections from large and metallic obstacles within the propagation channel. The random/periodic movement of people, robots, trucks, and other objects may also cause time varying channel conditions. All these propagation impairments reduce the reliability of wireless communications, so that mission-critical communications in industrial applications can result in important losses in terms of safety, time and money.

Knowledge of the propagation channel is needed to successfully design and evaluate robust wireless communications for industrial applications. However, there are limited works in the bibliography dealing with industrial multipath propagation. In this section we introduce the multipath propagation, noise and interference models that we have employed in our simulations during the development of this doctoral thesis.

One of the main problems that the wireless propagation implies is the dispersion of the transmitted signal. The received signal is not only coming directly from the transmitter, but from the combination of reflected, diffracted and scattered "copies" of the transmitted signal. This dispersion phenomena distorts in a great deal the received signals.

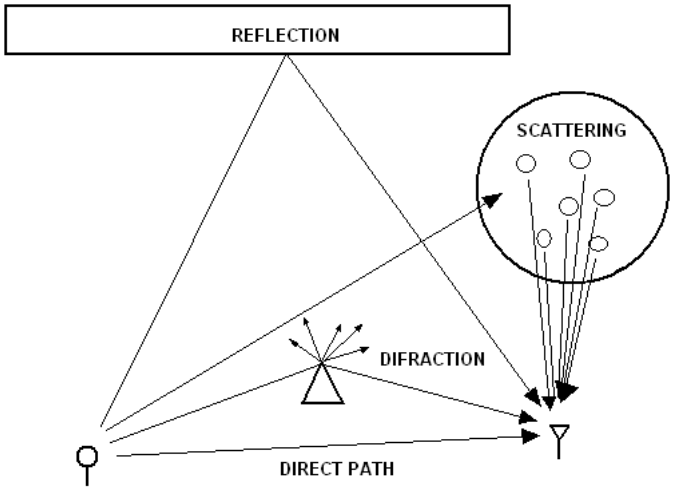

Figure 2.1: Wireless propagation in dispersive channels.

Reflection occurs when the transmitted signal "hits" a surface where part of

that signal's energy is reflected. Diffraction occurs when the signal is obstructed by a sharp object which derives secondary waves. Finally, scattering occurs when the signal impinges on a rough surface or between numerous small objects and it is reflected several times. Thus, the receiver gets the transmitted signal along with other "copies" of it, but with different phase and energy [14]. Figure 2.1 shows a graphical scheme of these phenomena.

Figure 2.2: An example of an industrial environment, a picture of an incinerator plant [15].

Since this thesis is aimed at dealing with industrial environments, it must be taken into account that the aforementioned dispersion phenomena imply more serious issues in such environments than in typical indoor offices or halls. Industrial environments consist of numerous heavy and metallic elements which act as reflectors within the propagation channel. Besides, since many surfaces are metallic, it is usual the reflected signal's energy to be higher than in other kind of environments (see Figure 2.2).

Considering all the aforementioned aspects, a variety of potentially suitable highly dispersive channel models are analysed in next sections.

2.2.1 IEEE 802.15.4a channel models

In [16] a discussion of the IEEE 802.15.4a channel modelling subgroup is introduced. It provides channel models for the following frequency ranges and environments:

- Ultra Wide Band (UWB) channels covering the 2-10 GHz frequency range, it covers indoor residential, indoor office, industrial, outdoor, and open outdoor

environments (with a distinction between Line Of Sight (LOS) and Non Line Of Sight (NLOS) properties).

- A model for body area networks in the 2-6 GHz frequency range.
- A model for indoor office-type environments in the 100-900 MHz frequency range.
- A narrowband model for a 1 MHz carrier frequency.

The document also provides Matlab programs to simulate these channel models.

For this thesis, only the first case (UWB channels covering the 2-10 GHz frequency range) for industrial environments is taken into account. Besides, it must be taken into consideration that this is an UWB channel model, so that it does not fit the scope of our research considering that it is aimed at ISM bands.

The IEEE 802.15.4a channel modelling subgroup develops stochastic channel models derived from measured real data. The main goal of these channel models, is to provide the chance of comparing different communication system proposals over these very channels. So that it must be borne in mind that they are not intended to provide information of absolute performance of those proposals over these channels. That is because the number of available measurements of real data on which the models are based, is insufficient for that purpose. Specific measurements for the industrial environment model were extracted from the campaign described in [17].

The aforementioned measurement data is used in order to estimate the parameters for the channel generation. On the other hand, the generic channel model is defined as

$$h_{discr}(t) = \sum_{l=0}^{L} \sum_{k=0}^{K} a_{k,l} e^{j\phi_{k,l}} \delta(t - T_l - \tau_{k,l}) \ . \tag{2.1}$$

All the calculations for parameter estimation and generation of the channel model have been omitted in order to make the reading lighter and more clear, for details about those aspects refer to [16].

2.2.2 TGn channel models

In [18] a set of geometric ray-tracing based channel models applicable to indoor Multiple Input Multiple Output (MIMO) WLAN systems are proposed. Some Single Input Single Output (SISO) WLAN channel models are also proposed in this study. However, considering the scope of this doctoral thesis, only the SISO approach has been taken into consideration during the revision of the state of the art. Next, the overall procedure to develop one of these channel models is explained:

- In these models distinct *clusters*[1] are identified first. The number of clusters varies from 2 to 6, depending on the model, this finding is consistent with numerous experimentally determined results reported in the bibliography.

- Then the power of each tap in a particular cluster is determined.

- Next Alpha Stable (αS), Angle of Arrival (AoA), and Angle of Departure (AoD) values are assigned to each tap and cluster (using statistical methods) that agree with experimentally determined values reported in the bibliography. Cluster αS was experimentally found to be in the 20 to 40 range, and the mean AoA was found to be random with a uniform distribution.

- With the knowledge of each tap power, αS, AoA and AoD, for a given antenna configuration, the channel matrix H can be determined.

The channel matrix H fully describes the propagation channel between all transmit and receive antennas. If the number of receive antennas is n and transmit antennas is m, the channel matrix H will have a dimension of $n \times m$. However, as aforementioned, in this revision of the state of the art only SISO models have been considered, so that the channel matrix H will have a dimension of 1x1.

The model can be used for both 2.4 GHz and 5.1 GHz ISM frequency bands, since the experimental data and published results for both bands were used to develop this channel model.

The implemented models can be classified in six of them, from the model A to de model F. Each one of these models differs from the others in aforementioned tap and cluster parameters, so that each one of them may be assigned to a certain physical environment. These are some examples:

- Model A for a typical office environment, NLOS conditions, and 0 ns rms delay spread.

- Model B for a typical large open space and office environments, NLOS conditions, and 15 ns rms delay spread.

- Model C for a large open space (indoor and outdoor), NLOS conditions, and 30 ns rms delay spread.

- Model D, same as model C, LOS conditions, and 50 ns rms delay spread (10 dB Ricean K-factor at the first delay).

[1]cluster may refer to the group of rays/taps reflected on a "scatterer"/""reflector" (according to the terminology used in the previous sections) element within the wireless channel.

- Model E for a typical large open space (indoor and outdoor), NLOS conditions, and 100 ns rms delay spread.

- Model F for a typical large open space (indoor and outdoor), NLOS conditions, and 150 ns rms delay spread.

This has been an overall explanation about TGn group's WLAN channel modelling, all the calculations for parameter estimation and generation of the channel model have been omitted in order to make the reading lighter and more clear. For further information and details about those aspects refer to [18].

TGn channel model's time variability

In the TGn channel models indoor wireless channels are assumed, where transmitter and receiver are stationary and people are moving in between. Those people moving around are the cause of channel's variation over time. As a result, a function $S(f)$ is defined for that indoor environment in order to fit the Doppler power spectrum measurements. $S(f)$ can be expressed as (in linear values, not dB values):

$$S(f) = \frac{1}{1 + A\left(\frac{f}{f_d}\right)^2} , \tag{2.2}$$

where A is a constant, used to define S(f)=0.1, at a given frequency $f = f_d$, so that $A = 9$. The Doppler spread f_d is defined as

$$f_d = \frac{\nu_o}{\lambda} ,$$

where ν_o is the environmental speed determined from measurements that satisfy (21), and λ is the wavelength defined by

$$\lambda = \frac{c}{f_c} ,$$

where c is the light speed and f_c is the carrier frequency. The value for ν_o is proposed equal to 1.2 km/h.

Figures 2.3 and 2.4 show the principal results of the Doppler spectrum model defined by Equation (2.2). In Figure 2.3 just the theoretical Doppler spectrum is shown, while in Figure 2.4 this theoretical Doppler spectrum is compared to the measured values it is based on.

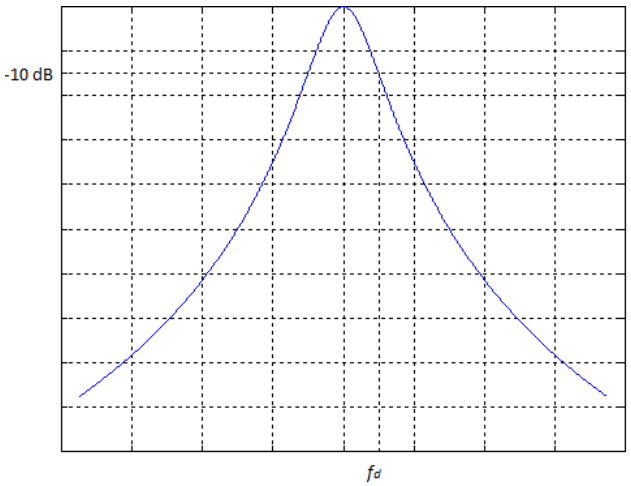

Figure 2.3: TGn's time varying channel model's "Bell" shape Doppler power spectrum [18].

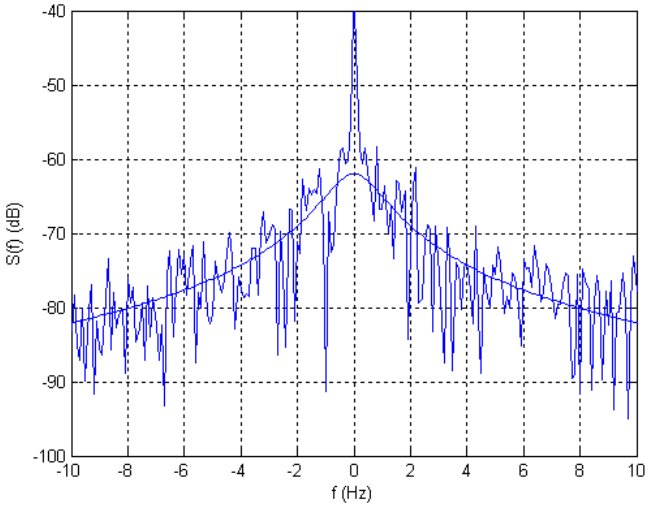

Figure 2.4: Measured Doppler power spectrum for a single delay tap vs. theoretical "Bell" shape fitting function [18].

2.2.3 WINNER channel models

The work in [19] presents WINNER II channel models for WLAN, Wireless Metropolitan Area Network (WMAN), and Wireless Wide Area Network (WWAN) communication systems. The models have been evolved from the WINNER I channel models described in [20] and WINNER II interim channel models described in deliverable D1.1.1. The implemented channel model scenarios are indoor office, large

indoor hall, indoor-to-outdoor, urban micro-cell, bad urban micro-cell, outdoor-to-indoor, stationary feeder, suburban macro-cell, urban macro-cell, rural macro-cell, and rural moving networks. This revision of the state of the art is focused on the *large indoor hall* scenario, since it may be the one which most approximates to an industrial environment characteristics. In fact, some of the measurements for the data corresponding to this scenario were carried out in an industrial hall [21], see Figure 2.5.

Figure 2.5: WINNER's *large indoor hall* measurements scenario [21].

The generic WINNER channel model follows a geometry-based stochastic channel modelling approach. The channel models are antenna independent, so that different antenna configurations and element patterns can be inserted. The channel parameters are determined stochastically, based on statistical distributions extracted from channel measurement. Those distributions are defined for, delay spread, delay values, angle spread, shadow fading, and cross-polarisation ratio. For each channel snapshot (or sampling moment), the channel parameters are calculated from those distributions. Channel realisations are generated by summing contributions of rays/taps with specific channel parameters like delay, power, AoA and AoD. Different scenarios are modelled by using the same approach, but different parameters.

WINNER's channel models are scalable from a SISO or MIMO link to a multi-link MIMO scenario including polarisation among other radio channel dimensions. The models can be applied not only to WINNER II systems, but also any other

wireless system operating in 2-6 GHz frequency range with up to 100 MHz bandwidth.

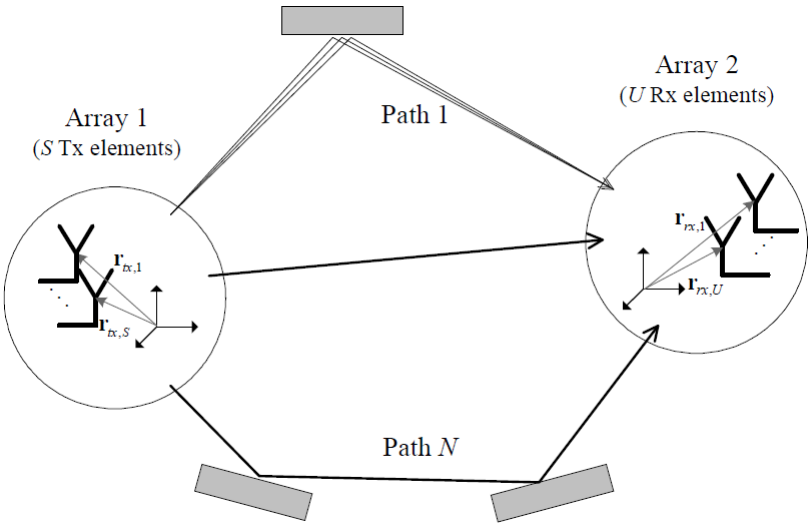

Figure 2.6: WINNER's generic channel model's layout [19].

Figure 2.6 shows the layout of a generic WINNER channel model. According to that scheme, a number of rays constitute a cluster or a path, both terms are equal as far as WINNER terminology concerns.

On the other hand, Equation (2.3) represents the analytical definition of the WINNER's generic channel model.

$$H_{u,s,n}(t;\tau) = \sum_{m=1}^{M} \begin{bmatrix} F_{rx,u,V}(\varphi_{n,m}) \\ F_{rx,u,H}(\varphi_{n,m}) \end{bmatrix}^T \begin{bmatrix} \alpha_{n,m,VV} & \alpha_{n,m,VH} \\ \alpha_{n,m,HV} & \alpha_{n,m,HH} \end{bmatrix} \begin{bmatrix} F_{tx,s,V}(\phi_{n,m}) \\ F_{tx,s,H}(\phi_{n,m}) \end{bmatrix} \times \cdots \tag{2.3}$$
$$\cdots e^{j2\pi\lambda_0^{-1}(\overline{\varphi}_{n,m}\cdot\overline{r}_{rx,u})} \cdot e^{j2\pi\lambda_0^{-1}(\overline{\phi}_{n,m}\cdot\overline{r}_{tx,s})} \cdot e^{j2\pi\nu_{n,m}t} \cdot \delta(\tau - \tau_{n,m}) \ ,$$

where $F_{rx,u,V}$ and $F_{rx,u,H}$ are the antenna element u field patterns for vertical and horizontal polarisations respectively, $\alpha_{n,m,VV}$ and $\alpha_{n,m,VH}$ are the complex gains of vertical-to-vertical and horizontal-to-vertical polarisations of ray n, m respectively (where n refers to a cluster/path and m to a ray/tap within that cluster/path). Further λ_0 is the wave length of carrier frequency, $\overline{\phi}_{n,m}$ is AoD unit vector, $\overline{\varphi}_{n,m}$ is AoA unit vector, $\overline{r}_{tx,s}$, and $\overline{r}_{rx,u}$, are the location vectors of element s and u respectively, and $\nu_{n,m}$ is the Doppler frequency component of ray n, m. If the radio channel is modelled as dynamic, all the above mentioned small scale parameters are time varying, i.e. function of t.

This has been an overall explanation about WINNER's generic channel model, all the calculations for parameter estimation and generation of the channel model have been omitted in order to make the reading lighter and more clear. For further information and details about those aspects refer to [19, 21].

WINNER channel model's time variability

For WINNER's time varying channel modelling, the most important feature to be taken into account is the mobile reflectors. In WINNER's project the channels with moving scatterers are referred as *nomadic channels*. These are the main steps to generate a WINNER time-varying channel:

1. Generate initial channel parameters (delays, powers, AoA/AoD etc.).
2. Assign which scatterers (or clusters in the WINNER terminology) are moving.
3. Calculate the Doppler frequencies for all moving rays in all the clusters containing movement (note that all or only part of the rays are moving in those clusters).
4. Generate the channel coefficients for each channel *segment* (see Figure 2.7).

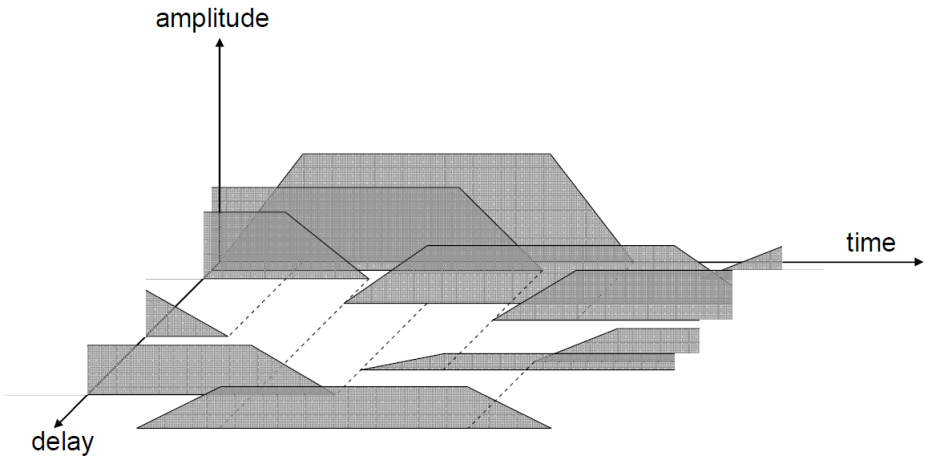

Figure 2.7: Winner model's time evolution scheme, transitions between channel segments [19].

Figure 2.7 shows the scheme of the WINNER's channel's time variation. During that variation some scatterers remain stationary, others keep changing their

position, others eventually stop affecting signal's propagation and others eventually begin to affect signal's propagation. In Figure 2.7 the effect of those scatterers is represented by those plane elements ramping up and down. In this context, a *segment* is a extremely short time gap in which channel characteristics remain constant. So that when modelling WINNER's time varying channels, the variation occurs from one segment to the next one.

2.3 Industrial Wireless Communications

Industrial wireless communications have been used for more than one decade. During this period, the use of wireless communications in industrial automation has been constantly increasing and they also have gained great scientific interest [22–26]. As in other fields, wireless technology can provide important benefits to industrial communications, such as devices layout flexibility and cost reduction in cable installation and maintenance. On the other hand, they also present significant drawbacks regarding communications robustness. The main challenge for current industrial wireless solutions are the high requirements of industrial automation applications concerning latency, synchronism and reliability.

Wireless communications for industrial automation typically consist on a set of sensors and actuators connected via wireless known as IWSAN. Their main task is to gather information about the industrial environment and make the elements within that network to act according to the collected data [27–30]. IWSANs are mostly used in monitoring and loop control applications [31–34]. Most of these technologies are based on existing standards like IEEE 802.11 (WLAN), IEEE 802.15.1 (Bluetooth) or IEEE 802.15.4 (ZigBee) and additionally proprietary protocol extensions are applied over them [35–39]. Some of the most extended industrial wireless solutions are WirelessHART, ISA 100.11a, WIA-PA, WISA, WSAN-FA and some solutions based on the IEEE 802.11 standards [40, 41].

In this section the aforementioned industrial wireless communication systems are introduced. For each of them, an overall description along with their main characteristics are provided. They are classified depending on the standard their PHYs are based on.

2.3.1 Systems based on IEEE 802.15.4

In this section the characteristics of the most extended IWSANs based on the IEEE 802.15.4 (ZigBee) are introduced: WirelessHART [42], ISA 100.11a [43] and WIA-PA [44]. Unlike other non-standard proprietary solutions, these ones are recognised as industrial wireless communication standards by international organisms. Thus, WirelessHART is defined as the IEC 62591 standard by the

International Electrotechnical Commission (IEC); the ISA 100.11a is a standard defined by the International Society of Automation (ISA) and WIA-PA is defined as the IEC 62601 standard.

The IEEE 802.15.4 standard [45] has become a communication standard for low data rate, low power consumption and low cost Wireless Personal Area Network (WPAN). The protocol focuses on very low cost communication, which requires very little or no underlying infrastructure. The basic framework supports a communication range of $\leq$10 m. The capacity of the system varies depending on the selected data rate of 20, 40, 100, and 250 kbps. The protocol provides flexibility for a wide variety of applications by effectively modifying its parameters. It also provides real-time guarantees by using a Guaranteed Time Slot (GTS) mechanism for time sensitive applications. Hence, two kinds of network configuration modes are provided in the IEEE 802.15.4 standard. The beacon enabled mode, where a Personal Area Network (PAN) Coordinator periodically generates beacon frames after every Beacon Interval (BI). In the non beacon enabled mode, all nodes can send their data by using an unslotted Carrier Sense Multiple Access - Collision Avoidance (CSMA-CA) mechanism which does not provide any time guarantees to deliver data frames.

The PHY Layer is responsible for transmission and reception of data using a selected radio channel according to the defined modulation and spreading techniques. The spreading in all frequency bands is based on Direct Sequence Spread Spectrum (DSSS). The different modulation schemes are Binary Phase-Shift Keying (BPSK), Amplitude Shift Keying (ASK) and Offset Quadrature Phase-Shift Keying (OQPSK). The choice of a modulation scheme depends on the desired data rate.

The IEEE 802.15.4 MAC layer provides features like: beacon management, channel access, GTS management, frame validation, acknowledgement frame delivery, association, and disassociation. In the beacon enabled mode, the PAN Coordinator uses a superframe structure in order to manage the communication between its associated nodes. The superframe structure is defined by means of two parameters: Beacon Order (BO) and Superframe Order (SO). The active period (Superframe Duration (SD)) is divided into 16 equally sized time slots for data transmission. Within the active period two medium access coordination functions are defined in IEEE 802.15.4: a mandatory Carrier Sense Multiple Access (CSMA) mechanism for the contention access period and an optional GTS mechanism for the Contention-Free Period (CFP). The contention access phase shall start immediately after the beacon and complete before the beginning of the CFP on a superframe slot boundary. The CFP shall start on a slot boundary immediately after the Contention Access Period (CAP) and it shall complete before the end of the active period of the superframe. The CFP can be activated by a request sent

from a node to the PAN coordinator.

- CSMA: Two versions of CSMA-CA are defined, the unslotted for the non beacon-enabled mode and the slotted CSMA-CA for the beacon-enabled mode. For both versions it is based on back-off periods.

- GTS: GTS provides real time guarantees for time sensitive applications. GTS can be activated by the request sent from a node to the PAN coordinator. At the reception of this request, the PAN coordinator checks whether there are sufficient resources available for the requested node in order to allocate requested time slot. Maximum of 7 GTSs can be allocated in one superframe.

Regarding the application fields of these systems, it is worth mentioning that they are specified for PA (e.g. chemical industry, oil refineries, paper factories, etc.) environments. Their characteristics make them unsuitable for FA applications. More details about this issue in Section 2.1.2.

WirelessHART

WirelessHART was developed by the Highway Addressable Remote Transducer Protocol (HART) Communication Foundation in 2007 [46] and in 2010 the IEC adopted it as the IEC 62591 standard [47]. The standard is defined as a simple, reliable and secure solution for WSAN. The network is formed by a number of field devices, gateways, a network manager and a security manager; as shown in Figure 2.8. The field devices are connected to process or plant equipment, and it can be connected in either star or mesh topology. Handheld devices and adapters to connect HART devices to WirelessHART networks are also allowed. The gateway connects the field device network with host applications. It buffers large sensor data, event notifications, and diagnostics and command responses. The network manager configures the networks, scheduling, communications between devices, managing message routes and monitoring network health. The network manager may be integrated into the gateway or host application. Finally, the security manager collaborates with the network manager in order to avoid intrusions or attacks against the network.

Field devices use an IEEE 802.15.4 transceiver, which transmits in the 2.4 GHz ISM band. DSSS and channel hopping are employed in order to ensure a secure and reliable communication. Latency is ensured through a Time Division Multiple Access (TDMA) with a timeslot of 10 ms. Each slot may be reserved to be used by a specific node or shared by several nodes which use CSMA-CA. The slot allocation is carried out by the network manager.

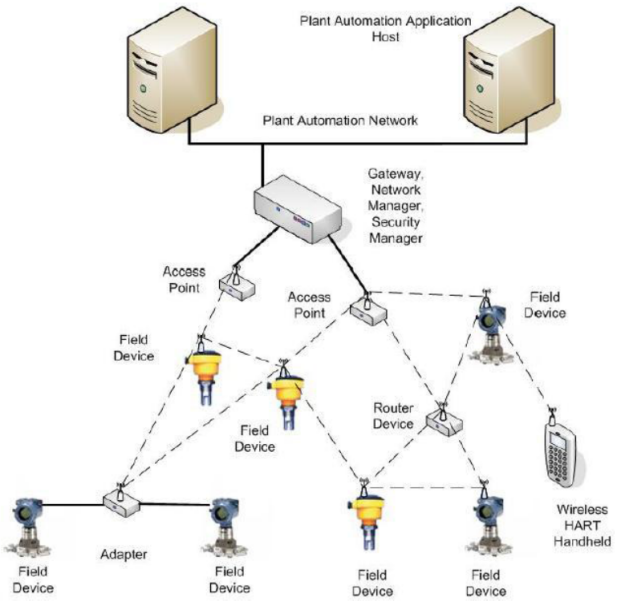

Figure 2.8: WirelessHART network representation [46].

ISA 100.11

The ISA 100 standards committee, which is part of the non-profit International Society of Automation (ISA) organization, developed the ISA 100.11a standard. It enables wireless industrial applications, such as process automation and FA. An ISA 100.11a network is composed of end devices and gateways, see Figure 2.9. Some of the end devices, which can be both sensor and actuator, are also in charge of routing functionalities. One or several gateways are in charge of providing connection between the WSAN and the user application, and it may provide security and network managers. Furthermore, the gateways also support connection with other standards.

The PHY is based on the IEEE 802.15.4 standard, but some additional features are included. The ISA 100.11a supports frequency hopping and also blacklisting to increase robustness against interference, being TDMA the access method used by the nodes. Some flexibility in the configuration of the TDMA mechanism is allowed: since timeslot size is configurable. As a result, it is possible that two ISA 100.11a devices may not be able to communicate. Every link in the network is associated to one or more slots in the TDMA frame. ISA100.11a also defines network and transport layers, based on 6LoWPAN, IPv6 and UDP [48].

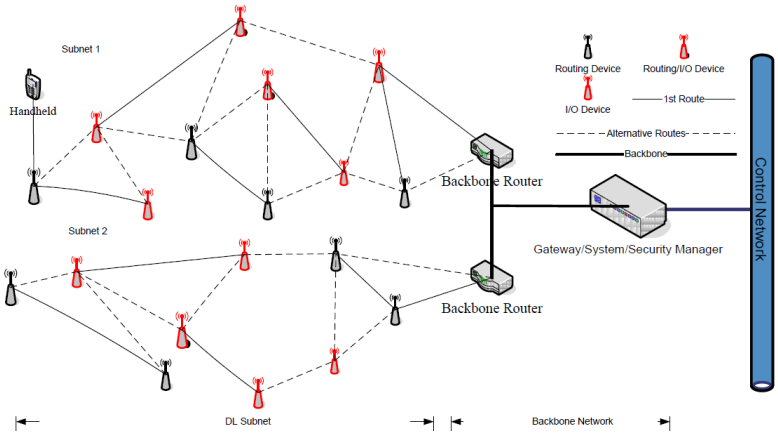

Figure 2.9: ISA 100.11a network representation [48].

WIA-PA

WIA-PA is the Chinese standard GB/T26790.1-2011, for measuring, monitoring and open loop control of production processes [49]. It was developed by the Shenyang Institute of Automation (SIA) and it was standardised by the IEC as the standard IEC 62601 [50].

WIA-PA adopts a hybrid mesh and star network and supports end devices, routers and gateways. Routers and gateways form a mesh network, and end devices construct a star network. Each star network is a cluster managed by a router. An example of a WIA-PA network is shown in Figure 2.10.

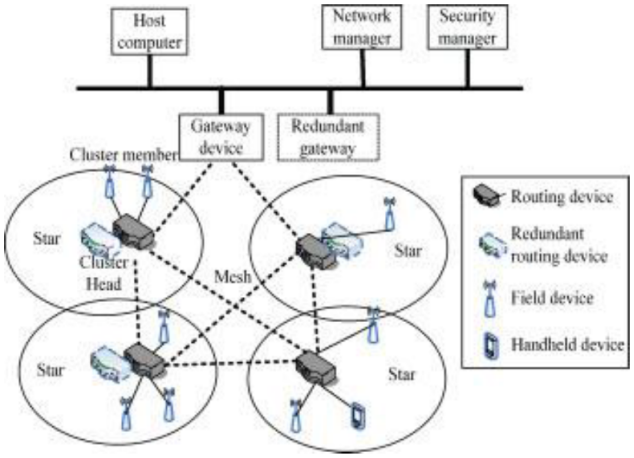

Figure 2.10: WIA-PA network representation [49].

Physical layer in WIA-PA is based on IEEE 802.15.4 and MAC layer is com-

patible with it. Some extensions to the MAC layer have been done to satisfy the industrial requirements. The contention-free period of the IEEE 802.15.4 MAC is used to carry out the communication between devices and cluster heads, while the nodes used the contention period to join the network. The inactive period can be used to sleep or for inter-cluster and intra-cluster communications.

2.3.2 Systems based on IEEE 802.15.1

In this section the characteristics of the most extended IWSANs based on the IEEE 802.15.1 (Bluetooth) are introduced: WISA and WSAN-FA. Unlike the industrial wireless communication standards introduced in Section 2.3.1, these ones are proprietary solutions. Thus, WISA is a proprietary solution developed by ABB and WSAN-FA was developed by the Profibus and Profinet user organization (PNO).

The IEEE 802.15.1 standard [51] specifies the PHY and the MAC sublayer of the well-known Bluetooth technology and it operates in the 2,4 GHz ISM band. A typical application for the 802.15.1 would be for instance a connection between a cell-phone and a headset or a headphone and an audio device. However, the system is also attractive for the use in industry applications, since its medium access method allows a deterministic data delivery.

According to 802.15.1 every physical channel used, is called a piconet consisting of one master, and up to seven slaves. The master device within a piconet coordinates the traffic within a piconet and starts the connection setup procedure. Furthermore, the wired and the wireless network are connected via the master device. The other devices are called slave devices. These are only able to directly communicate with their master. Slave devices within a piconet are either in an active or inactive operation mode. An active slave device communicates with the master device, inactive devices are in an energy saving state and only start a communication upon a wake up call by the master device.

Piconet traffic is based on TDMA with a duplex scheme, allowing the master to communicate in odd-numbered time slot. The slaves are only permitted to reply in time slots which are even-numbered and after they have been polled by the master. The channel access is divided into slots, each of 625 μs length. A data transmission may occupy the channel for 1, 3 or 5 consecutive slots. A Frequency Hopping Spread Spectrum (FHSS) modulation with 79 different 1 MHz channels is used to deal with the ISM band requirements. In order to avoid problems with the coexistence to other technologies, an Adaptive Frequency Hopping (AFH) can be used to render occupied frequencies.

The MAC protocol is mainly divided into Synchronous Connection Oriented (SCO) and Asynchronous Connectionless frames. The SCO transmission is attractive for industrial usage. The SCO transport mechanism reserves time slots on the

physical channel. It is therefore able to provide Quality of Service (QoS) guarantees. The transmission of an SCO packet takes 366 μs and typically transmits data with a rate of 64 kb/s. This is done by reserving periodic slots for a specific communication between the master and a slave device. An extension to the SCO data transmission is the eSCO data transmission. It also uses reserved time slots and has the advantage that it can deal with different, but still static, transmission rates and is able to transport non voice data. Nonetheless, in most cases, it is necessary to have more than one piconet, because of the existing slave limitation to seven.

As for the application fields of these systems, it is worth mentioning that they are specified for FA (e.g. assembly line production) environments. Their characteristics regarding timeliness and latency make them more suitable than systems based on the IEEE 802.15.4 for FA applications. More details about this issue in Section 2.1.2.

WISA

The WISA system [52] [53] is a proprietary solution developed by Asea Brown Boveri (ABB) and is targeted at typical FA applications. Its PHY is based on the standard IEEE 802.15.1-2005. It has been designed to cover wireless communication as well as wireless power supply. This enables truly wireless connected sensors and actuators without having the need for a separate power supply.

In a system that needs to achieve the delivery of messages with a very high probability of success and high number of devices, the medium access is important. The medium access in WISA are TDMA, Frequency Division Duplex (FDD) and Frequency Hopping (FH). The WISA frequency hopping scheme guarantees that the frequencies used in successive frames are widely spread. The downlink transmission from the base station to the wireless devices is always active, for the purpose of establishing frame and slot synchronization for the devices, but also to send acknowledgements and data.

In order to save power, uplink transmissions from a sensor only occur when it has data to send. The requirement of wireless real-time communication combined with a need for a high number and high density of devices, makes efficient use of the available bandwidth very important. A number of input modules (base stations) can be distributed in the plant, with short-range communication to local sensors/actuators. The input modules (base stations) are connected to the control network via any field bus and communicate with the local wireless devices. A sophisticated input module (base station) ensures that the complexity resides in the input module rather than in the wireless sensors or actuators. One input module can handle up to 120 devices (sensors) or 13 wireless sensor input/output pads. Since in typical applications only sensor and actuator devices are targeted

the capacity of the system is very limited. It is possible to exchange only a few bytes of payload.

WSAN-FA

The WSAN-FA was developed by the PNO and is partly based on the previously introduced WISA system [39]. It also uses the PHY layer of IEEE 802.15.1-2005 and provides a combination of frequency hopping and TDMA as medium access technique. The whole system is specifically designed for the sensors and actuators on the field level. WSAN-FA is able to address up to 120 wireless nodes in the system, targeting applications of real-time class 2. The reliability is achieved by allowing up to four retransmissions on different frequencies. In this case the update time must be decreased. Moreover, a blacklisting of certain channels is provided to minimise interference with other system. However, the capacity of the system is limited due to the same reason as for WISA.

2.3.3 Systems based on IEEE 802.11

In this section the characteristics of some systems based on the IEEE 802.11 (WLAN) and which are used in industrial wireless communications are introduced: Wireless Networks for Industrial Automation - Factory Automation (WIA-FA) and Real-Time (RT)-WiFi. WIA-FA is defined as IEC/PAS 62948 by the IEC and RT-WiFi is a MAC protocol based on IEEE 802.11 PHY that aims to provide real-time data delivery.

In todays IEEE 802.11 systems only DSSS and OFDM based modulation types are relevant. In the DSSS, the data symbols are spread over the full bandwidth of a devices transmitting frequency. The data signal at the sending station is combined with a higher data rate bit sequence, or chipping code, that divides the user data according to a spreading ratio. The chipping code is a redundant bit pattern for each bit that is transmitted, which increases the signals resistance to interference. OFDM is a multi-carrier modulation that splits the radio signal into multiple smaller sub-signals that are then transmitted simultaneously at different frequencies to the receiver. OFDM is used in all recent standard amendment 802.11a/g/n/ac due to the increased robustness especially in environments with many interferers. It can be used with different modulation schemes and Forward Error Correction (FEC) code rates ranging from BPSK with a code rate of 1/2 to 256 Quadrature Amplitude Modulation (QAM) with a code rate of 5/6.

As for the application fields of these systems, it is worth mentioning that they are used in FA (e.g. assembly line production) environments. Their characteristics regarding timeliness and latency make them more suitable than systems based on

the IEEE 802.15.4 for FA applications. More details about this issue in Section 2.1.2.

WIA-FA

WIA-FA is the first wireless technology specification developed specifically for factory, high-speed, automatic, control applications. As WIA-PA, it was developed by the SIA, and currently is defined as IEC/PAS 62948 [54].

Access to the WIA-FA network is through one of the optionally redundant gateway devices, connected to one or several access devices. Multiple access devices may communicate with the field devices in parallel and form multiple, again optionally redundant, star topologies. Each access device forms a star topology with the field devices. These access devices have the same address and are transparent to the field devices.

WIA-FA network protocol defines the PHY, MAC and Application Layer (AL) layers. MAC layer are based on multiple access devices: TDMA, Frequency Division Multiple Access (FDMA), retransmission and aggregation, while the PHY layer is based on the IEEE 802.11-2012 standard [55].

WIA-FA MAC layer is designed to guarantee real-time, reliable and secure communication between WIA-FA field devices and access devices by:

- Adopting a TDMA data-transport mechanism based on the "superframe" concept. Superfames are used to avoid transmission collisions between frames, and ensure reliability and real-time performance of transmission, while supporting frame aggregation/disaggregation, etc.

- MAC layer management functions include defining device joining, leaving, time synchronization, remote attribute get/set, etc. WIA-FA superframe is a collection of timeslots cyclically repeating at a constant rate. Though the length of a timeslot is configurable, each timeslot is only used for transmitting one frame. A WIA-FA superframe timeslot, together with the radio channels, are assigned to a link with each individual device link specified by a timeslot and a channel. The default superframe consists of beacon timeslots used by a field device to join the network, management timeslots, and data timeslots.

Each WIA-FA network has only one Network Manager (NM), which resides in the gateway device where it implements the network management function. The WIA-FA network management performs the following functions:

- Allocating the unique 8-bit or 16-bit short address for all devices in the network.

- Constructing and maintaining the redundant star topology.
- Allocating communication resources for communications of WIA-FA devices.
- Monitoring the status of the WIA-FA network, including device status and channel condition.

RT-WiFi

RT-WiFi is a MAC protocol based on IEEE 802.11 physical layer and aims to provide real-time data delivery for a wide range of wireless control systems from low-speed industrial process control to high-speed mechanical device control [56].

The core of the RT-WiFi protocol is the TDMA based MAC layer. Since there is no centralized channel access controller of a regular WiFi network, it adopts CSMA-CA to avoid collision. This mechanism helps to improve the network throughput but is not feasible for supporting high-speed real-time traffic with stringent timing requirements. Since only one node can access a certain channel in a given time slot, RT-WiFi provides collision free and deterministic communication.

There are three key components in the RT-WiFi MAC protocol to ensure real-time communication: a timer for maintaining global synchronization among all RT-WiFi nodes and triggering timing events; a link scheduler for coordinating the access to shared media, and executing the dedicated event at scheduled time points; and a flexible channel access controller which dynamically configures the hardware parameters for executing the timing event according to the target application behaviour. These components allow to adjust design trade-offs including sampling rate, real-time performance, communication reliability, and compatibility to existing Wi-Fi networks.

Other works about IEEE 802.11 in industrial communications

In addition to the already introduced RT-WiFi and WIA-FA, the use of the IEEE 802.11 standard family in the automation industry, in general, has been a relevant research topic for more than a decade. There is an extensive bibliography about this subject, of which some examples are given next.

Few years after the standardization of the IEEE 802.11, the authors in [57] presented results of bit error measurements taken with an IEEE 802.11-compliant radio modem in an industrial environment and draw some conclusions for the design of MAC protocols. In [58] the authors show the results of some experiments in which wired fieldbus application layers are tested over the IEEE 802.11 PHY layer. [59] addresses the problem of supporting soft-real-time traffic over IEEE 802.11-based WLANs in the presence of competing non-real-time traffic within an

industrial environment, by means of a middleware located between the MAC and the network layers. In [60] an analysis of the RT performance that can be achieved in QoS-enabled 802.11e networks is carried out, particularly oriented to soft-real-time industrial applications. [61] introduces two rate adaptation techniques for IEEE 802.11 devices to combat the Signal to Noise Ratio (SNR) reduction typical in industrial wireless scenarios. Contrary to what has been exposed up to now, the IEEE 802.11ah amendment is analysed as a candidate for PA applications, and not for FA, in [62, 63] (along with other application fields). Finally, in [64, 65] the benefits that the characteristics introduced in the IEEE 802.11n amendment (for both, PHY and MAC layers) might provide are analysed and assessed.

2.4 Cognitive radio

A CR communication system consists on knowing certain information about its environment and actuating depending on it [66]. For example, based on that information, a CR system could conveniently switch between different bands, avoiding occupied bands and taking advantage of other underused bands of the spectrum. Thus, a CR system could even use licensed bands belonging to other services while these bands are not being used. The advances in Software Defined Radio (SDR) promote the opportunity of developing the paradigm of CR. That is because SDR allows to change the communication parameters of a radio system during execution time by software (microprocessors) or dynamic reconfiguration (Field Programmable Gate Array (FPGA) devices).

As for the interaction methods with the medium of the CR there are two possibilities [67]: *overlay* mode and *underlay* mode. *Overlay* consists on the CR system accessing a certain band without interfering with the legitimate users of this band (primary users). *Underlay* mode, on the other hand, consists on transmitting even along with a primary user in its band, as long as the power of the interference caused by the CR system does not exceed a certain threshold.

In order to obtain the information about its medium, a CR system employs *spectrum sensing* techniques. Thanks to the information obtained by *spectrum sensing* the CR system will be able to establish the optimal configuration.

The MAC techniques based on CR are supposed to provide better performance than the conventional ones because they have certain intelligence. Also, in variable environments, such as industrial wireless channels, MAC techniques based on CR are expected to provide higher throughput and robustness due its adaptability.

2.4.1 Physical layer in Cognitive Radio systems

For years, multi-carrier modulations have been considered strong candidates for PHY layers of CR communication systems [68]. The main reason for this, is the flexibility that multi-carrier systems can provide to a CR system. If a multi-carrier CR system knows the state of the spectrum, it can configure the PHY layer so that only sub-carriers corresponding to free spectrum spaces are activated or even conveniently allocate different power levels for each sub-carrier [69, 70]. Figures 2.11 and 2.12 represent this idea, only sub-carriers which do not affect the primary users are employed.

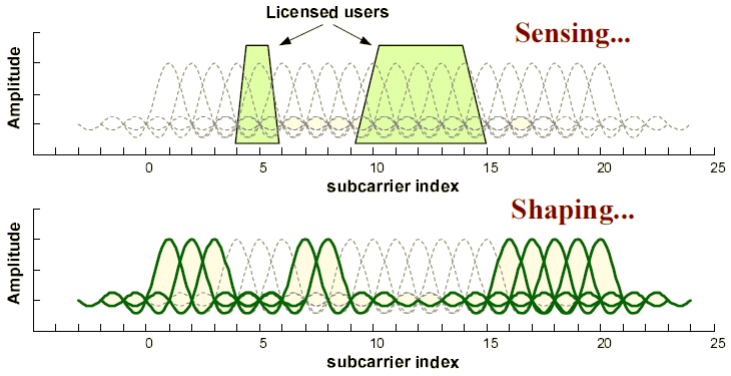

Figure 2.11: Spectrum sensing and spectrum shaping in OFDM systems [71].

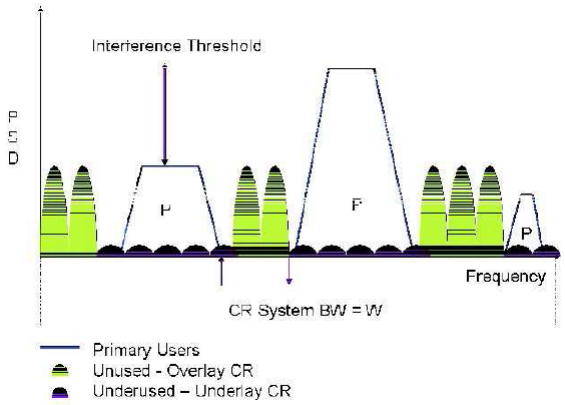

Figure 2.12: Primary users identification [72].

In [71, 72] the authors analyse OFDM as PHY layer for CR systems. The main advantage of OFDM is its adaptability due to the possibility to configure sub-

carriers and other parameters such as modulation order, coding rate and power of each sub-carrier.

However, besides the well known drawbacks of OFDM like its sensitivity to non lineal distortion and to synchronization errors, it presents another principal disadvantage which supposes an additional problem when used in CR systems. The sidelobes generated by the OFDM sub-carriers could interfere with adjacent bands belonging to primary users. This phenomenon is represented in Figures 2.11 and 2.12.

Although nowadays OFDM is the predominant multi-carrier scheme in the industry, a lot of research have been done on FMC schemes in order to overcome the aforementioned OFDM's problems [73,74]. The main features that these FMC schemes provide are waveform flexibility and narrower spectrum of the sub-carriers. For this reason, FMC modulations are promising options for the PHY layer of CR systems.

The PHYDYAS project is an example of the relevance of employing FMC modulation schemes with more restrained spectrum than OFDM in CR systems. PHYDYAS was a European research project within the 7th Framework Programme (FP7) and its main goal was researching on the impact of FMC modulation techniques on CR [75]. The conventional OFDM scheme is a block processing technique, which lacks waveform flexibility and makes an inefficient use of the spectrum. In contrast, a FMC technique offers efficient spectrum usage and can provide independent sub-channels, while maintaining or enhancing the high data rate capability.

More efficient spectrum usage of FMC modulations is accomplished by using longer and spectrally well-shaped prototype filters. Because of that, the sidelobe levels are considerably lower than in the case of OFDM as can be seen in Figure 2.13. Here the spectrums of an OFDM sub-carrier and prototype filter designed by PHYDYAS are compared. In this way, a good spectral containment for all the sub-channels can be obtained and this also results in a good resistance against narrowband interference. In fact, any sub-channel overlaps significantly only with its neighbouring sub-channels. Then, in order to make two multi-carrier signals independent, it is sufficient to leave an empty sub-channel between them, providing better flexibility and SE than OFDM for CR applications.

Among the different options of FMC techniques, in the PHYDYAS project FMC schemes based on the OFDM-Offset Quadrature Amplitude Modulation (OQAM) model were considered, which is the most extended model in the bibliography. In the aforementioned PHYDYAS project FBMC-OQAM is used to denote the filter bank based MCM adopting the model of OFDM-OQAM.

In this thesis we analyse some of these FMC techniques and we evaluate them taking into consideration their suitability for CR systems, besides other criteria

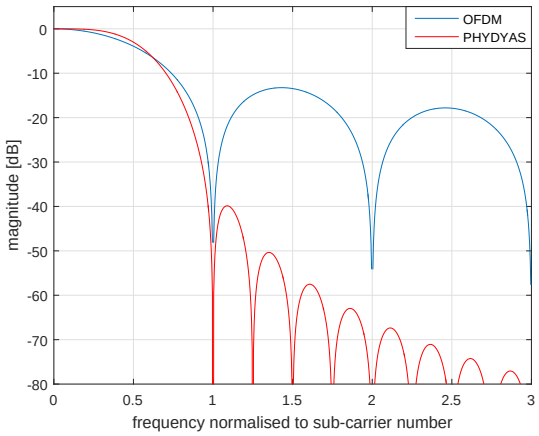

Figure 2.13: Comparison of sub-channel filter magnitude responses in the case of an OFDM sub-carrier and PHYDYAS prototype filter.

too. Some of those FMC systems are introduced in Section 2.5.1 and the most relevant ones for the development of this thesis are analysed more in detail in Chapter 3.

2.5 Filtered Multi-Carrier modulations in industrial communications

Filtered Multi-Carrier (FMC) modulations have been gaining interest for both science and industry. From the point of view of our investigation, we already introduced their potential for CR applications. However, we also have to analyse their suitability for harsh environmental and stringent timeliness and latency conditions. Looking at the bibliography, FMC modulation techniques might be considered upcoming technologies within 5G communications as replacement to the more extended OFDM modulation. [76–79]. 5G is aimed at covering a wide range of application fields. Services and applications such as autonomous vehicle, drone-based delivery, smart home and factory, remote surgery, and artificial intelligence based personal assistant are some examples of the use cases and needs that 5G communications will have to cope with [80]. Among the whole set of services that 5G is meant to cover, requirements in terms of latency, reliability, throughput, scalability and energy-efficiency may differ considerably from one application to another. In accordance with this variety of scenarios and use cases, the International Telecommunication Union (ITU) defined three representative service categories: Enhanced Mobile Broadband (EMBB), Massive Machine-

Type Communication (MMTC) and Ultra-Reliable and Low-Latency Communications (URLLC) [81] (see Figure 2.14).

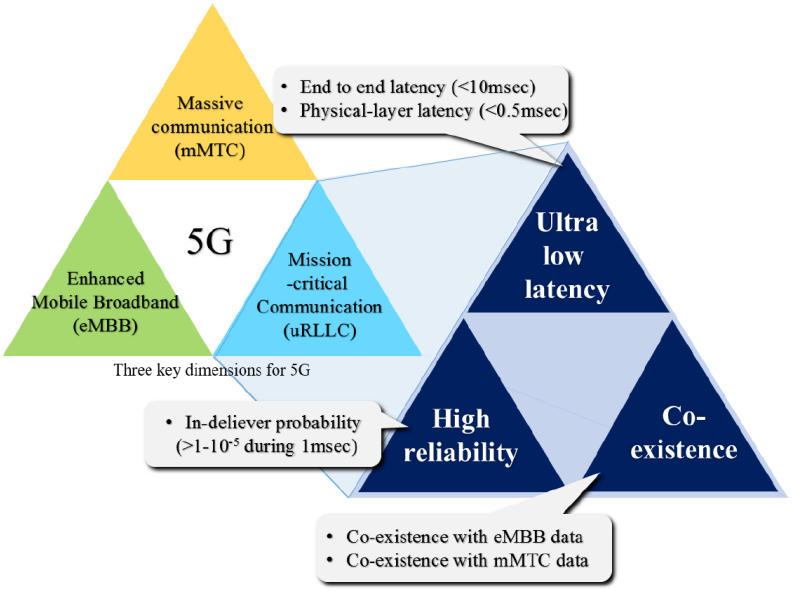

Figure 2.14: 5G service categories [82].

Each one of these categories comprises a set of use cases that share some similarities regarding their requirements. EMBB addresses the human-centric use cases for access to multi-media content, services and data. The EMBB service category is expected to bring new application areas and improve the already existing mobile broadband applications in terms of throughput, performance and user experience. MMTC use cases, on the other hand, are characterized by a very large number of connected devices typically transmitting a relatively low volume of data with no latency restrictions. For this kind of applications, devices are usually required to be low cost and battery efficient. Finally, and more accordingly to the scope of our research, URLLC use cases, also referred to as Critical Machine-Type Communication (CMTC), have stringent requirements regarding characteristics such as reliability, latency and availability. Some examples of URLLC use cases include wireless control of industrial automation processes, remote medical surgery, distribution automation in a smart grid, transportation safety, etc.

Considering the scope of our research, among the aforementioned service categories of 5G, our interest lies on URLLC and CMTC, and specially on wireless communications for FA among the use cases comprised in these service categories (see Figure 2.15). Such applications require very high reliability to minimize the error rate; availability to ensure wireless connectivity and coverage; and very low latency to enable real-time control. In order to achieve these characteristics, al-

though the average volume of data transported to and from devices may not be large, wide instantaneous bandwidths and high throughputs might be useful in order to meet reliability and latency requirements. On the other hand, other, still not mentioned characteristics, such as low device cost and energy consumption, are not as critical as for MMTC applications.

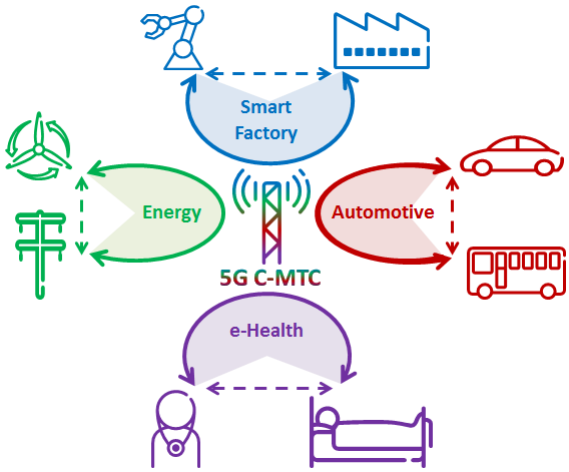

Figure 2.15: 5G CMTC use cases [83].

Enhancements and enablers for EMBB and MMTC are already in the scope of current standardization both in 3rd Generation Partnership Project (3GPP) and Institute of Electrical and Electronics Engineers (IEEE). URLLC on the other hand, is still in the early-standardization phase of 5G New Radio (NR). However, the application of 5G communications to URLLC use cases such as industrial automation has gain great scientific interest from both the academic field and the industry.

2.5.1 Filtered Multi-Carrier modulation candidates for 5G

Considering that the scope of this doctoral thesis focuses on PHY layer modulations for industrial wireless communications and the use of 5G for future URLLC applications such as industrial FA, we analyse the bibliography related to modulation techniques aiming at 5G applications. The main characteristics of the modulation techniques which are considered for 5G applications are the multi-carrier structure and the filtering of their sub-carriers for efficient spectrum usage and waveform flexibility. Although this principles are common for all the 5G candidates, many variations and schemes exist, which provide different properties more or less appropriate depending on the application they are meant for. In this section, we briefly introduce the main and most elemental 5G waveform candi-

dates. In Chapter 3, on the other hand, we give an in-depth analysis of the FMC modulation candidates that we have employed in our research, providing specific results and conclusions.

FBMC

Filter Bank Multi-Carrier (FBMC) waveform consists in a set of parallel data that are transmitted through a bank of modulated filters [84–86]. The prototype filter, parametrized by the overlapping factor K, can be chosen to have very low adjacent channel leakage. One may differentiate between two main variants of FBMC: one based on complex QAM signalling, referred to as Filtered Multi Tone (FMT), and another based on real valued OQAM symbols, referred to as FBMC-OQAM. The latter ensure orthogonality in real domain to maximize spectral efficiency. The first variant FMT is currently employed in standards like Telecommunication Equipment Distribution Service (TEDS), and achieves orthogonality among subcarriers by physically reducing their frequency domain overlapping, thus reducing the SE in a similar proportion as OFDM.

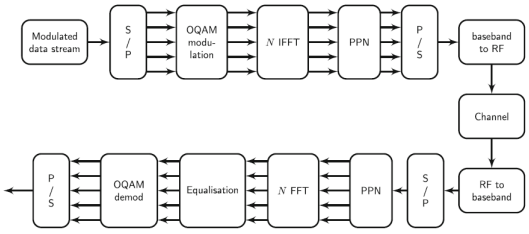

Figure 2.16: FBMC transceiver [87].

FBMC-OQAM, on the contrary, is able to achieve the maximum SE by imposing the orthogonality in the real domain only. Given the SE optimality of FBMC-OQAM, this variant is universally considered as the baseline FBMC modulation [88–92]. Multiple alternative ways of implementing FBMC-OQAM in a computationally efficient manner are existing, although the most important are Polypahse Network (PPN) and Frequency Spreading (FS) implementations. In PPN architecture, OQAM symbols feed an Fast Fourier Transform (FFT) of size $NFFT$ and then into a PPN. The receiver applies matched filtering before a FFT of size $NFFT$ and multi-tap equalization is performed in a per carrier basis. We address the topic of the computationally efficient FBMC-OQAM implementation in Section 3.2.

In Frequency Shift - FBMC (FS-FBMC), OQAM symbols are filtered in frequency domain. The result then feeds an Inverse Fast Fourier Transform (IFFT) of size $K \cdot NFFT$, followed by an overlap and sum operation. At the receiver side,

a sliding window selects $K \cdot NFFT$ points every $NFFT/2$ samples [18]. A FFT of size $K \cdot NFFT$ is applied followed by filtering by the prototype matched filter.

GFDM

GFDM waveform is based on the time-frequency filtering of a data block, which leads to a flexible, non-orthogonal waveform [93–95]. A data block is composed of K carriers and M time slots, and transmits $N = KM$ complex modulated data. In this paper, we consider that the data is cyclic filtered by a Root Raised Cosine (RRC) filter that is translated into both frequency and time domains as it is customarily done. To avoid Inter-Symbol Interference (ISI), a Inter-Carrier Interference (ICI) is added at the end of each block of symbols. To further improve the spectral location, a windowing process can be added in the transmitter.

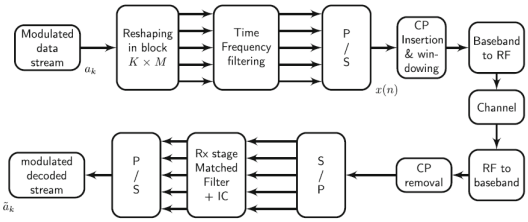

Figure 2.17: GFDM transceiver [87].

Several receiver architectures have been investigated in the literature for GFDM, and we consider in this paper a matched filter receiver scheme: each received block is filtered by the same time and frequency translated filters as in the transmission stage. As the modulation is non-orthogonal, it is necessary to implement an intrinsic interference pre-cancelling scheme, which improves the performance but severely increases the complexity of the receiver. More recently, OQAM was also considered in GFDM to allow the use of less complex linear receivers.

UFMC

Universal Filtered Multi-Carrier (UFMC) waveform is a derivative of OFDM waveform combined with post-filtering, where a group of carriers is filtered by using a frequency domain efficient implementation [96, 97]. This sub-band filtering operation is motivated by the fact that the smallest unit used by the scheduling algorithm in frequency domain in 3GPP Long Term Evolution (LTE) is a resource block, which is a group of 12 carriers. The filtering operation leads to a lower OOB leakage than for OFDM. The UFMC transmitter is composed of B sub-band filtering that modulate the B data blocks. The transmitted signal uses no CP, but there is still a spectral efficiency loss due to the time transient (tails) of the shaping

filter. The Rx stage is composed of a $2NFFT$ point FFT, which is then decimated by a factor 2 to recover the data. A windowing stage can also be inserted before the FFT. It introduces interference between carriers but is interesting to consider for asynchronous uplink transmissions as it helps to separate contiguous users.

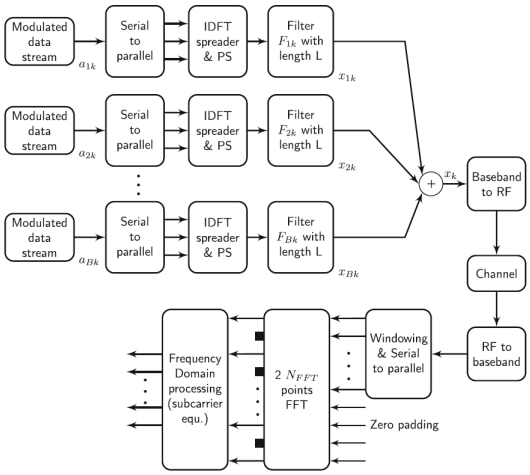

Figure 2.18: UFMC transceiver [87].

2.6 Critical review of the state of the art

In this section we introduce a critical review and a discussion about the state of the art resources we analysed during our research. Thus, we give a summary and the conclusions we obtained from the analysis introduced in this chapter.

As far as industrial automation scenarios concern, in this work we distinguish between two subtypes based on a classification shown in the bibliography: PA and FA. In this sense, according to the scope of our investigation, we must clarify and establish that the environments and industrial applications we focus on correspond to FA scenarios explained in Section 2.1.2, due to their harsh environmental and stringent timeliness and latency conditions. In Section 2.5 we also make reference to another classification shown in the bibliography, which is based on the application fields of 5G. The URLLC or CMTC category of this classification comprises mission-critical, highly reliable and low-latency communication. Hence, as for the connection between FA, URLLC and CMTC, we consider URLLC and CMTC as more general categories which comprise FA scenarios.

Regarding the characterization of industrial environments, as discussed in Section 2.2, differences from one scenario to another might be significant. Besides, there is no standard wireless industrial channel model for the ISM bands. These

facts make it more difficult to carry out a rigorous wireless industrial channel characterization. From the channel models we analysed in Section 2.2, we chose the TGn channel models for our simulations, because it fits the ISM bands our research focuses on. On the other hand, WINNER presents channel models with several scenarios and a wide range of modelling options. However, considering the features we employ from these channel models, WINNER does not provide any significant advantage over TGn, while this one results a simpler, more extended and computationally more efficient option. As aforementioned, there is no specifically industrial wireless channel model, and TGn is not so either. However, we employ the most frequency dispersive models of TGn in our simulations, in order to emulate low-band transmissions (below 6 GHz and a bandwidth of several MHz) in large indoor spaces with strong multipath effect.

In Section 2.3 we analyse the current state of the art solutions for wireless industrial communications. As aforementioned, PA applications do not carry a major challenge in terms of latency and timeliness and state of the art solutions. For instance, schemes based on the IEEE 802.15.4 (ZigBee), can already address them. On the contrary, current state of the art solutions are not capable of addressing the stringent real-time requirements of FA applications along with the harsh environmental conditions of such scenarios. As discussed in Sections 2.1.2, 2.3.2 and 2.3.3, some applications in FA are addressed by current state of the art solutions based on IEEE 802.15.1(Bluetooth) or IEEE 802.11 (WiFi). However, the most critical applications like the closed-loop controls cannot be addressed by these technologies. A lot of research has been carried out on the enhancement of these techniques, but still there is no wireless communication solution for the most challenging FA applications. Therefore, new techniques and technologies must be proposed in order to definitely address the wireless communications issue in FA scenarios.

Among the upcoming technologies, FMC modulations and CR might be promising solutions for wireless industrial communications in FA. As aforementioned, CR might be specially useful considering that industrial wireless communications are meant to work in the unlicensed and highly occupied ISM bands. We already discussed the compatibility of FMC modulations and CR, which is an important factor to consider in our research. Moreover, the robustness of these FMC modulation schemes against highly frequency selective industrial wireless channels must be taken into consideration in order to decide if these are suitable solutions. In this sense, considering that these FMC schemes are modulation candidates for 5G, which comprises URLLC and CMTC scenarios as discussed before, bibliography suggests that they might be suitable options as PHY layer modulations for wireless communications in FA. It is worth mentioning that we carry out an in depth analysis of some FMC modulations and we evaluate their suitability for highly

dispersive channels in Chapter 3.

Chapter 3

Evaluation of WCP-COQAM, GFDM-OQAM and FBMC-OQAM for Industrial Wireless Communications with Cognitive Radio

MCM schemes are widely adopted in wireless communication systems, being OFDM the most extended one among them. Despite the features and benefits that OFDM offers in wireless communications, it also presents significant drawbacks such as high OOB radiation. Considering this fact and the upcoming applications and needs in wireless communications, a lot of research, specially on new waveforms for the PHY communication layer of 5G, has been carried out in order to overcome OFDM's limitations [98–100]. As a result, several pulse-shaping techniques exist which allow sub-carrier filtering in MCM systems in order to get better frequency localization. We refer to these filtered MCM systems as Filtered Multi-Carrier (FMC) modulations. These techniques provide good frequency localization and reduce the OOB radiation. The most extended FMC schemes in the bibliography are FBMC-OQAM and GFDM.

In Section 2.5 we discuss, based on the bibliography, the possibilities that 5G might provide to URLLC applications such as wireless communications in FA. Moreover, in Section 2.4 we discuss, based on the bibliography too, the compatibility between CR and 5G FMC modulation candidates. Considering the conclusions we obtain (see Section 2.6), in this chapter we evaluate the possible suitability for wireless industrial communications of some of the 5G FMC modulation candidates. Specifically, in this chapter we analyse FBMC-OQAM, GFDM-OQAM and also

WCP-COQAM modulation systems. Although WCP-COQAM [101–106] is not as extended as the other two schemes in the bibliography, it shares several similarities and properties with both, FBMC-OQAM and GFDM-OQAM, which make it an interesting FMC scheme to be analysed. Besides analysing WCP-COQAM, we provide some additional details with respect to the bibliography about its orthogonality against multipath channels and SE.

Among the industrial environment characteristics discussed in Section 2.2, in this chapter we focus on severe multipath effect, so that we evaluate the performance of the aforementioned FMC systems in terms of BER, Power Spectral Density (PSD) and SE under highly dispersive channels. We compare these results with OFDM and we use the SE to represent the cost of using CP extensions, sub-carrier filtering and windowing schemes in the analysed FMC systems. Based on those analysis and results, we aim at providing a notion about the suitability of these FMC modulation schemes for industrial wireless communications based on CR.

From the analysis and the assessment of the aforementioned FMC systems we provide the following contributions:

1. This chapter complements the work in [101–103], by bringing additional details about how windowing affects the protection against multipath channels and the SE in WCP-COQAM. We state the conditions to provide full orthogonality in multipath channels and we show how windowing reduces SE in WCP-COQAM compared to GFDM-OQAM. We explain all these details in Section 3.1.3, 3.1.4 and 3.3, while in Section 3.4.3 we give an example with some specific results and we discuss them.

2. While most research about the aforementioned FMC modulations is focused on Mobile Broadband (MBB) communications, here we simulate and assess some of these modulation schemes under different conditions. We simulate low-band transmissions through large indoor spaces and severe multipath channels in order to model some of the industrial wireless characteristics. Under these conditions and by means of BER, PSD and SE analysis, we evaluate the suitability of the aforementioned FMC systems for wireless industrial communications based on CR.

The chapter is organised as follows: in Section 3.1 we explain the theoretical background of the FMC systems we are going to analyse; in Section 3.2 we introduce an efficient implementation scheme for the analysed FMC systems; in Section 3.3 we give more detailed explanations about WCP-COQAM and make some clarifications with respect to the bibliography; in Section 3.4 we present the results obtained from our simulations, based on which we compare and discuss the per-

formance of the considered FMC systems; in Section 3.5 we state the conclusions we obtained from our research.

3.1 Filtered Multi-Carrier modulations

The FMC systems we analyse are based on OQAM instead of classical IQ modulations (e.g., N-PSK, N-QAM). The reason why we focus on OQAM based schemes is that FMC systems cannot simultaneously keep good Time-Frequency Localization (TFL), Nyquist symbol rate and orthogonality between transmitted symbols if conventional IQ modulations are used, as it is stated by the Balian-Low Theorem (BLT) [107]. According to BLT, ISI and ICI introduced by the prototype filters of these FMC systems make it impossible to achieve perfect reconstruction of complex valued symbols transmitted at Nyquist rate. Consequently, in case matched filter receivers are used, FBMC and GFDM perform worse than OFDM in terms of BER. One solution to overcome the constraints defined by the BLT is to send alternately real and imaginary valued symbols at twice the Nyquist rate instead of complex symbols. This technique is known as OQAM. This strategy allows the filtered data symbols to remain orthogonal and keep both good TFL and Nyquist symbol rate, all at the same time.

Hence, we first introduce the OQAM technique and next we explain the rest of the FMC schemes.

3.1.1 OQAM

OQAM consists, basically, in splitting one complex symbol into two semi-symbols, one real and one imaginary. After this operation, the whole OQAM symbol's duration remains equal to the duration of the original complex symbol, while the duration of each semi-symbol is half the whole symbol, as shown in Figure 3.1. This symbol structure implies an oversampling by two with respect to the original sampling rate of the complex symbol. It is worth mentioning that this oversampling does not carry any change in the total bandwidth of the transmitted signal when OQAM is used in MCM systems. As we explain in Section 3.1.2, when the multi-carrier OQAM signal is serialized its symbol rate is the same as it would be in a conventional IQ modulation.

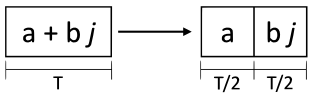

Figure 3.1: Complex to pure real and imaginary operation.

The OQAM scheme discussed up to now can reduce ISI caused by pulse shaping processes. Since imaginary and real semi-symbols are transmitted alternately, interference coming from adjacent semi-symbols can be ignored in the receiver (i.e., interference caused by a real semi-symbol to its adjacent imaginary semi-symbol can be ignored, as well as interference caused by a imaginary semi-symbol to its adjacent real semi-symbol can be ignored).

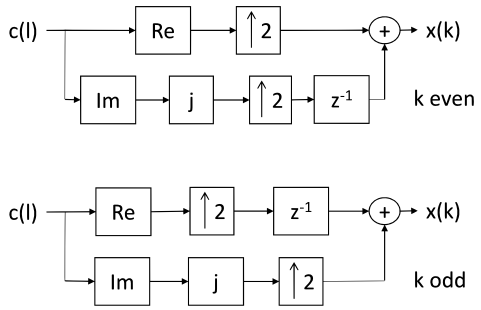

Figure 3.2: Block diagram of the OQAM symbols arrangement in a multi-carrier system.

Similarly in frequency domain, pulse shaping makes adjacent sub-carriers overlap with each other, thus causing severe ICI. If those sub-carriers are organised so that real and imaginary ones are alternated one next to the other, ICI from adjacent sub-carriers will be avoided because interference coming from them can be ignored in the receiver. Figure 3.2 shows the block diagram of a OQAM MCM system. Figure 3.3, on the other hand, shows the demodulation process to recover the original complex data symbols.

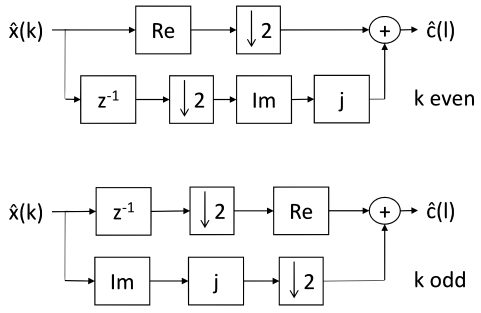

Figure 3.3: Block diagram of the OQAM demodulation process in a multi-carrier system.

More details about OQAM can be found in [91].

3.1.2 FBMC-OQAM

FBMC consists in filtering each sub-channel in order to get well localized sub-carriers. Figure 3.4 shows the basic representation of a FBMC-OQAM trans-multiplexer. The main blocks are the OQAM pre-processing or modulator block, the synthesis filter bank, the analysis filter bank and OQAM post-processing or demodulator.

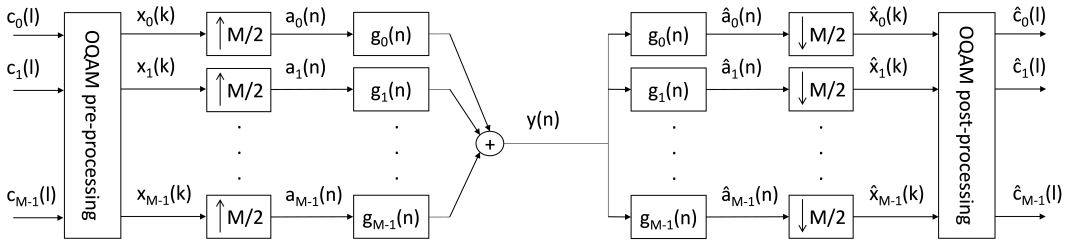

Figure 3.4: Basic representation of a FBMC-OQAM transmultiplexer.

The key components of the FBMC-OQAM scheme are the Synthesis Filter Bank (SFB) and the Analysis Filter Bank (AFB), which are formed by one filter per sub-channel. We call SFB to the filter bank in the transmitter and AFB to the filter bank in the receiver. These filter banks are the set of filters defined as

$$g_m(n) = p(n) exp\left(j\frac{2\pi mn}{M}\right) , \tag{3.1}$$

where m is the sub-channel index; $p(n)$ is the prototype filter of length L_p and $n = 0, ..., L_p - 1$. The exponential factor corresponds to the mth sub-carrier, where M is the total number of sub-carriers.

Note that the FBMC-OQAM scheme works as a multi-rate system. Before filtering the $x_m(k)$ OQAM data symbols they are up-sampled by $M/2$ using a zero padding process to get the oversampled signal $a_m(n)$.

$$a_m(n) = \sum_{k\in\mathbb{Z}} x_m(k)\delta(n - kM/2) , \quad n \in \mathbb{Z} . \tag{3.2}$$

The reason why the up-sampling factor is $M/2$ and not M is that OQAM pre-processing already introduces an up-sampling factor of 2. Thus, the FBMC-OQAM signal can be expressed as

$$y(n) = \sum_{m=0}^{M-1} \sum_{l\in\mathbb{Z}} a_m(l) g_m(n - l) , \quad n \in \mathbb{Z} . \tag{3.3}$$

At the receiver side, the FBMC-OQAM signal $y(n)$ is demodulated so that, in first place, each sub-channel is filtered in order to get only its corresponding signal.

$$\hat{a}_m(n) = \sum_{l\in\mathbb{Z}} y(l)g_m(n-l) \ , \quad n \in \mathbb{Z} \ , \tag{3.4}$$

where $m = 0, ..., M-1$.

Then, $\hat{a}_m(n)$ is sampled in the time domain, so that the estimation of the original OQAM signal $x_m(k)$ is obtained.

$$\hat{x}_m(k) = \hat{a}_m(kM/2) \ , \quad k \in \mathbb{Z} \ . \tag{3.5}$$

If a non-ideal transmission channel is assumed, a LR-FDE must be performed at this point. That is,

$$\hat{x}_m^{eq}(k) = \frac{\hat{x}_m(k)}{H_{m,k}} \ , \tag{3.6}$$

where $H_{m,k}$ represents the channel frequency response at the m sub-carrier and k sub-symbol. We refer as LR-FDE to the Frequency Domain Equalization (FDE) performed for each sub-symbol k with a single frequency point per sub-carrier, as it is done in OFDM.

It must be borne in mind that, since no CP is employed, this kind of equalization might present error floors caused by the ICI and ISI introduced by the channel. In order to avoid this problem the number of sub-carriers must be sufficiently high to be narrower than channel's coherent bandwidth.

3.1.3 GFDM-OQAM

In [101,102] the idea of GFDM-OQAM is introduced, although the authors refer to this scheme as Filter Bank Multi-Carrier - Circular Offset Quadrature Amplitude Modulation (FBMC-COQAM) or just as Circular Offset Quadrature Amplitude Modulation (COQAM). As shown in Figure 3.5, the structure of a GFDM-OQAM transmultiplexer is similar to the structure of a FBMC-OQAM transmultiplexer. GFDM-OQAM is also based on OQAM modulation and sub-channel filtering. The difference is that in GFDM-OQAM filtering is performed by a circular convolution instead of the linear convolution used in FBMC-OQAM. This way, the modulation system now adopts a block based signal structure, so that a CP can be added to provide orthogonality against multipath channels without affecting signals TFL.

We consider a GFDM-OQAM system with M sub-channels and K complex valued data symbols in each block (i.e. $2K$ OQAM symbols in each block). Thus, if we consider $y(n)$ as one GFDM-OQAM block, it can be expressed as

$$y(n) = \sum_{m=0}^{M-1} \sum_{l=0}^{MK-1} a_m(l)\tilde{g}_m(n-l+MK-1) \ , \tag{3.7}$$

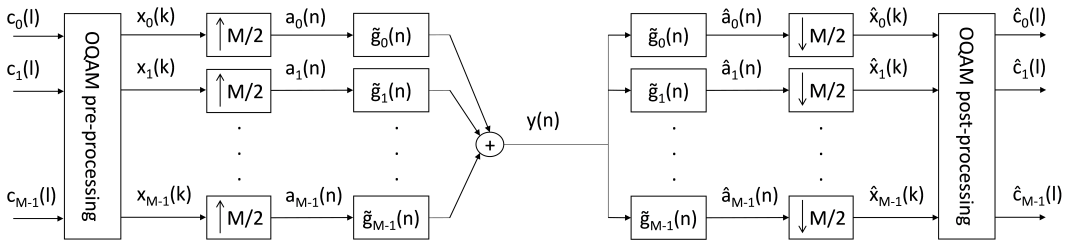

Figure 3.5: Basic representation of a GFDM-OQAM transmultiplexer.

where $n = 0, ..., MK - 1$ and $\tilde{g}_m$ filters are obtained by the periodic repetition of g_m filters defined in Eq. (3.1). So that

$$\tilde{g}_m(k) = g_m[mod(k, MK)] \ . \tag{3.8}$$

At the receiver side, if a non-ideal transmission channel is assumed, the GFDM-OQAM block $y(n)$ is equalised so that,

$$y_{eq} = idft\left[\frac{dft(y, MK)}{H^{HR}}\right] \ . \tag{3.9}$$

H^{HR} denotes the MK points High Resolution (HR) channel frequency response. This equalization is different from the one used in FBMC-OQAM or in OFDM. On the one hand, it is applied over a whole block with a channel frequency response of MK points, instead of over each sub-symbol and M points; on the other hand, it is performed prior to the inherent Discrete Fourier Transform (DFT) operation of the demodulation process. We refer to this kind of equalization as HR-FDE.

Once the GFDM-OQAM block is equalised, each sub-channel is filtered in order to get only its corresponding signal. Once again, the difference between FBMC-OQAM and GFDM-OQAM receivers consists on the circular convolution.

$$\hat{a}_m(n) = \sum_{l=0}^{MK-1} y_{eq}(l)\tilde{g}_m(n - l + MK - 1) \ , \tag{3.10}$$

where $m = 0, ..., M - 1$.

Then, $\hat{a}_m(n)$ is sampled in the time domain, so that the estimation of the original OQAM signal $\hat{x}_m(k)$ is obtained, just as it is shown in Eq. (3.5).

3.1.4 WCP-COQAM

WCP-COQAM is introduced in [103]. This technique can be considered as a GFDM-OQAM system with a windowing process, which improves the PSD with respect to GFDM-OQAM.

In WCP-COQAM both the CP and the windowing are related. The CP is divided in two parts: the GI and the Window Interval (WI) (referred as RI in [103]). So that the total length of the CP will be equal to the sum of the lengths of the GI and WI parts:

$$L_{CP} = L_{GI} + L_{WI} \ , \tag{3.11}$$

where GI is the part of the CP aimed at preventing against multipath channels and WI is the part which will be used for windowing.

Let us consider a GFDM-OQAM signal $s_{_G}$ [1] as a queue of several GFDM-OQAM blocks, each with its CP extension of length L_{CP}. Equally, we will consider M to be the total number of sub-carriers and K the number of symbols in each block. Then the lth block of a WCP-COQAM signal is defined as

$$s_{_W}(k) = \sum_{r=l-1}^{l+1} s_{_G}(k + rL_{WI}) w(k - rQ) \ , \tag{3.12}$$

where $k = 0, ..., MK + L_{CP} - 1$; $Q = MK + L_{GI}$ and the window function $w(k)$ is defined by

$$w(k) = \begin{cases} \text{window coeff.}, & k = 0, , L_{WI} - 1 \\ 1, & k = L_{WI}, , MK + L_{GI} - 1 \\ \text{window coeff.}, & k = Q, , MK + L_{CP} - 1 \\ 0, & \text{otherwise} \ . \end{cases} \tag{3.13}$$

In our work we use a Hamming window for the window coefficients. Figure 3.6 shows the block diagram that represents this whole process.

It must be noted from Eq. (3.12) and (3.13) that the samples of the CP corresponding to the WI part and also the last L_{WI} samples of the block are multiplied by the window coefficients and they are overlapped with the WI regions of the previous and next blocks, respectively. By overlapping the WI regions, these extra samples are prevented from reducing SE, as shown in Figure 3.7.

The receiver structure is depicted in Figure 3.8. It is worth noticing that, Figure 3.8 only shows the recovery process of one GFDM-OQAM block from a received WCP-COQAM signal. Once the GFDM-OQAM signal is recovered, the demodulation process is equal to GFDM-OQAM.

For this scheme, perfect synchronization and an ideal channel are assumed. So, in the first place, the first $MK + L_{GI}$ samples of one WCP-COQAM block are

[1] For the sake of readability, from this point on parameters corresponding to OFDM will be expressed with the sub-index O, parameters corresponding to GFDM-OQAM will be expressed with the sub-index G and parameters corresponding to WCP-COQAM will be expressed with the sub-index W.

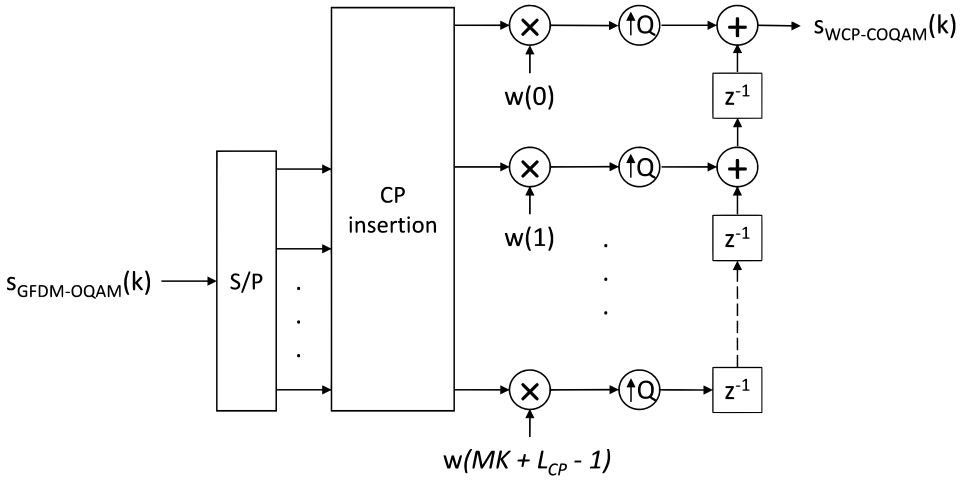

Figure 3.6: Block diagram of the cyclic prefix insertion and windowing operation for WCP-COQAM [103].

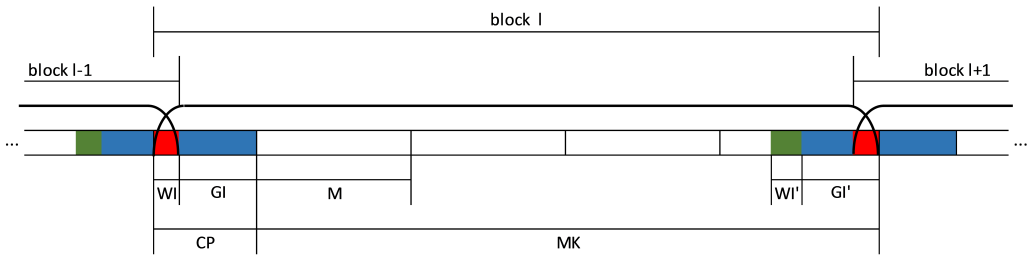

Figure 3.7: Overlapping of adjacent WCP-COQAM blocks.

taken. Next, the first L_{GI} (which correspond to the CP extension) samples are removed, while the last L_{WI} samples are left to process them within the next block. Finally, in order to get all the samples back to their original positions within the original GFDM-OQAM block, a cyclic shift is carried out, which can be expressed as

$$s'_{_G}(k) = s[mod(k + L_{WI}, MK)] \,, \tag{3.14}$$

where $k = 0, , MK - 1$; $s'_{_G}(k)$ is the estimation of the original $s_{_G}(k)$ signal and $s(k)$ is the signal after the removal of the windowing effect and the CP.

From this point on, the process continues the same as in GFDM-OQAM. At the receiver side, if a non-ideal transmission channel is assumed, the estimated GFDM-OQAM block $s'_{_G}(k)$ is equalised as in Equation (3.9).

Then, each sub-channel is filtered in order to get only its corresponding signal, like in Equation (3.10). Finally, $\hat{a}_m(n)$ is sampled in the time domain, so that the estimation of the original OQAM signal $\hat{x}_m(k)$ is obtained, just as it is shown in Equation (3.5).

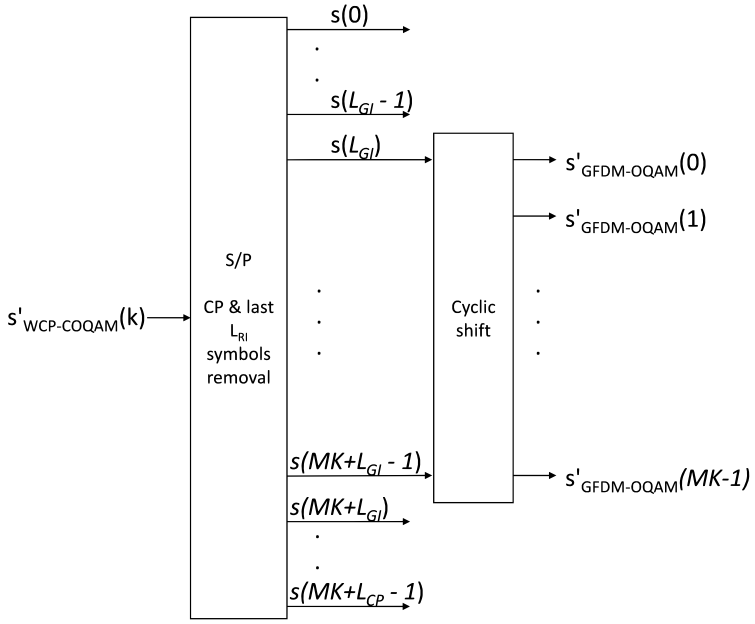

Figure 3.8: Block diagram of one GFDM-OQAM block recovery process from a WCP-COQAM block [103].

3.2 Efficient implementation of FMC systems based on polyphase filters

In the previous section we explained the fundamentals of the analysed FMC systems from a theoretical point of view, giving the basic idea behind these modulation schemes and their corresponding analytical expressions. However, the fundamental and direct filtering and modulation schemes shown in Figures 3.4 and 3.5 are not computationally efficient structures for practical implementations. Filtering operations are performed at the high sampling rate, after the zero padding operations, leading to a high number of unnecessary calculations. Therefore, for practical FMC implementations different filter bank structures are used. In our simulations we employ the so-called polyphase filter bank structures. These polyphase structures consist of a filter bank section where the prototype filter and its coefficients are divided into several sub-filters, and a transform section implementing the modulation. Their main advantage is that they offer significant simplification because filtering operations are done at the lower sampling rate and no unnecessary calculations are performed. In this section, polyphase structures for SFBs and AFBs and their application in the analysed FMC systems are introduced.

3.2.1 Polyphase structure of synthesis and analysis filter banks

Figure 3.9 shows the graphical representation of a FBMC-OQAM transmitter based on a polyphase structure. The key point of this implementation scheme and the main difference with respect to the scheme shown in the previous section is the SFB. While the filter bank defined in Equation (3.1) consists on repeating the whole prototype filter and modulating it over every sub-carrier, in a polyphase filter bank the coefficients of the prototype filter are distributed among all the sub-filters $g_m(k)$ and the modulation is previously performed by the IFFT. Thus, the sub-filters are defined as

$$\begin{aligned} g_m(k) &= p\left(m + k\frac{M}{2}\right) && k \text{ even} \\ g_m(k) &= 0 && k \text{ odd}\ , \end{aligned} \tag{3.15}$$

where m is the sub-channel index, M is the total number of sub-carriers, p is the prototype filter of length L_p and $k = 0, ..., \frac{2L_p}{M} - 1$.

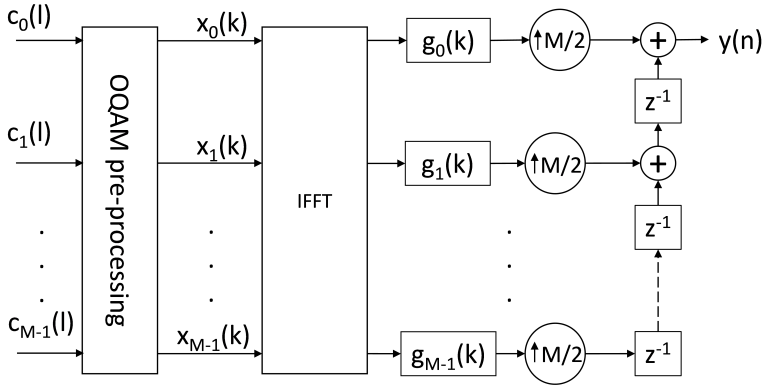

Figure 3.9: PHYDYAS polyphase structure of the synthesis filter bank.

It is worth noting that the model shown in Figure 3.9 and the transmitter shown in Figure 3.4 and defined in Equation (3.3) are equivalents, as far as their response concerns. In fact, here we use the same nomenclature in order to represent and make visible that for certain $c_m(l)$ input data symbols we get the same $y(n)$ output for both transmitter models, regardless of the employed SFB structure.

As for the receiver, Figure 3.10 shows the graphical representation of a FBMC-OQAM receiver based on a polyphase structure. As it happens with the transmitter side, at the receiver the key point and the main difference with respect to the basic model explained in the previous section consists on the filter bank too. We refer to the filter bank of the receiver as AFB. The $g_m(k)$ sub-filters of the

AFB are defined as in Equation (3.15) and the demodulation is performed by the FFT.

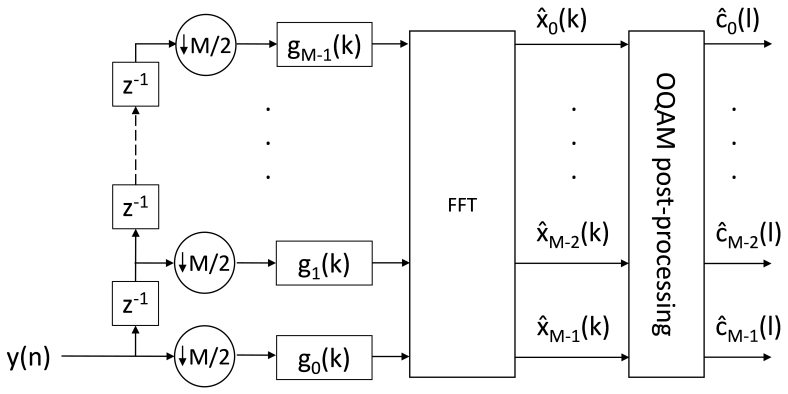

Figure 3.10: PHYDYAS polyphase structure of the analysis filter bank.

The receiver model shown in Figure 3.10 and the one shown in Figure 3.4 and defined in Equations (3.4) and (3.5) are equivalents, as far as their response concerns. Again, here we use the same nomenclature in order to represent and make visible that for certain $y(n)$ FBMC-OQAM received signal we get the same $\hat{x}_m(k)$ estimated OQAM symbols (and therefore, the same $\hat{c}_m(k)$ complex data symbols too) for both receiver models, regardless of the employed AFB structure.

The filter bank structures shown until now correspond to a FBMC-OQAM transmultiplexer and they are based on the schemes provided by the PHYDYAS project [91].

3.2.2 Polyphase filter banks for GFDM-OQAM and WCP-COQAM

A transmultiplexer formed by the polyphase filter banks introduced in the previous section corresponds to a FBMC-OQAM system and this structure is not directly applicable to a GFDM-OQAM or WCP-COQAM system. As explained in Section 3.1.3, the key points and the main differences of GFDM-OQAM and WCP-COQAM with respect to FBMC-OQAM are the circular filtering and the block-wise signal structure. In this section we explain how to use the polyphase filter bank structures introduced above to implement efficient GFDM-OQAM and WCP-COQAM transmultiplexers.

In order to implement a GFDM-OQAM or WCP-COQAM transmultiplexer based on polyphase structure, on the one hand, we need to adapt the scheme introduced in the previous section to a circular filtering operation, which can be

carried out without modifying the SFB nor the AFB. On the other hand, a block-wise signal structure must be adopted instead of the continuous signal structure of FBMC-OQAM expressed in Equation (3.3). In our simulations of GFDM-OQAM and WCP-COQAM we take advantage of the polyphase SFB and AFB introduced in Section 3.2.1. In order to adapt them to the circular filtering we perform a tail-biting operation at the output of the polyphase filter banks. Performing a tail-biting operation over the output of a linear convolution is the equivalent of performing a circular convolution.

Next, we explain how the polyphase structure FBMC-OQAM transmultiplexer introduced above, is transformed to a GFDM-OQAM transmultiplexer based on polyphase filter bank structure. Note that, as explained in Section 3.1.4, the only difference between GFDM-OQAM and WCP-COQAM is their CP extension and the windowing; and that they share the same SFB and AFB, regardless of whether they present a polyphase structure or not. Hence, the adaptations of the polyphase filter banks introduced below, are valid for both, GFDM-OQAM and WCP-COQAM.

In the first place, we assume a block-wise transmission. So we define Equation (3.16), which represents the FBMC-OQAM transmission of a complex data symbol block of length K,

$$y(n) = \sum_{m=0}^{M-1} \sum_{l=0}^{MK-1} a_m(l) g_m(n-l) \ , \tag{3.16}$$

where $n = 0, ..., 2MK-1$ and $g_m(n)$ is the filer bank defined in Equation (3.1). Since the analytical expression of Equation (3.16) and the polyphase SFB represented in Figure 3.9 are equivalent, we can consider the $y(n)$ signal as the output of the SFB, assuming a complex data symbol block of length K as the input.

Once the equivalent FBMC-OQAM signal $y(n)$ is obtained, tail-biting operation is performed at the output of the SFB as expressed in Equation (3.17), in order to apply the effect of circular filtering of GFDM-OQAM.

$$y'(l) = y(l) + y(l + MK) \ , \quad l = 0, ..., MK-1 \ . \tag{3.17}$$

Thus, we get the signal $y'(l)$ of length MK which is equivalent to the GFDM-OQAM block defined in Figure 3.5 and Equation (3.7).

For a WCP-COQAM transmitter based on a polyphase structure, the first step is getting the $y'(l)$ signal, just as for GFDM-OQAM. Hence, the SFB stage is equal for both FMC systems. Once the $y'(l)$ GFDM-OQAM signal is obtained, the process to construct the WCP-COQAM signal is the same as described in Section 3.1.4.

At the receiver side, the tail-biting operation must be applied to the signal $\hat{x}_m(k)$ at the output of the AFB. Assuming a GFDM-OQAM block $y'(l)$ defined

in Equation (3.17) as the input of the AFB, after the downsampling, filtering and FFT operations, we get an estimated OQAM block $\hat{x}_m(k)$ of length $4K-1$. At this point, tail-biting operation is performed at the output of the AFB as expressed in Equation (3.18), in order to apply the effect of circular filtering of GFDM-OQAM.

$$\hat{x}'_m(l) = \hat{x}_m(l) + \hat{x}_m(l+2K) \ , \quad l = 0, ..., 2K-1 \ . \tag{3.18}$$

Thus, we get the signal $\hat{x}'_m(l)$ of length $2K$ which is equivalent to the estimated OQAM block $\hat{x}_m(k)$ shown in Figure 3.5.

For a WCP-COQAM receiver based on a polyphase structure, the first step is getting the equivalent GFDM-OQAM block $y'(l)$. The process to obtain the corresponding GFDM-OQAM block from the received WCP-COQAM signal is the same as described in Section 3.1.4. Once the equivalent GFDM-OQAM block $y'(l)$ is obtained, the SFB stage is equal for both FMC systems.

3.3 Orthogonality condition and spectral efficiency analysis of WCP-COQAM

Several analysis on FMC modulation schemes are available in the bibliography, some of them even including WCP-COQAM modulation scheme [101–106]. However, for the best our knowledge, none of them addresses the implications of windowing in the WCP-COQAM waveform as we do here.

In this section, we contribute with some additional details regarding how windowing affects on the orthogonality against multipath channels and the SE in WCP-COQAM. Specifically, we state the condition that the GI region of the CP extension must fulfil in order to provide full orthogonality in the presence of multipath channels. Besides, we also compare WCP-COQAM and GFDM-OQAM (due to the similarities between both FMC systems) in terms of SE and we show that, in this aspect, the former is outperformed by the latter if equal multipath protection is assumed.

3.3.1 Orthogonality condition

In WCP-COQAM multipath channel protection is directly related to the CP extension and also to the windowing process. In order to explain this fact, we show in detail the steps to form a WCP-COQAM block starting from a basic GFDM-OQAM block (as seen in Section 3.1.3).

Once a GFDM-OQAM block is formed the CP extension is added to it. Figure 3.11.a shows the details of this first stage in the construction of WCP-COQAM signal, where M is the total number of sub-carriers; K is the number of symbols

per block; WI is the region of length L_{WI} devoted to windowing and overlapping; GI is the region of length L_{GI} that protects against multipath channel effect; and the CP extension has a total length of $L_{CP} = L_{WI} + L_{GI}$. CP', WI' and GI' are those last samples of the block which are copied in order to form the CP extension. As it is represented in Figure 3.11.a, before the windowing is applied, this signal can be considered as a GFDM-OQAM block with CP extension.

Figure 3.11.b represents the WCP-COQAM block right after windowing is applied. As shown in Figure 3.7 and Eq. (3.12) and (3.13), the window function is applied on the first and the last L_{WI} samples, so that these samples are somehow distorted. Because of that, CP, WI and GI are no longer equal to CP', WI' and GI' respectively.

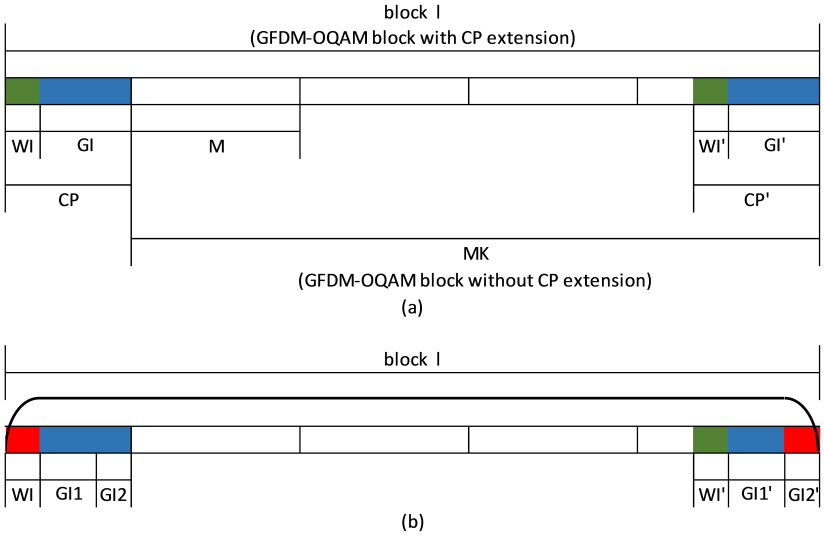

Figure 3.11: Windowing operation of a WCP-COQAM block. a) A WCP-COQAM block before windowing is equal to a GFDM-OQAM block with CP extension. b) The first and the last L_{WI} samples of a WCP-COQAM block are distorted by the window.

Since the last L_{WI} samples are affected by the window, we define a new region for them which we call GI2'. Thus, now the original GI and GI' regions are divided in GI1, GI2 and GI1', GI2' respectively, so that WI $\neq$ WI', GI1 = GI1', GI2 $\neq$ GI2'. As for the length of these regions $L_{WI} = L_{WI'} = L_{GI2} = L_{GI2'}, L_{GI1} = L_{GI1'}$. Note that GI1 and GI1' are now the only really redundant parts. Because of that, only GI1 and not the whole GI (as it is explained in [103]) acts as a real guard interval against multipath channels when FDE is performed. Hence, $L_{GI1} \geq L_{CH} - 1$ must be fulfilled in order to maintain full orthogonality through a multipath channel, where L_{CH} is the transmission channel length. Thus, considering that $L_{GI2} = L_{WI}$

and so $L_{GI1} = L_{GI} - L_{GI2} = L_{GI} - L_{WI}$, we can define the full orthogonality condition for WCP-COQAM as

$$L_{GI} \geq L_{CH} - 1 + L_{WI} \, . \tag{3.19}$$

It is worth mentioning that the FDE should be performed for samples between GI2 and GI1', inclusive, because that is the section corresponding to the cyclic convolution between GI1 and GI1' with the transmission channel.

3.3.2 Spectral efficiency analysis

Figure 3.12 shows how overlapping between adjacent blocks is performed in WCP-COQAM. Every windowed region is overlapped with the next or the previous block, so that the WI region of each block is overlapped with the GI2' region of the previous block. Thus, the samples within WI regions do not suppose an overload and they do not affect the SE. Based on this fact, in [103] the authors claim that the use of the window function has no effect on SE. While it is true that the samples in WI have no effect on SE, claiming that the windowing does not affect the SE is not precise, at least if the orthogonality condition defined in Eq. (3.19) is to be fulfilled. Note that the use of the window function and overlapping of WI and GI2' regions distort those samples in GI2' region. This and the fact that FDE is performed between GI2 and GI1', inclusive, implies that the GI2 region is necessary in order to recover those samples originally placed in the GI2' region. At this point, we conclude that both GI1 and GI2 are essential parts within the GI region of WCP-COQAM.

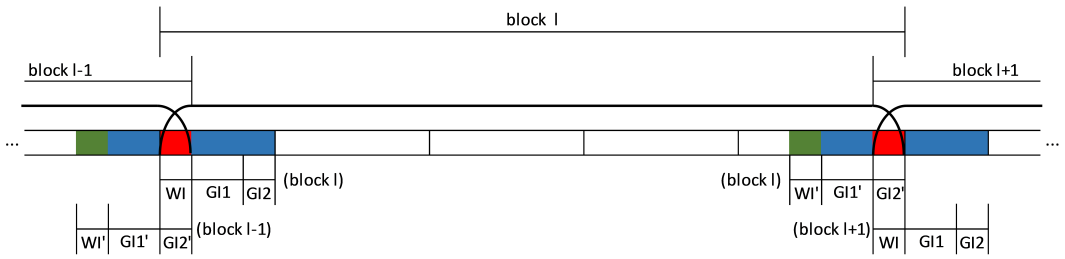

Figure 3.12: Overlapping between adjacent WCP-COQAM blocks and CP extensions structure.

In order to make a fair analysis of SE in WCP-COQAM we compare it to GFDM-OQAM, because both modulation schemes only differ in windowing and overlapping processes. In order to maintain a homogeneous notation between

GFDM-OQAM and WCP-COQAM, we assume the following considerations:

$$\begin{aligned} CP_G &= GI_G = GI1_G \\ \\ CP_W &= [WI_W, GI_W] \\ GI_W &= [GI1_W, GI2_W] \ . \end{aligned} \tag{3.20}$$

The criterion we applied for this comparison is to provide equal protection against multipath channels for both modulations, so that $L_{GI1_G} = L_{GI1_W}$. Thus

$$\begin{aligned} SE_G &= \frac{MK}{L_{GI_G} + MK} = \frac{MK}{L_{GI1_G} + MK} \\ \\ SE_W &= \frac{MK}{L_{GI_W} + MK} = \frac{MK}{L_{GI1_W} + L_{GI2_W} + MK} \ . \end{aligned} \tag{3.21}$$

From this analysis it is clear that if full orthogonality is to be maintained, the windowing process brings an extra GI2 region to the CP which has effects on the SE of a WCP-COQAM signal. In particular, SE is reduced by a factor of $(L_{GI1} + L_{GI2} + MK)/(L_{GI1} + MK)$ compared to a windowless system with equal multipath channel protection.

3.4 Simulation results and discussion

In this section we show and discuss the results obtained from the simulations of the systems previously described. Based on these results we assess the performance of the simulated systems in terms of BER, PSD and SE. In our analysis we prioritize robustness against highly dispersive channels, so that we use the BER of transmissions through Rayleigh fading multipath channels in order to assess the robustness of the FMC systems. In addition to BER, we also take into consideration the PSD of the transmitted signals, for it is an important factor when it comes to CR systems. Regarding SE, we use it to represent the cost of the CP extensions, windowing process and convolution tails caused by the prototype filters in FBMC-OQAM, so that we can obtain a fair comparison between different FMC systems.

Since we are evaluating MCM systems, we consider appropriate taking OFDM as the reference system in order to assess the modulation schemes we are analysed. Table. 3.1 shows the configuration parameters we used in most of our simulations. We choose parameters suitable for low-band transmissions in ultra-reliable and low-latency indoor scenarios. For that, we consider aspects like sub-carrier bandwidth and transmission channel's coherence bandwidth; data block duration and window length for PSD improvement.

Table 3.1: Basic simulation parameters

	OFDM	FBMC-OQAM	GFDM-OQAM	WCP-COQAM
Signal bandwidth	20 MHz			
IQ modulation	QPSK			
M (sub-carriers)	512			
K (symbols/block; overlapping factor)	1	4	4	4
L_{CP} (samples)	32	-	32	224
L_{WI} (samples)	-	-	-	96
L_{GI} (samples)	32	-	32	128
L_{GI1} (samples)	-	-	-	32
L_{GI2} (samples)	-	-	-	96
Prototype filter	-	PHYDYAS [91]		
L_p (samples)	-	2048		

3.4.1 Robustness against multipath channels

In this subsection we analyse the robustness of each MCM system against multipath channels. In order to make a fair comparison we simulate every system with equal protection against multipath channels, matching effective GI lengths (L_{GI_O}, L_{GI_G} and L_{GI1_W}). These parameters are selected as shown in Table. 3.1.

The equalization technique we use in our simulations is one tap Zero-Forcing (ZF) FDE for all the MCM systems. While block-wise modulation schemes OFDM, GFDM-OQAM and WCP-COQAM employ CP extensions to prevent from ISI caused by the transmission channel, FBMC-OQAM could be considered a special case in this aspect. It is not a block-wise modulation and it employs no CP extension like the other MCM systems. Therefore, a FBMC-OQAM transmission is not prevented against the ISI introduced by the channel. In such conditions, one tap FDE can be successfully performed only if the sub-carrier bandwidth is narrower than the channel's coherence bandwidth (i.e. channel frequency response at each sub-carrier is considered to be flat). In this case, we employ a high number of sub-carriers, as stated in 3.1, with a bandwidth close to channel's coherence bandwidth. Thus, we consider acceptable the use of one tap FDE also for FBMC-OQAM. An in-depth analysis about the doubly dispersive channels' impact on FBMC systems is given in [108].

We simulated transmissions through a time invariant Rayleigh fading channel model with exponential PDP, whose Root Mean Square (RMS) delay spread and channel length are $t_{rms} = 185$ ns and $L_{CH} = 22$ taps, respectively. Besides,

we simulate uncoded and coded communications, with turbo codes, soft decoding and a code rate of 1/3. In Figure 3.13 we compare the BER vs. E_b/N_0 of the MCM systems over these channel models, assuming perfect synchronization and full Channel State Information (CSI). We got these BER curves by running simulations with a confidence interval of $\pm 1.8 \cdot 10^{-7}$ and a confidence level of 99.9% for the lowest BER given value.

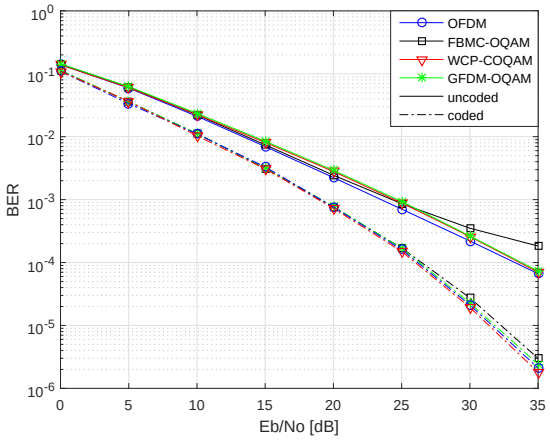

Figure 3.13: BER curves of the analysed MCM systems in a multipath channel.

Here we show that, for uncoded transmissions, in terms of error rate, FBMC-OQAM performs slightly worse than the rest of MCM systems under the simulated conditions. While at low E_b/N_0 values every MCM system provides similar BER, an error floor appears at high E_b/N_0 values because of the lack of GI in FBMC-OQAM. On the other hand, although OFDM, GFDM-OQAM and WCP-COQAM provide similar performance in terms of BER providing equal multipath effect protection, OFDM slightly outperforms the other two FMC schemes due to its perfect orthogonality.

Finally, it is worth noting that for coded transmissions all the simulated MCM systems present similar BER curves, so that they provide similar robustness against multipath channels in the described conditions.

3.4.2 Power Spectral Density analysis

PSD is a relevant characteristic in order to design a CR communication system suitable for scenarios with high spectrum occupation. In this subsection we compare the spectrums of the signals of the analysed MCM systems, in order to assess their potential suitability for CR based systems.

Figure 3.14 shows the spectrums of OFDM, GFDM-OQAM, WCP-COQAM and FBMC-OQAM signals one on top of the other. For this test we only activate the 32 central sub-carriers, in order to make the power leakage into adjacent sub-carriers visible.

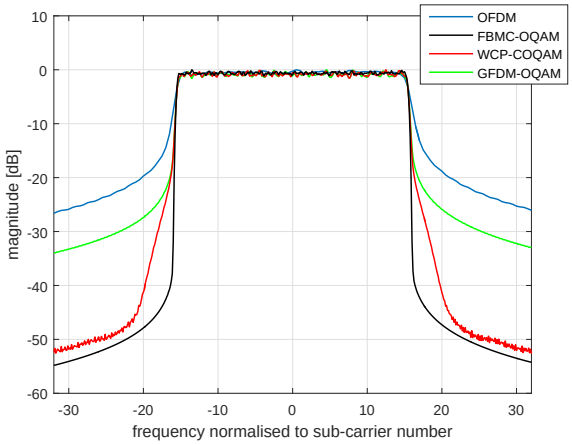

Figure 3.14: PSD of the analysed MCM systems with some sub-carriers deactivated.

As shown in Figure 3.14, the FMC systems carry significant reduction of OOB radiation compared to OFDM. However, even between these FMC schemes there is still a remarkable difference. In this sense, FBMC-OQAM outperforms both GFDM-OQAM and WCP-COQAM. On the other hand, thanks to the windowing, WCP-COQAM shows considerably lower OOB radiation than GFDM-OQAM. It is worth mentioning that the longer the WI region is, the narrower WCP-COQAM signal's spectrum gets. Since extra samples within the GI region are needed for windowing, as described in Section 3.3, PSD improvement of WCP-COQAM over GFDM-OQAM comes at the cost of lower SE. More detailed analysis on SE is given in Section 3.4.3.

3.4.3 Spectral Efficiency analysis

In this subsection we analyse SE in order to evaluate the cost of obtaining higher robustness against dispersive channels and better PSD by means of CP extensions and windowing. For this analysis we consider the parameters defined in Table. 3.1, so that effective multipath channel protection is equal for OFDM, GFDM-OQAM and WCP-COQAM. Eq. (3.22) shows the SE values of the three block-wise MCM system.

$$SE_O = \frac{MK_O}{L_{GI_O} + MK_O} = 0.9412$$

$$SE_G = \frac{MK_G}{L_{GI_G} + MK_G} = 0.9846 \tag{3.22}$$

$$SE_W = \frac{MK_W}{L_{GI_W} + MK_W} = 0.9412 \ .$$

Here we show a particular case with some specific parameters. On the one hand, GFDM-OQAM presents higher SE than OFDM because its GI precedes K symbols, while in OFDM the GI precedes only one symbol. On the other hand, because of the windowing operation, the CP extension of WCP-COQAM, specifically the GI part, has L_{GI2} extra samples with respect to GFDM-OQAM and that is the reason why WCP-COQAM also presents lower SE than GFDM-OQAM. However, under these conditions, with a high number of sub-carriers, we can conclude that the differences in the SE between OFDM, GFDM-OQAM and WCP-COQAM are not really significant.

Regarding FBMC-OQAM, once again, we consider it different from the rest of MCM systems because it is not a block-wise modulation and it uses no GI protection for multipath effect. So its SE depends on the length of the transmitted frames with respect to the convolution tails. For long data transmissions its SE will tend to 1 while for short data transmissions should tend to 0.5, assuming a minimum amount of data samples equivalent to a GFDM-OQAM or WCP-COQAM block. This calculation is simple if we introduce 4 complex data symbols (8 OQAM symbols) in Eq. (3.2)

$$a_m(n) = \sum_{k=0}^{7} x_m(k)\delta(n - kM/2) \ , \quad n = 0, ..., 8M/2 - 1 \ , \tag{3.23}$$

and we introduce this up-sampled data in Eq. (3.3). The resultant $y(n)$ signal will contain 4095 samples, of which half will correspond to actual data and the rest to convolution tails from sub-carrier filtering.

Considering the low latency scenarios our research focuses on, SE might suppose a significant drawback for FBMC-OQAM comparing to GFDM-OQAM and WCP-COQAM during short data transmissions.

3.5 Summary and conclusions

In this chapter we make a comparison between three FMC modulation schemes and a reference OFDM system, in order to assess their suitability for industrial wireless communications based on CR. For that, we simulate low-band communications and highly dispersive indoor channel scenarios. Under these conditions, we show the performance and features of these MCM systems from different points of view.

Regarding robustness against multipath channels, we conclude that all the analysed MCM systems provide similar performance under the simulated conditions. Although for uncoded transmissions FBMC-OQAM presents an error floor at high E_b/N_0 values, this error floor is corrected when coding is used.

In terms of PSD and OOB radiation, these FMC schemes provide more restrained spectrum than OFDM. Specially FBMC-OQAM outperforms the rest of the modulation schemes in this aspect, so it could be a suitable candidate for the CR scenarios considered in our research. On the other hand, although not as good as FBMC-OQAM, WCP-COQAM still has considerably better PSD than GFDM-OQAM, which only provides less than 10 dB of improvement in OOB radiation with respect to OFDM. Therefore, we conclude that circular filtering only is not sufficient and windowing must be applied in order to ensure more efficient use of the spectrum. Moreover, we consider that, due to its also restrained spectrum, WCP-COQAM might be another suitable modulation scheme for CR applications.

As for the SE analysis, as discussed in Section 3.4.3, the difference between OFDM, GFDM-OQAM and WCP-COQAM is not really significant for the parameters we used in our simulations. On the other hand, FBMC-OQAM might suffer from severe degradation of SE during short data transmissions in the low latency scenarios we consider in our research.

Chapter 4

CFO and STO synchronization and channel estimation techniques for WCP-COQAM

Synchronization has been one of the crucial research topics in OFDM because of its sensitivity to timing and frequency errors and it is also a relevant research area in FMC systems. A lot of research has been carried out about the aforementioned FMC systems assuming ideal CFO and STO conditions. However, in practical implementations, frequency offset arises from the frequency mismatch of the transmitter and receiver oscillators. As for time offset, due to the delay of the signal transmission between transmitter and receiver, it is likely for the latter to start sampling a new frame at the incorrect time instant. Besides, time offset is also caused by the sampling time mismatch between the transmitter and receiver clocks.

Along with CFO and STO synchronization, channel estimation is another crucial research field in wireless communications. In addition to ideal CFO and STO conditions, full CSI is commonly assumed in many researches, just as we do in Chapter 3. Regarding practical applications though, the transmission channel is usually unknown and it must be estimated at the receiver. Moreover, the transmission channel often varies through time, which causes Doppler effect on the received signal, thus distorting the signal and hindering its equalization. Channel estimation is usually performed either based on a preamble prior to the transmitted data or on pilot symbols transmitted scattered along with the data symbols. In this chapter we address the latter option due to its superior capacity to deal with channel variation and residual CFO.

In the following sections we address the issues of CFO and STO synchronization and time varying channel estimation for WCP-COQAM. We focus on WCP-COQAM due to the conclusions obtained from Chapter 3, where we con-

clude that it provides better PSD than GFDM-OQAM and fits more properly the low-latency requirements of FA applications than FBMC-OQAM. However, it is worth mentioning that the estimation techniques we show here for WCP-COQAM are totally compatible and applicable to GFDM-OQAM because both modulation schemes share the same symbol and filtering structure.

From the research we introduce in this chapter, we provide the following contributions:

1. We propose a CFO and a STO synchronization technique for WCP-COQAM, adapted from time-frequency synchronization techniques for GFDM and OFDM available in the bibliography. For the best of our knowledge this specific issue has not been addressed in the bibliography, so here we present simulation results that show that the synchronization techniques we propose in this chapter can be suitable solutions for the CFO and STO issue in WCP-COQAM systems.

2. In this chapter we propose a robust and low-latency pilot-based channel estimation technique for short WCP-COQAM transmissions. The simulation results we present here show that the channel estimation technique we introduce provides significantly higher robustness against time-variant and highly frequency selective channels than the solutions from the bibliography.

3. Based on the time-frequency synchronization and channel estimation techniques we propose in this chapter, we evaluate the overall performance of WCP-COQAM in terms of BER under more realistic conditions by simulating actual time-frequency offset and channel estimation impairments. For the best of our knowledge, there are no such results in the scientific bibliography.

In this chapter, beginning with Section 4.1, we explain the CFO and STO estimation methods that we apply on WCP-COQAM. First, we introduce the preamble structure we employ to perform the estimations. Then, we explain the procedures we follow to estimate the CFO on the one hand and the STO on the other hand. Afterwards, we show and discuss some simulation results in order to analyse the performance of the estimation techniques we are introducing. In Section 4.2 we introduce a pilot-based channel estimation method for WCP-COQAM in time-varying channels scenarios. Before giving the solution, we explain the inherent problems of pilot-based channel estimation in FMC systems based on OQAM, and then we introduce our pilot-based channel estimation technique proposal. Afterwards we present the results obtained from our simulations and we discuss the performance of our channel estimation technique. To conclude the chapter, in Section 4.3 we state the conclusions we obtained from the CFO, STO and channel estimation techniques we present in this chapter.

4.1 Preamble based CFO and STO synchronization

In this section we introduce a preamble based time-frequency synchronization method for WCP-COQAM. Based on synchronization algorithms for OFDM [109] and GFDM [110], we adapt them in order to make them suitable for WCP-COQAM.

4.1.1 Preamble structure

We begin explaining how we construct the preamble we use in our simulations. It consists on a data-aided training sequence, so we employ an arbitrary IQ complex data symbol sequence. From this IQ sequence, the preamble is constructed as a WCP-COQAM signal, so that its waveform matches the one of the following data transmission. At the receiver, this preamble sequence is known. The preamble sequence is depicted in Figure 4.1.

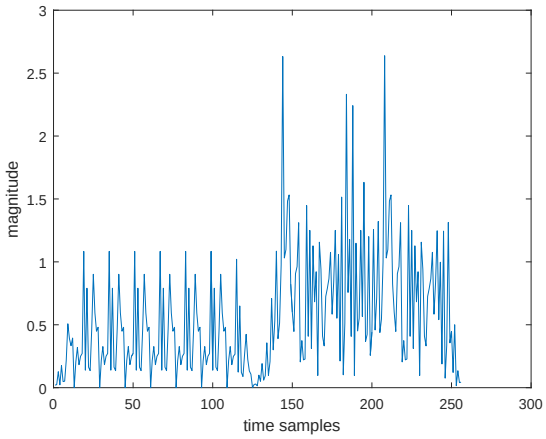

Figure 4.1: Magnitude of WCP-COQAM preamble in time domain.

The preamble is formed by two blocks referred as p_1 and p_2, each of them with: $M = 64$ sub-carriers, $K = 1$ subsymbol per block, $L_{CP} = 64$, $L_{GI} = 48$ and $L_{WI} = 16$. It is worth mentioning that, unlike in WCP-COQAM ordinary data transmission, p_1 and p_2 do not overlap between them and neither do p_2 and the first transmitted data block. Thus, we keep preamble blocks independent in order to provide higher accuracy to the correlation operations for CFO and STO estimations.

First preamble block p_1 is aimed at estimating the CFO and performing the coarse STO estimation. Its repetitive structure allows to make these estimations by means of the autocorrelation of the received signal. We designed p_1 so that it

originally has 4 identical parts, which allows to estimate the CFO up to ± 2 times the separation between contiguous sub-carriers, and the CP and window are added. Although the repetitions introduced by the CP do not count for the possibility of estimating wider CFO spans, the longer the repetitive sequence is, the more stable the autocorrelation will be, making CFO estimation more accurate.

Second preamble block p_2, on the other hand, is aimed at performing the fine STO estimation by means of the cross correlation between the received signal and the preamble training sequence known at the receiver. p_2, in addition to the structure already defined aimed at the cross correlation, contains $M = 64$ pilots which are also used to estimate channel's frequency response. As we explain in Section 4.1.3, this channel estimation is not aimed at channel knowledge and equalization, but at providing more accurate STO estimation.

Note that this preamble, except for the windows, adopts the same signal structure as a GFDM-OQAM preamble. Therefore, this preamble would be valid for a GFDM-OQAM system too, even with the windows. In fact, windowing improves the PSD of the preamble and enhances the accuracy of the correlation operations performed for CFO and STO estimations. Hence, a windowed preamble would be feasible for a GFDM-OQAM system, just as it would for a GFDM system as shown in [110].

4.1.2 Time-frequency synchronization based on correlation metrics

In this section we explain how we use the preamble sequence defined above in order to perform the CFO and STO estimations.

At the receiver we take a sequence $y(n)$ from the received signal. This sequence must contain the transmitted preamble, so the amount of collected samples must be chosen based on that criterion. In our simulations we take $3(M+L_{CP})$ samples, which is the equivalent of one preamble sequence and a half in length. First of all, according to [110], we perform an autocorrelation of $y(n)$ in order to detect the repetitive pattern of p_1 and thus the beginning of the preamble prior to the transmitted signal:

$$r_{yy}(k) = \sum_{n=k}^{k+M/4-1} y(n)^* y(n + M/4) \, , \tag{4.1}$$

where $k = 0, ..., M + L_{CP} - 1$.

The greatest values of $|r_{yy}|$ indicate the points where the autocorrelation operation went through the periodic section of the preamble p_1. Thus, it is possible to identify preamble's starting point and to calculate the delay introduced by the STO. However, having more than 2 repetitive parts within $y(n)$ creates a plateau

effect on the autocorrelation sequence r_{yy}. Hence, r_{yy} on its own is an inaccurate metric. As done in [110], this ambiguity can be solved by summing the autocorrelation sequence r_{yy} over $M + L_{CP}$, so that

$$\mu_1(k) = \sum_{n=k}^{k+M+L_{CP}} r_{yy}(n) \ , \tag{4.2}$$

where $k = 0, ..., M + L_{CP} - 1$. This operation cancels the plateau region of r_{yy} and gives a metric with a single highest point which approximately indicates the value of STO. μ_1 and the rest of the metrics explained below are graphically represented in Figure 4.2.

From the metric μ_1 we make a coarse estimation of STO:

$$\hat{\text{STO}}' = \underset{k}{\text{argmax}}[|\mu_1(k)|] \ . \tag{4.3}$$

On the other hand, we use the angle of $\mu_1(\hat{\text{STO}}')$ to estimate the CFO, so that

$$\hat{\text{CFO}} = 2 \cdot \frac{\angle\mu_1(\hat{\text{STO}}')}{\pi} \ . \tag{4.4}$$

Once we estimate the CFO, we use it to correct the frequency offset of the received signal:

$$y'(n) = y(n) \cdot exp\left(-j2\pi\frac{\hat{\text{CFO}}}{M}n\right) \ . \tag{4.5}$$

After correcting the CFO of the received signal, we perform a cross correlation between $y'(n)$ and p_2, known at the receiver, in order to carry out a fine STO estimation. Unlike in [110], our preamble contains a block which is not composed by repetitive parts and we take advantage of that sequence in order to get a more accurate metric by means of cross correlation. The calculation of this metric is expressed as

$$\mu_2(k) = \sum_{n=k}^{k+M+L_{CP}-1} y'(n + M + L_{CP})^* p_2(n - k) \ , \tag{4.6}$$

where $k = 0, ..., M + L_{CP} - 1$.

Although μ_2 already gives us an accurate estimation of the STO by means of strong peaks in the cross correlation sequence we multiply μ_1 and μ_2 in order to remove the side peaks caused by CP repetition within the preamble. Hence, we get the last metric

$$\mu_3(k) = \mu_1(k) \cdot \mu_2(k) \ . \tag{4.7}$$

From the metric μ_3 we make a fine estimation of STO:

$$\hat{\text{STO}} = \underset{k}{\text{argmax}}[|\mu_3(k)|] \, . \tag{4.8}$$

Figure 4.2 shows a graphical representation of the metrics that we calculate during the STO and CFO estimation process.

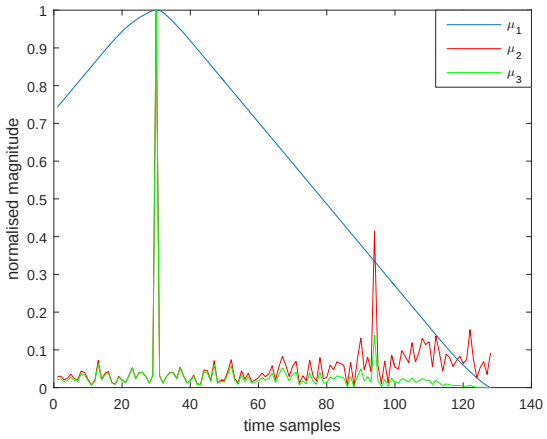

Figure 4.2: Graphical representation of μ_1, μ_2 and μ_3 metrics for STO estimation in a flat channel scenario.

Up to this point we focused only on the principles of CFO and STO estimations and we assumed flat channel scenarios. In real applications though, and specially in industrial environments, wireless channels are characterised by multipath effect, which means that the receiver will receive "several copies" of the transmitted signal. These repetition of the same signal will affect the cross correlation defined in Equation (4.6) by generating several peaks instead of a single one. Figure 4.3 graphically represents this scenario.

At this point μ_3 gives several peaks, caused by the multipath effect of the channel, among which one of them corresponds to the STO value. We have to bear in mind that the strongest peak should not necessarily correspond to the STO value, because the strongest channel path could be not the first one. So Equation (4.8) is no longer valid for multipath channel scenarios. In order to get the fine STO estimation, we must choose a threshold γ and consider the first peak in μ_3 above this threshold the one corresponding to the STO, so that

$$\hat{\text{STO}} = \underset{k}{\text{argfirst}}[|\mu_3(k)| > \gamma] \, . \tag{4.9}$$

The threshold γ must be low enough to avoid missing the peaks corresponding to the first channel paths and high enough to avoid taking a noise sample prior to

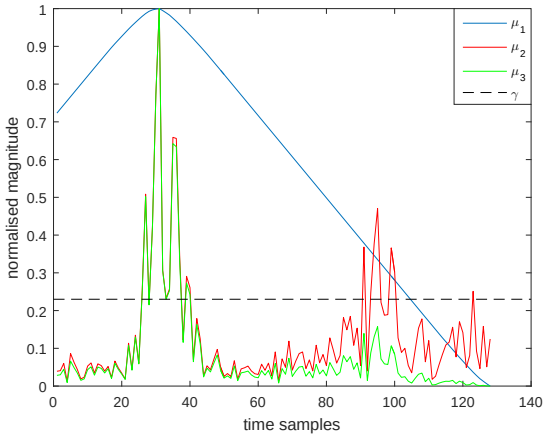

Figure 4.3: Graphical representation of μ_1, μ_2 and μ_3 metrics for STO estimation in a multipath channel scenario.

the actual first channel path as the starting point. This threshold strongly depends on the channel impulse response properties and, for the best of our knowledge, there is no specific formula in the bibliography for its calculation. Therefore, for our simulations we choose a specific threshold γ experimentally deduced, so that the BER is minimized for the channel model we use. We do so in order to focus on the calculation of the metrics and assess the best results this technique could provide under the simulated conditions, independently of the errors that the calculation of the threshold might cause.

4.1.3 Fine STO estimation based on channel impulse response

In this section we introduce another fine STO estimation method. This estimation technique uses the channel impulse response in order calculate the STO and it is based on the idea introduced in [109]. We start applying this method from the coarse STO estimation defined in Equation (4.3). Remember that in actual channels $\hat{STO}' \geq$ STO due to the multipath effect. Then, assuming $\hat{STO}'$ as the actual STO, we perform the channel estimation.

We make the channel estimation in frequency domain. At the receiver, once frequency and coarse time synchronizations are performed, we extract the sequence corresponding to the second symbol of the preamble $\hat{p}_2$ from the received and synchronized signal $y'(n)$.

$$\hat{p}_2 = y'(\hat{STO}' + L_{p_1}), ..., y'(\hat{STO}' + L_{p_1} + L_{p_2} - 1) \ , \tag{4.10}$$

where L_{p_1} and L_{p_2} are the lengths of p_1 and p_2 respectively.

Then, the CP and the window effect are removed and, finally, the resultant sequence is divided by the second symbol of the actual and known preamble p_2 (after removing its CP and window) in frequency domain, in order to estimate the channel frequency response. This operation is represented in Equation (4.11).

$$\begin{aligned} \hat{p}_2' &= [\hat{p_2}(L_{GI}), ..., \hat{p_2}(M + L_{GI} - 1)] \\ p_2' &= [p_2(L_{GI}), ..., p_2(M + L_{GI} - 1)] \ . \end{aligned} \tag{4.11}$$

Thus, channel frequency response $\hat{H}$ is estimated as

$$\hat{H} = \frac{dft(\hat{p}_2', M)}{dft(p_2', M)} \tag{4.12}$$

and channel impulse response $\hat{h}$ is given by

$$\hat{h} = idft(\hat{H}, M) \ . \tag{4.13}$$

We must bear in mind that we perform the channel estimation assuming the value of $\hat{STO}'$ as the actual STO. This will cause an offset in the taps of the estimated channel impulse response $\hat{h}$. And this offset will correspond to the difference between $\hat{STO}'$ and the actual STO value. These channel impulse response estimation and offset issues are graphically represented in Figure 4.4.

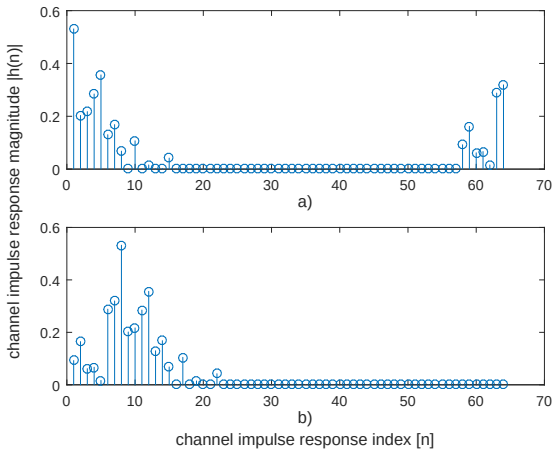

Figure 4.4: Graphical representation of the STO estimation based on channel impulse response.

Figure 4.4-a shows the estimated channel impulse response $\hat{h}$ and Figure 4.4-b shows the actual channel impulse response h. The difference between $\hat{STO}'$ and

the actual STO value causes a forward in $\hat{h}$. The number of forwarded taps will be equal to the difference between $\hat{STO}'$ and the actual STO value in time samples. Therefore, we get the fine STO estimation $\hat{STO}$ by subtracting the number of forwarded taps of $\hat{h}$ to the coarse STO estimation $\hat{STO}'$. So that

$$\hat{STO} = \hat{STO}' - \tau \ , \tag{4.14}$$

where τ represents the number of forwarded taps of $\hat{h}$.

Figure 4.4 represents a noiseless ideal scenario, in which identifying the offset taps of $\hat{h}$ presents no difficulty. In real scenarios with Additive White Gaussian Noise (AWGN), however, actual offset taps of $\hat{h}$ and purely noisy taps might be confused, thus causing errors in the calculation of the real STO value, as represented in Figure 4.5.

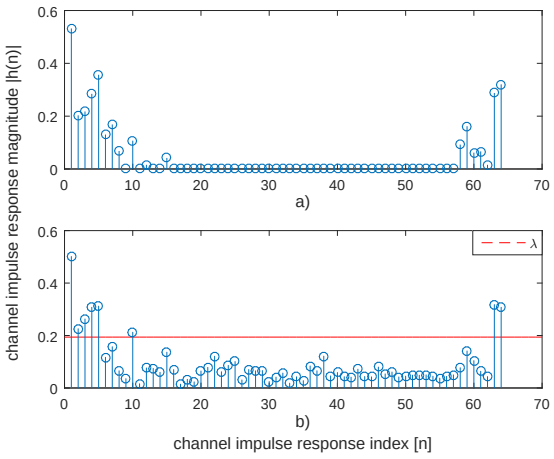

Figure 4.5: Graphical representation of the STO estimation based on channel impulse response in a scenario with AWGN.

In order to separate the offset taps from the noisy ones we propose a method based on the use of a threshold defined as λ. Note that λ should be low enough to not miss the offset taps of $\hat{h}$ and high enough to avoid wrongly picking up a noisy tap, similarly to what happen with the threshold γ, as explained in Section 4.1.2. However, unlike the threshold γ, which strongly depends on the channel impulse response characteristics, the threshold λ we introduce here is mainly dependent on the noise power level. Hence, we define it as

$$\lambda = \frac{\sqrt{P_N}}{\eta} \ , \tag{4.15}$$

where $\eta \in [1.5, 2]$. We established this span experimentally in order to fulfil the aforementioned criterion about the value of λ. The value of η, actually, does

depend on the channel impulse response characteristics. Thus, if the first channel taps are expected to have low energy, η should tend to its maximum value; on the other hand, if the first channel taps are expected to have relatively high energy, then η should tend to its minimum value.

Figure 4.6 represents the situation in which a noisy tap is detected as the first offset tap of $\hat{h}$. In case this happens, channel impulse response must be re-estimated after the calculation of $\hat{STO}$. In such situation, $\hat{STO}$ would be smaller than the actual STO and the re-estimated channel impulse response $\hat{h}_r$ would be like shown in Figure 4.6-b. In this case, the difference between $\hat{STO}$ and the actual STO value is equal to the offset of noisy taps at the front position of $\hat{h}_r$. Therefore, we get the new fine STO estimation $\hat{STO}_r$ by adding the number of taps at the front position of $\hat{h}_r$ to the previous fine STO estimation $\hat{STO}$. So that

$$\hat{STO}_r = \hat{STO} - \tau_r \ , \tag{4.16}$$

where τ_r represents the number of noisy taps at the front position of $\hat{h}_r$.

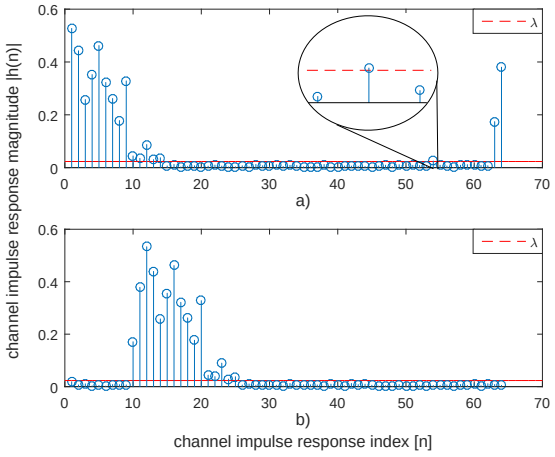

Figure 4.6: Graphical representation of the second stage in STO estimation based on channel impulse response.

We repeat this operation until we get a $\hat{h}_r$ with no noisy taps at the front position.

4.1.4 Performance analysis

In this section we show the performance of the simulated synchronization techniques used for WCP-COQAM. These results correspond to the preamble and techniques described above and the simulations have been carried out under the conditions specified in Table 4.1.

Table 4.1: Simulation parameters for synchronization performance analysis

Transmitted signal bandwidth	20 MHz
IQ modulation	QPSK
M (number of sub-carriers)	64
K (subsymbols per block) data symbols	4
K (subsymbols per block) preamble	1
L_{CP}	64
L_{WI}	16
L_{GI}	48
Prototype filter	PHYDYAS [91]
Filter length (L_p)	256
Channel model	16 taps; $t_{rms} = 150$ ns
CFO range	± 2 sub-carriers
STO range	0-32 samples

We measure MSE of CFO and STO estimations and the BER of simulated transmissions with confidence intervals of $\pm 1.2 \cdot 10^{-8}$, $\pm 2.5 \cdot 10^{-5}$ and $\pm 3.5 \cdot 10^{-6}$ respectively, with a confidence level of 99.9% for their lowest error rate given value. We represent them in Figures 4.7, 4.8 and 4.9, respectively.

We simulated the CFO as a random frequency offset ± 2 times the separation between contiguous sub-carriers. Figure 4.7 shows how the preamble and the CFO estimation technique explained above are able to achieve MSE levels of almost a millionth part of the separation between contiguous sub-carriers.

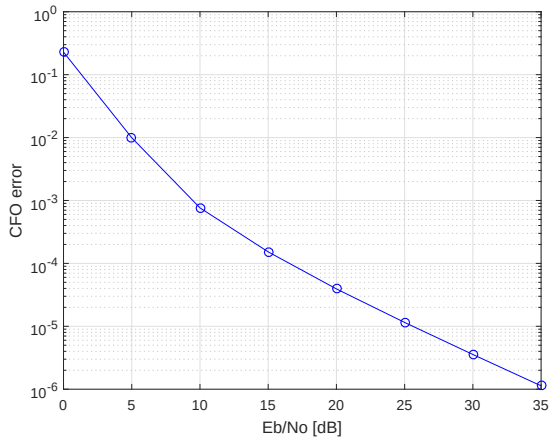

Figure 4.7: Mean Square Error of CFO estimation.

On the other hand, we simulated the STO as a uniformly distributed random

integer number of samples between 0 and 32, which, during the simulations, are added at the beginning of the received signal. Figure 4.8 shows the MSE curves of the STO estimation techniques explained in Sections 4.1.2 and 4.1.3. Results show that the STO estimation based on channel impulse response outperforms the one based on cross correlation metrics, which is thanks to the lower dependence of channel response characteristics of the former, as explained in Section 4.1.3.

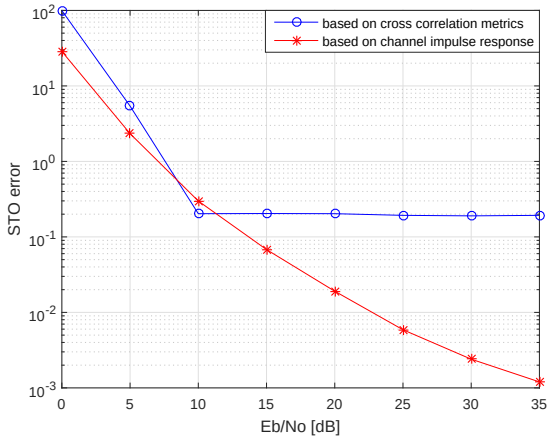

Figure 4.8: Mean Square Error comparison of STO estimation based on cross correlation metrics and based on channel impulse response.

We evaluate the overall performance by comparing the BER curves of a WCP-COQAM system with the synchronization techniques explained in this chapter and the same system without CFO and STO. The CFO and STO estimations we employ for these simulations are explained in Sections 4.1.2 and 4.1.3, respectively. We chose the STO estimation based on channel impulse response due to its better results shown in Figure 4.8. BER curves in Figure 4.9 show that the simulated synchronization techniques under CFO and STO conditions provide an overall performance close to a system under ideal time-frequency synchronization conditions.

We simulate the transmission of a single WCP-COQAM data block in order avoid additional errors caused by residual CFO. Since in this chapter we consider time varying channels, dynamic channel estimation is necessary, which additionally might be a way to deal with residual CFO. Hence, we omit this issue in this section and we address it in Section 4.2.

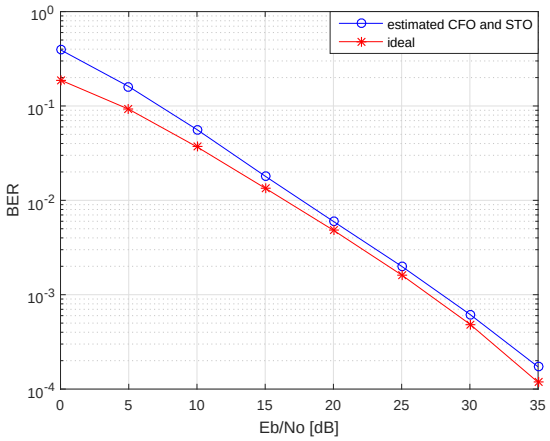

Figure 4.9: BER curves comparison of a WCP-COQAM system with CFO and STO estimation and ideal conditions.

4.2 Pilot aided time varying channel estimation for WCP-COQAM

In this section we analyse pilot-based channel estimation methods for GFDM and FBMC-OQAM and adapt them to WCP-COQAM modulation scheme. Besides, according to the Ultra-Reliability and Low-Latency (URLL) requirements of industrial communications [111], we propose a robust pilot-based channel estimation technique for short WCP-COQAM transmissions.

Before starting this section, we sum up the basics of WCP-COQAM. We do this for the sake of readability, because some expressions used in this section differ slightly from the ones shown in Chapter 3. The details that we do not specify here are assumed to be as explained in Chapter 3.

In this section, we express a WCP-COQAM block $s_{_G}(n)$, before the CP and the window are applied, as

$$s_{_G}(n) = \sum_{m=0}^{M-1} \sum_{k=0}^{2K-1} x_{m,k} \tilde{g}_m(n - kM/2 + MK - 1) \ , \tag{4.17}$$

where M is the total number of sub-carriers; K is the number of complex valued sub-symbols in each block (i.e. $2K$ OQAM sub-symbols in each block); $n = 0, ..., MK - 1$ and $x_{m,k}$ are the OQAM data symbols distributed along the time-frequency grid.

In the receiver, the first L_{GI} and the last L_{WI} samples of a WCP-COQAM received block $r_{_W}$ are removed.

$$r = [r_{_W}(L_{GI}), ..., r_{_W}(MK + L_{GI} - 1)] \ . \tag{4.18}$$

At this point, HR-FDE can be performed over the block r as in Equation (3.9).

After CP and window removal and equalization, the remaining samples are shifted L_{WI} positions in order to recover the WCP-COQAM signal $\hat{s}_{eq}(n)$:

$$\hat{s}_{eq}(n) = r_{eq}[mod(n + L_{WI}, MK)] \,, \tag{4.19}$$

where $n = 0, ..., MK - 1$.

Once the WCP-COQAM block $\hat{s}_{eq}(n)$ is recovered, the OQAM data symbols distributed along the time-frequency grid are obtained by the following equation:

$$\hat{x}_{m,k} = \sum_{l=0}^{MK-1} \hat{s}_{eq}(l)\tilde{g}_m(kM/2 - l + MK - 1) \,, \tag{4.20}$$

where $k = 0, ..., 2K - 1$ and $m = 0, ..., M - 1$.

Another equalization method is also possible, instead of the HR-FDE defined in Equation (3.9). The demodulation/filtering process to recover the OQAM data symbols in the time-frequency grid might be done before equalization. Thus, we change the expression of Equation (4.20), so that $y_{m,k}$ and $s(l)$ denote $\hat{x}_{m,k}$ and $\hat{s}_{eq}(l)$ signals without being equalized respectively:

$$y_{m,k} = \sum_{l=0}^{MK-1} s(l)\tilde{g}_m(kM/2 - l + MK - 1) \,. \tag{4.21}$$

At this point a LR-FDE must be performed over $y_{m,k}$ as in Equation (3.6).

4.2.1 Pilot based channel estimation principles for OQAM systems

In this section we focus on pilot-based channel estimation techniques for WCP-COQAM, instead of preamble based ones, in order to address the time varying channel estimation issue. For the best of our knowledge, there is no work about channel estimation for WCP-COQAM available in the bibliography. However, considering that WCP-COQAM employs OQAM data symbols and it is a FMC based on circular filtering, channel estimation techniques used for FBMC-OQAM and GFDM might be valid references.

The pilot-based channel estimation techniques for both FBMC-OQAM and GFDM shown in the bibliography [112–115] are based on the same principle involving the per sub-symbol LR-FDE expressed in Equation (3.6). An M points channel frequency response is estimated for each sub-symbol. For that, pilots are scattered between data symbols throughout the time-frequency grid. As a consequence of using an LR-FDE, low frequency selectivity is usually assumed in the scattered pilot-based approaches [116].

From [112], we take into consideration the fact that channel estimation based on LR-FDE and scattered pilots is performed for GFDM. Considering the block-wise nature and the circular filtering of WCP-COQAM, it would seem reasonable to employ the same channel estimation scheme. However, due to the OQAM data (and consequently pilot) structure of WCP-COQAM, a straightforward application of GFDM channel estimation is not feasible. Because of this, the pilot design and detection procedure in WCP-COQAM will be similar to FBMC-OQAM's.

In pilot-based channel estimation solutions for FBMC-OQAM, the principle consists on transmitting real pilot symbols at certain positions which are known by the receiver.

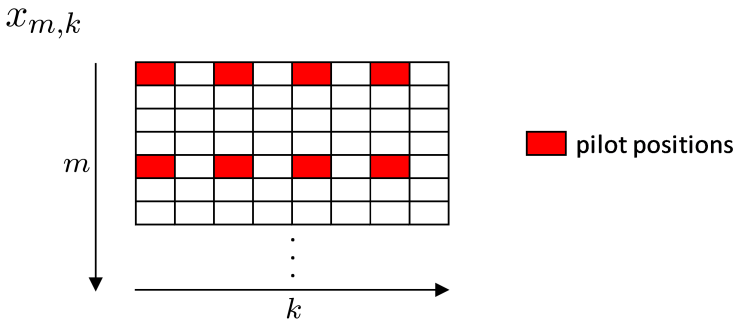

Figure 4.10: Graphical representation of pilots distribution along time-frequency grid $x_{m,k}$.

Assuming a pilot position (m_0,k_0), the corresponding received pilot symbol after the analysis filter bank can be expressed as

$$y_{m_0,k_0} = H_{m_0,k_0}(x_{m_0,k_0} + jI_{m_0,k_0}) \ . \tag{4.22}$$

The factor jI_{m_0,k_0} is the intrinsic interference caused by the filters and the adjacent data symbols. Assuming a correct time-frequency localization of the prototype filter and the use of real valued pilots, the intrinsic interference will be purely imaginary.

$$I_{m_0,k_0} = \sum_{(m,k)\neq(m_0,k_0)} x_{m,k}\langle g\rangle_{m_0,k_0} \ , \tag{4.23}$$

where

$$\langle g\rangle_{m_0,k_0} = \sum_m \sum_n g_m(n) g_{m_0}(k_0 M/2 - n) \ . \tag{4.24}$$

The factor I_{m_0,k_0} depends on the data symbols transmitted around the pilot, which are unknown at the receiver. That is why a coherent channel estimation cannot be performed:

$$\hat{H}_{m_0,k_0} = \frac{y_{m_0,k_0}}{x_{m_0,k_0} + jI_{m_0,k_0}} \ . \tag{4.25}$$

One idea to overcome this problem is to avoid the intrinsic interference by making it to be zero:

$$I_{m_0,k_0} = 0 \ . \tag{4.26}$$

In [113] the authors propose to transmit an Auxiliary Pilot (AP) in order to fulfil the Equation (4.26) by pre-cancelling the intrinsic interference introduced by the data symbols. This AP is adjacent to the pilot x_{m_0,k_0} and it is transmitted at (m_0, k_1) position known at the receiver, where $k_1 = k_0 + 1$.

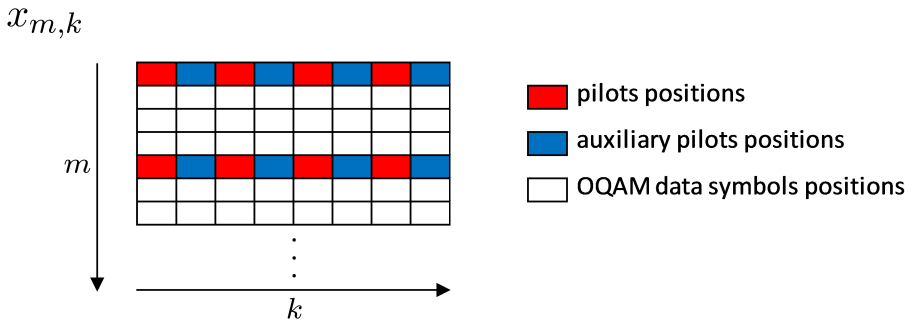

Figure 4.11: Graphical representation of pilots and auxiliary pilots distribution along $x_{m,k}$ time-frequency grid.

The intrinsic interference can be divided in two factors now: the one corresponding to the AP, $I^A_{m_0,k_0}$; and the one corresponding to the adjacent data symbols, $I^D_{m_0,k_0}$. So that

$$I_{m_0,k_0} = I^D_{m_0,k_0} + I^A_{m_0,k_0} \ . \tag{4.27}$$

On the one hand we have that

$$I^D_{m_0,k_0} = \sum_{(m,k)\neq(m_0,k_0)\cup(m_0,k_1)} x_{m,k}\langle g\rangle_{m_0,k_0} \ , \tag{4.28}$$

and on the other hand

$$I^A_{m_0,k_0} = x_{m_0,k_1}\langle g\rangle_{m_0,k_0} \ . \tag{4.29}$$

Considering Equation (4.27) and in order to fulfil (4.26) we conclude that

$$I^A_{m_0,k_0} = -I^D_{m_0,k_0} \ . \tag{4.30}$$

Consequently, the value of the AP is given by

$$x_{m_0,k_1} = -\frac{I^D_{m_0,k_0}}{\langle g\rangle_{m_0,k_0}} \ . \tag{4.31}$$

Using this approach the term I_{m_0,k_0} becomes zero and the coherent channel estimation in Equation (4.25) can be performed at the receiver. After $\hat{H}_{m_0,k_0}$ estimation for all the pilot positions, channel frequency response over the whole time-frequency grid is estimated by interpolation. Two one-dimensional interpolations are performed, first in time domain and the second one in frequency domain.

The main drawback of this solution is the possibly high transmit power needed for the AP in order to fulfil the condition in Equation (4.26). Such symbol power levels, besides increasing the Peak to Average Power Ratio (PAPR), also can break prototype filter's time-frequency localization and distort the rest of the data symbols due to the high ICI and ISI.

In order to avoid this problem, instead of pre-cancelling all the intrinsic interference by forcing it to be zero at the pilot position, the authors in [115] propose to pre-cancel it partially and make it to adopt a certain value from a set $\mathcal{X}$ of possible discrete values known at both the transmitter and the receiver. That is:

$$I_{m_0,k_0} = X \ , \tag{4.32}$$

where X is one of the possible values within the set $\mathcal{X}$. Considering this condition and applying it to Equations (4.27) and (4.30), we obtain that

$$I^A_{m_0,k_0} = X - I^D_{m_0,k_0} \tag{4.33}$$

and

$$x_{m_0,k_1} = \frac{X - I^D_{m_0,k_0}}{\langle g \rangle_{m_0,k_0}} \ . \tag{4.34}$$

The criterion to choose the appropriate X from the whole set $\mathcal{X}$ is minimizing the power of the AP x_{m_0,k_1}. Hence, the appropriate value of X will be the one that fulfils the following minimization problem:

$$min|X - I^D_{m_0,k_0}| \ , \quad X \in \mathcal{X} \ . \tag{4.35}$$

That is, the closest X value to the intrinsic interference introduced by the data symbols $I^D_{m_0,k_0}$. With X defined, the value of the AP x_{m_0,k_1} is calculated as in Equation (4.34).

At the receiver side, although the set $\mathcal{X}$ is known, which one of the X values has been chosen for the intrinsic interference term is unknown. Hence, X must be estimated before performing the actual channel estimation. Once X is estimated, channel frequency response at the pilot position (m_0, k_0) can be also estimated:

$$\hat{H}_{m_0,k_0} = \frac{y_{m_0,k_0}}{x_{m_0,k_0} + j\hat{X}} \ . \tag{4.36}$$

As aforementioned, channel frequency response over the whole time-frequency grid is estimated by interpolation.

The authors in [115] propose an estimation method for X based on the amplitude of the received pilot symbol $|y_{m_0,k_0}|$. This method consists on associating ranges of $|y_{m_0,k_0}|$ values to their corresponding pilot symbols plus intrinsic interference amplitude $|x_{m_0,k_0} + jX|$ for each possible $X \in \mathcal{X}$ value.

Without loss of generality, they assume the real pilot x_{m_0,k_0} to be always 1. The amplitude of the pilot symbols plus intrinsic interference $|1 + jX|$ must be delimited, so that $|X| \in [|X|_{min}, |X|_{max}]$. Besides, the amplitude of the pilot plus intrinsic interference $|1 + jX|$ must be different and uniformly distributed for each value of X, in order to avoid any ambiguity when performing amplitude based estimation of X at the receiver. Hence, the fewer X values there are in $\mathcal{X}$, the larger the difference between the possible $|1 + jX|$ values will be, so that the estimation of X at the receiver will be easier. However, based on Equation (4.34), the larger the resolution of $\mathcal{X}$ is, the higher x_{m_0,k_1} AP power might be. Inversely, if the resolution of $\mathcal{X}$ is lower, x_{m_0,k_1} AP power might be acceptable, but error rate in the estimation of X would be higher.

Although this partial pre-cancelling method eases the issue of high AP power, it still presents considerable problems. The main of them is that the pilot estimation method is based on the amplitude of the received pilot symbol, which is not reliable in highly dispersive channels. Furthermore, for this kind of scenarios, finding a trade-off between x_{m_0,k_1} AP power and error rate in the estimation of X might not always be possible.

4.2.2 Proposed robust channel estimation method

The channel estimation methods analysed in Section 4.2.1 present several drawbacks: they are only valid for low frequency selective channels, high AP transmission power, intrinsic interference pre-cancellation need and estimation of intended intrinsic interference X are some of them. These problems are consequences of using LR-FDE and dealing with OQAM pilots/data-symbols and the intrinsic interference issues. In this section we propose a channel estimation technique for WCP-COQAM that avoids LR-FDE and OQAM based pilot structures. Instead, we employ HR-FDE based on the WCP-COQAM block and CP structure as in Equation (3.9) in order to provide full orthogonality against multipath channel effect; and we design the pilots structure and perform the channel estimation in the IQ domain instead of OQAM, in order to avoid any problem related to the intrinsic interference.

At the transmitter, before OQAM processing is performed, complex valued pilots and their positions are defined:

$$a_{m_0,l_0} = a^R_{m_0,l_0} + j a^I_{m_0,l_0} \ , \tag{4.37}$$

where the value of a_{m_0,l_0} and the position (m_0, l_0) are known at the transmitter

and the receiver. Here, $a_{m,l}$ are complex valued IQ symbols extended through the time-frequency grid so that $m \in [0, M-1]$ and $l \in [0, K-1]$.

In this estimation method, we place equal pilots at every l sub-symbol of each m_0 sub-carrier. We do this in order to avoid ISI between the pilots within the same sub-carrier and in order to minimize channel estimation errors.

Assuming good TFL of the prototype filter and equal pilots at every l sub-symbol of each sub-carrier, every intrinsic interference is avoided after OQAM symbols are demodulated to IQ symbols. Therefore, no pilot estimation is required at the receiver and the received pilots can be expressed as

$$b_{m_0,l_0} = \mathcal{H}_{m_0,l_0} \cdot a_{m_0,l_0} \ . \tag{4.38}$$

Thus a coherent channel frequency response estimation at pilot positions can be performed.

$$\hat{\mathcal{H}}_{m_0,l_0} = \frac{b_{m_0,l_0}}{a_{m_0,l_0}} \ . \tag{4.39}$$

Once channel frequency response estimation at pilot positions is done, we proceed to calculate MK point channel frequency response for HR-FDE. First, the mean values of the K pilots within each pilot sub-carrier is calculated:

$$\hat{H}^{LR}_{m_0} = mean(\hat{\mathcal{H}}_{m_0,0}, ..., \hat{\mathcal{H}}_{m_0,K-1}) \ . \tag{4.40}$$

Finally, $\hat{H}^{LR}$ is interpolated to MK points in order to get $\hat{H}^{HR}$ for the HR-FDE shown in Equation (3.9).

Note that in order to perform this channel estimation, the receiver must go over the demodulation process twice. In the first stage the HR-FDE is skipped and the demodulation process is carried out as shown in Equation (4.21). Then, the $y_{m,k}$ OQAM symbols are demodulated into the $b_{m,l}$ IQ symbols, so that our channel estimation can be performed. Once the HR channel frequency response is estimated, HR-FDE is performed and demodulation process continues as shown in Equations (4.19) and (4.20).

4.2.3 Performance analysis

The authors in [112] claim that HR-FDE is not suitable for time-variant channel environments because of the channel variation during the transmission of a whole GFDM block. Comparing with one OFDM symbol or one FBMC-OQAM sub-symbol, a GFDM block is K times longer. For this reason, they propose Low Resolution (LR) channel equalization and estimation for time-variant channels, as explained in Section 4.2.1. This very reasoning is directly applicable to the WCP-COQAM case, considering its block-wise structure. However, if we consider

highly dispersive channels, modulation systems based on LR channel estimation and equalization require a high number of sub-carriers, which makes sub-symbols transmissions longer. On the other hand, systems based on block structure, CP and HR equalization and channel estimation, can support a low number of sub-carriers without loss of orthogonality, which implies shorter transmission times.

In this section we analyse these issues by comparing the results of different channel estimation methods used in a WCP-COQAM system. Considering that our investigation is aimed at industrial wireless communications, we simulate transmissions through highly dispersive channels under different conditions, such as number of sub-carriers and channel's time variability. Thus, we evaluate the suitability of these channel estimation techniques for strong frequency selectivity, different time variability levels and different block transmission durations.

For the case of LR channel estimation we simulate the partial intrinsic interference pre-cancellation technique introduced in [115] and explained in Section 4.2.1. Since in the original work the estimation process of the intended intrinsic interference X is not fully detailed, we assume perfect knowledge of the pilots at the receiver in our simulations. By employing our own techniques for the estimation of X we might penalise the performance of this channel estimation technique. Table 4.2 shows the simulation parameters we use.

Table 4.2: Basic simulation parameters

f_0 (carrier frequency)	2.4 GHz
Signal bandwidth	20 MHz
M (sub-carriers)	64 or 1024
Channel properties	16 taps; t_{rms} = 150 ns
IQ constellation	QPSK
K (sub-symbols/block; overlapping factor)	4
L_{CP} (samples)	64
L_{WI} (samples)	16
L_{GI} (samples)	48
Prototype filter	PHYDYAS [91]

We measure MSE of the analysed channel estimation techniques and BER of WCP-COQAM with 64 and 1024 sub-carriers with confidence intervals of $\pm 1.4 \cdot 10^{-6}$, $\pm 2.1 \cdot 10^{-6}$ and $\pm 5.2 \cdot 10^{-6}$ respectively, with a confidence level of 99.9% for their lowest error rate given value. We represent them in Figures 4.12, 4.13 and 4.14, respectively.

First we analyse the performance of the channel estimation techniques themselves. Figure 4.12 shows the MSE against E_b/N_0 of the aforementioned LR channel estimation technique and the HR channel estimation method introduced in Section

4.2.2. For these simulations channel response is assumed to be time-invariant.

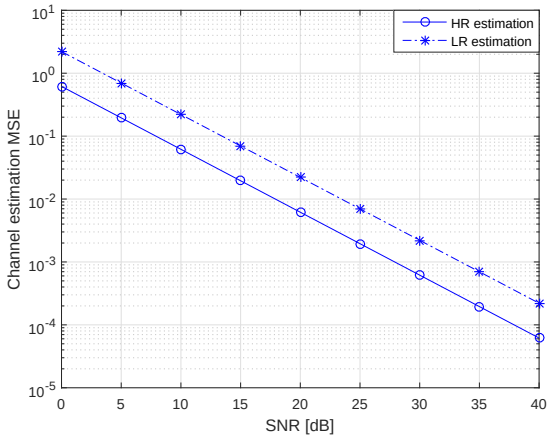

Figure 4.12: Mean Square Error of the analysed channel estimation techniques.

Figure 4.12 shows that the error rate for HR channel estimation is lower than for the LR channel estimation, which means that the former technique is more precise than the latter for time-invariant channels.

Next, we evaluate the robustness of a WCP-COQAM system using one channel estimation technique or the other. For that, we analyse the BER of the system under different conditions.

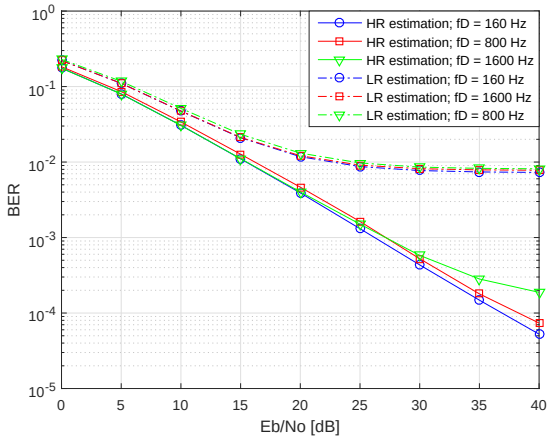

Figure 4.13: BER curves of a WCP-COQAM system with 64 sub-carriers for different estimation techniques and different Doppler frequencies.

Figure 4.13 shows BER curves of an uncoded short block transmission system with 64 sub-carriers for both channel estimation techniques at different Doppler

frequencies. We chose those Doppler frequencies assuming fixed transmitter and receiver and the wireless channel between them formed by moving scatterers at maximum speeds of 10 m/s, 50 m/s and 100 m/s. We assigned these values based on the assumption that scatterers in an industrial wireless channel should mainly consist on people walking across the wireless channel and few machines performing some periodic and rapid movements. According to the TGn time varying channel model introduced in Section 2.2.2, these conditions are modelled by a bell shaped Doppler spectrum, which we model using Matlab's channel object. Both, scatterer maximum speed and Doppler spectrum, are given as parameters to the channel object.

We see that for short block transmissions with a low number of sub-carriers, the penalisation because of the channel's time variability in the HR-FDE based systems is much lower than the one caused by the channel's ICI in LR-FDE based systems.

Figure 4.14 shows BER curves of an uncoded long block transmission system with 1024 sub-carriers for both channel estimation techniques at the same Doppler frequencies.

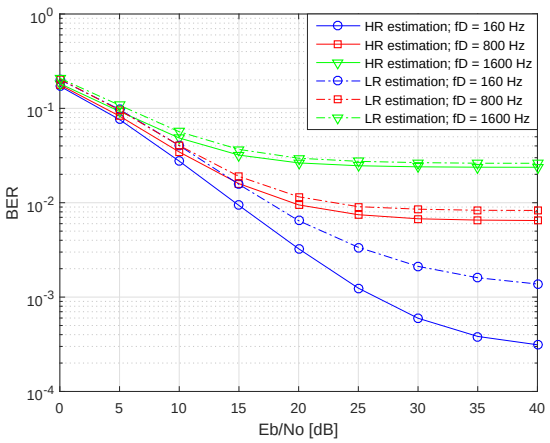

Figure 4.14: BER curves of a WCP-COQAM system with 1024 sub-carriers for different estimation techniques and different Doppler frequencies.

In this case, even with long block transmissions and narrower sub-carriers, HR-FDE based systems still present better BER performance than the LR-FDE based ones. Channel's time variation's effect over each sub-symbol in LR-FDE based systems, is lower than over a whole block in HR-FDE. However, assuming a highly dispersive channel scenario, time variation in combination with the remaining ICI from LR-FDE, make these systems perform worse than the ones based on HR-FDE. On the other hand, despite the perfect orthogonality provided

by HR-FDE, if channel's variability arises above certain level, the channel variation through such a long block transmission makes both, channel estimation and equalization, infeasible.

4.3 Summary and conclusions

In this chapter we present results on synchronization and channel estimation for WCP-COQAM, which, for the best of our knowledge, have not been published in the bibliography.

Regarding time-frequency synchronization, we show that techniques similar to those previously used for GFDM and OFDM can be adapted to WCP-COQAM. Moreover, our results show that the performance of those time-frequency synchronization techniques used on WCP-COQAM is similar to that of GFDM or OFDM shown in the bibliography. Besides, BER results show that the simulated synchronization techniques under CFO and STO conditions, provide an overall performance close to a system under ideal time-frequency synchronization conditions.

As for channel estimation, we analyse some of the most extended techniques for FBMC-OQAM and we adapt them to WCP-COQAM. We also propose a pilot-based estimation technique for WCP-COQAM and we compare its performance with the techniques from the bibliography adapted to WCP-COQAM.

Although, according to the bibliography, HR based channel estimation and equalization should not be aimed at time-variant channel scenarios, we base our proposal on this principle. We employ the HR-FDE and block-wise structure provided by WCP-COQAM in order to take advantage of full orthogonality against multipath channels and short block transmission.

Results show that in highly dispersive channel scenarios HR-FDE provides higher robustness even for time-varying channels. Moreover, for short block transmissions with low number of sub-carriers, our proposal shows good BER performance even for the highest channel variability level and clearly outperforms the simulated LR-FDE based systems.

Finally, we consider robustness against multipath channels and short transmission times essential in industrial wireless communications for FA applications. Therefore, and also considering the conclusions stated in 3.5, we conclude that the channel estimation method for WCP-COQAM we propose in this chapter might be a suitable technique for industrial automation scenarios with CR.

Chapter 5

Conclusions and future work

Before stating the main conclusions obtained from this doctoral thesis, we make a summary of this report in order to recall its contents and connect them to the conclusions shown below.

In Chapter 1 we explain the context in which this thesis has been carried out: the main problems which motivate this research, its reach and scope, the main objectives of this doctoral thesis, the hypotheses that have conducted this project and the methodology followed to carry out the research.

In Chapter 2 we take into consideration several aspects and research fields related to this doctoral thesis. We provide a general analysis of the state of the art and some theoretical background related to the work introduced in this thesis.

In Chapter 3 we analyse FBMC-OQAM, GFDM-OQAM and WCP-COQAM FMC modulations in depth. We simulate these modulation schemes in low-band transmissions through large indoor spaces and severe multipath channels, emulating industrial halls. Based on these results, we aim at providing a notion about the suitability of FMC modulation techniques for industrial wireless communications based on CR.

In Chapter 4 we address the issues of CFO and STO synchronization and time varying channel estimation for WCP-COQAM. We analyse CFO and STO synchronization techniques for GFDM and OFDM available in the bibliography and we adapt them in order to propose synchronization techniques for WCP-COQAM. Additionally, we also propose a robust and low-latency pilot-based channel estimation technique for short WCP-COQAM transmissions.

We conclude this thesis report by stating the conclusions and the main contributions that we obtained from the whole research carried out during this doctoral thesis. Finally, we propose a set of tasks that would complement and enhance the work done in this doctoral thesis.

5.1 Conclusions

Referring to the objectives and hypotheses stated in Sections 1.3 and 1.4 respectively, and based on the results shown and discussed in this thesis report, we introduce the following conclusions.

Firstly, regarding the robustness property our research focuses on and considering the results shown in Sections 3.4 and 4.2.3, we conclude that the block-wise FMC modulations with CP GFDM-OQAM and WCP-COQAM provide higher robustness against multipath channels, assuming certain SE and timeliness requirements. That is, FBMC-OQAM needs sub-carriers narrower than the channel's coherence bandwidth in order to provide similar robustness to GFDM-OQAM and WCP-COQAM against multipath channels. In highly frequency selective channels it implies a high number of sub-carriers. With a high number of sub-carriers, as discussed in Section 3.4.3, FBMC-OQAM might suffer from severe degradation of SE during short data transmissions in the low latency scenarios we consider in our research. On the other hand, GFDM-OQAM and WCP-COQAM can adopt shorter block structures with few sub-carriers and keep orthogonality and robustness against multipath channels thanks to the CP. Thus, we address the first hypothesis stated in Section 1.4 and we consider it as fulfilled.

Related to the robustness against multipath channels and concerning block-wise FMC modulations with CP, as discussed in Section 3.4.1, although OFDM, GFDM-OQAM and WCP-COQAM provide similar performance in terms of BER providing equal multipath effect protection, OFDM slightly outperforms the other two FMC schemes due to its perfect orthogonality. Thus, although it practically means no significant difference, our second hypothesis is not strictly fulfilled.

Secondly, as for the compatibility with CR techniques, we evaluate it based on PSD and OOB radiation presented by the analysed FMC schemes. In this sense, as discussed in Section 3.4.2, these FMC modulations provide more restrained spectrum than OFDM. Specially FBMC-OQAM outperforms the rest of the modulation schemes in this aspect, so it might provide good compatibility with CR techniques in certain scenarios. On the other hand, WCP-COQAM provides a PSD close to FBMC-OQAM and significantly better than GFDM-OQAM. Therefore, it is worth noting that circular filtering is not sufficient and windowing must be applied in order to ensure a more efficient use of the spectrum. Finally, we consider that, due to its also restrained spectrum, WCP-COQAM might provide good compatibility with CR applications.

Considering all the aforementioned conclusions and the first goal we define in Section 1.3, we conclude that WCP-COQAM is the modulation technique that best fits the requirements we take into consideration for our research in terms of robustness, CR compatibility and timeliness.

As far as our second objective defined in Section 1.3 concerns, we propose a

time-frequency synchronization technique for WCP-COQAM, based on schemes previously used for GFDM and OFDM. As for channel estimation, we analyse some of the most extended techniques for FBMC-OQAM and we adapt them to WCP-COQAM. As explained in 4.2, we propose a pilot-aided HR based channel estimation technique for WCP-COQAM which employs the HR-FDE and block-wise structure of WCP-COQAM in order to take advantage of full orthogonality against multipath channels and short block transmission. Furthermore, we evaluate the overall performance of WCP-COQAM in terms of BER under more realistic conditions by simulating actual time-frequency offset and channel estimation impairments and their respective synchronization and estimation techniques. Results show that in highly dispersive channel scenarios HR-FDE provides higher robustness than LR-FDE based systems of the bibliography, even for time varying channels. Hence, based on these conclusions, we consider our second goal and our third hypothesis fulfilled.

5.2 Contributions

In this section we list the main contributions of this doctoral thesis and we show the publications in the scientific bibliography derived from them.

- In this thesis we complement the work in [101–103], by bringing additional details about how windowing affects the protection against multipath channels and the SE in WCP-COQAM. We state the conditions to provide full orthogonality in multipath channels and we show how windowing reduces SE in WCP-COQAM compared to GFDM-OQAM.

- While most research about the FMC modulations we analyse in this thesis is focused on MBB communications, here we simulate and assess some of these modulation schemes under different conditions. We simulate low-band transmissions through large indoor spaces and severe multipath channels in order to model some of the industrial wireless characteristics. Under these conditions and by means of BER, PSD and SE analysis, we evaluate the suitability of the aforementioned FMC systems for wireless industrial communications based on CR.

- We propose a CFO and a STO synchronization technique for WCP-COQAM, adapted from time-frequency synchronization techniques for GFDM and OFDM available in the bibliography. Moreover, we also propose a robust and low-latency pilot-based channel estimation technique for WCP-COQAM short transmissions. For the best of our knowledge, these specific issues have not been addressed in the bibliography, so we present simulation results that

show that the synchronization and channel estimation techniques we propose in this thesis can be suitable solutions for WCP-COQAM modulation technique.

- Based on the time-frequency synchronization and channel estimation techniques we propose in this thesis, we evaluate the overall performance of WCP-COQAM in terms of BER under more realistic conditions by simulating actual time-frequency offset and channel estimation impairments. For the best of our knowledge, there are no such results in the scientific bibliography.

These are the works about PHY layer FMC modulations on which the author of this thesis appears as principal author.

- A. Lizeaga, M. Mendicute, P. M. Rodríguez, and I. Val, "Evaluation of WCP-COQAM, GFDM-OQAM and FBMC-OQAM for industrial wireless communications with Cognitive Radio," in *2017 IEEE International Workshop of Electronics, Control, Measurement, Signals and their Application to Mechatronics (ECMSM)*, May 2017.

- A. Lizeaga, P. M. Rodríguez, I. Val, and M. Mendicute, "Evaluation of 5G Modulation Candidates WCP-COQAM, GFDM-OQAM and FBMC-OQAM in Low-Band Highly Dispersive Wireless Channels," *Journal of Computer Networks and Communications*, 2017.

- A. Lizeaga, M. Mendicute, P. M. Rodríguez, and I. Val, "Robust Pilot-Aided Channel Estimation for WCP-COQAM in Industrial Wireless Communications," in *2018 IEEE Wireless Communications and Networking Conference (WCNC)*, 2018 - (*submitted*).

These are the works about CR on which the author of this thesis appears as a co-author.

- P. M. Rodríguez, Z. Fernández, R. Torrego, A. Lizeaga, M. Mendicute, and I. Val, "Low-complexity Cyclostationary-based Modulation Classifying Algorithm," *AEU - International Journal of Electronics and Communications*, vol. 74, 02 2017.

- P. M. Rodríguez, I. Val, A. Lizeaga, and M. Mendicute, "Evaluation of cognitive radio for mission-critical and time-critical WSAN in industrial environments under interference," in *Factory Communication Systems (WFCS), 2015 IEEE World Conference on*, pp. 1–4, May 2015.

5.3 Future work

Considering the current state of our research and the work carried out during this doctoral thesis, the next logical step should be to model more realistic wireless industrial environments. In order to do that, in addition to the issues that we do address in this thesis, like time varying and highly frequency selective channels, RFI also must be taken into consideration. Presence of RFI is one of the main characteristics in wireless industrial environments. This RFI might be caused by either other wireless communications transmitting in the same frequency band or impulsive noise introduced by excessive electromagnetic noise caused by large coils, motors, etc. There are several RFI characterization models in the bibliography, so that the study and application of them, or even the proposal of a new one if the need arises, should be addressed in order to provide greater rigour to the evaluation of these FMC modulations in wireless industrial scenarios.

Considering the heterogeneous characteristics of FA scenarios and therefore, the lack of a generalist and valid FA environment characterization model and the difficulty to do it; we consider that the simulations of different use cases could help evaluating the actual validity of WCP-COQAM for FA wireless communications. Based on such use cases we might provide successful configurations of WCP-COQAM wireless systems for different FA environments.

Another mandatory task is the implementation of the WCP-COQAM scheme we propose on a hardware platform. Going from simulations to hardware based experiments in a laboratory would provide more realistic results, evaluations and conclusions to the research we carried out in this doctoral thesis.

Finally, in order to really propose a solution for wireless communications in FA, we should integrate the WCP-COQAM system proposed in this doctoral thesis and the CR techniques proposed in [1]. Considering that robust MCM systems like OFDM and current conventional MAC techniques cannot address the requirements of FA applications, we must search compatibility and performance optimization between WCP-COQAM and CR in order to surpass current robustness and reliability standards.

References

[1] P. M. Rodríguez, *Spectrum handoff strategy for cognitive radio-based MAC in industrial wireless sensor and actuator networks*. PhD thesis, Mondragon Unibertsitatea, 2016.

[2] P. M. Rodríguez, I. Val, A. Lizeaga, and M. Mendicute, "Evaluation of cognitive radio for mission-critical and time-critical WSAN in industrial environments under interference," in *Factory Communication Systems (WFCS), 2015 IEEE World Conference on*, pp. 1–4, May 2015.

[3] P. M. Rodríguez, R. Torrego, F. Casado, Z. Fernández, M. Mendicute, A. Arriola, and I. Val, "Dynamic Spectrum Access Integrated in a Wideband Cognitive RF-Ethernet Bridge for Industrial Control Applications," *Journal of Signal Processing Systems*, vol. 83, no. 1, pp. 19–28, 2016.

[4] P. M. Rodríguez, Z. Fernández, R. Torrego, A. Lizeaga, M. Mendicute, and I. Val, "Low-complexity Cyclostationary-based Modulation Classifying Algorithm," *AEU - International Journal of Electronics and Communications*, vol. 74, 02 2017.

[5] S. Vitturi, "Wireless networks for the factory floor: requirements, available technologies, research trends and practical applications," in *IEEE International Conference on Emerging Technologies and Factory Automation*, 2014.

[6] A. Frotzscher, U. Wetzker, M. Bauer, M. Rentschler, M. Beyer, S. Elspass, and H. Klessig, "Requirements and current solutions of wireless communication in industrial automation," in *2014 IEEE International Conference on Communications Workshops (ICC)*, pp. 67–72, June 2014.

[7] C. Lu, A. Saifullah, B. Li, M. Sha, H. Gonzalez, D. Gunatilaka, C. Wu, L. Nie, and Y. Chen, "Real-TimeWireless Sensor-Actuator Networks for Industrial Cyber-Physical Systems," *Proceedings of the IEEE*, vol. 104, no. 5, pp. 1013–1024, 2016.

[8] K. Pister, T. Phinney, P. Thubert, and S. Dwars, "Industrial Routing Requirements in Low-Power and Lossy Networks." RFC 5673, 2009.

[9] W. Ikram and N. F. Thornhill, "Wireless communication in process automation: A survey of opportunities, requirements, concerns and challenges," in *UKACC International Conference on Control 2010*, pp. 1–6, Sept 2010.

[10] G. Bianchi, "Performance analysis of the IEEE 802.11 distributed coordination function," *IEEE Journal on Selected Areas in Communications*, vol. 18, pp. 535–547, March 2000.

[11] G. Buttazzo, *Hard real-time computing systems: predictable scheduling algorithms and applications*, vol. 24. Springer Science & Business Media, 2011.

[12] Y. Bang, J. Han, K. Lee, J. Yoon, J. Joung, S. Yang, and J.-K. K. Rhee, "Wireless network synchronization for multichannel multimedia services," in *2009 11th International Conference on Advanced Communication Technology*, vol. 02, pp. 1073–1077, Feb 2009.

[13] J. Cao, A. Chen, I. Widjaja, and N. Zhou, "Online Identification of Applications Using Statistical Behavior Analysis," in *IEEE GLOBECOM 2008 - 2008 IEEE Global Telecommunications Conference*, pp. 1–6, Nov 2008.

[14] R. S. B. Ahmad, R. S. Burton, and E. Mustafa, *Multi-Carrier Digital Communications Theory and Applications of OFDM*. Springer Science and Business Media, Inc., 2004.

[15] J. Karedal, S. Wyne, P. Almers, F. Tufvesson, and A. Molisch, "UWB channel measurements in an industrial environment," in *Global Telecommunications Conference, 2004. GLOBECOM '04. IEEE*, vol. 6, pp. 3511 – 3516 Vol.6, nov.-3 dec. 2004.

[16] A. Molisch, K. Balakrishnan, C. Chong, S. Emami, A. Fort, J. Karedal, J. Kunisch, H. Schantz, U. Schuster, and K. Siwiak, "IEEE 802.15.4a channel model - final report," in *Converging: Technology, work and learning. Australian Government Printing Service*, Online]. Available, 2004.

[17] J. Karedal, S. Wyne, P. Almers, F. Tufvesson, and A. Molisch, "Statistical analysis of the UWB channel in an industrial environment," in *Vehicular Technology Conference, 2004. VTC2004-Fall. 2004 IEEE 60th*, vol. 1, pp. 81 – 85 Vol. 1, sept. 2004.

[18] V. Erceg, L. Schumacher, P. Kyritsi, A. Molisch, D. S. Baum, A. Y. Gorokhov, C. Oestges, Q. Li, K. Yu, N. Tal, B. Dijkstra, A. Jagannatham,

C. Lanzl, V. J. Rhodes, J. Medbo, D. Michelson, M. Webster, V. Erceg, E. Jacobsen, D. Cheung, C. Prettie, M. Ho, S. Howard, B. Bjerke, L. Jengx, H. Sampath, S. Catreux, S. Valle, A. Poloni, A. Forenza, and R. W. Heath, "Indoor MIMO WLANTGn Channel Models," tech. rep., IEEE P802.11 Wireless LANs, 2004.

[19] P. Kyosti, J. Meinila, L. Hentila, X. Zhao, T. Jamsa, C. Schneider, M. Narandzic, M. Milojevic, A. Hong, J. Ylitalo, V.-M. Holappa, M. Alatossava, R. Bultitude, Y. Jong, and T. Rautiainen, "IST-4-027756 WINNER II, D1.1.2 V1.2, WINNER II Channel Models, Part I Channel Models," tech. rep., Winner Information Society Technologies, 2007.

[20] D. S. Baum, H. El-Sallabi, T. Jamsa, J. Meinila, P. Kyosti, X. Zhao, D. Laselva, J.-P. Nuutinen, L. Hentila, P. Vainikainen, J. Kivinen, L. Vuokko, P. Zetterberg, M. Bengtsson, K. Yu, N. JaJald, T. Rautiainen, K. Kalliola, M. Milojevic, C. Schneider, and J. Hansen, "IST-2003-507581 WINNER, D5.4 v. 1.4, Final Report on Link Level and System Level Channel Models," tech. rep., Winner Information Society Technologies, 2005.

[21] P. Kyosti, J. Meinila, L. Hentila, X. Zhao, T. Jamsa, C. Schneider, M. Narandzic, M. Milojevic, A. Hong, J. Ylitalo, V.-M. Holappa, M. Alatossava, R. Bultitude, Y. Jong, and T. Rautiainen, "IST-4-027756 WINNER II, D1.1.2 V1.0, WINNER II Channel Models, Part II Radio Channel Measurement and Analysis Results," tech. rep., Winner Information Society Technologies, 2007.

[22] A. Willig, K. Matheus, and A. Wolisz, "Wireless Technology in Industrial Networks," *Proceedings of the IEEE*, vol. 93, no. 6, pp. 1130–1151, 2005.

[23] A. Willig, "Recent and Emerging Topics in Wireless Industrial Communications: A Selection," *Industrial Informatics, IEEE Transactions on*, vol. 4, no. 2, pp. 102–124, 2008.

[24] V. C. Gungor, B. Lu, and G. P. Hancke, "Opportunities and Challenges of Wireless Sensor Networks in Smart Grid," *Industrial Electronics, IEEE Transactions on*, vol. 57, no. 10, pp. 3557–3564, 2010.

[25] I. A. Silva, L. A. A. Guedes, P. B. Portugal, and F. C. Vasques, "Reliability and availability evaluation of wireless sensor networks for industrial applications," *Sensors*, vol. 12, no. 1, pp. 806–838, 2012.

[26] S. Vitturi, P. Pedreiras, J. Proenza, and T. Sauter, "Guest Editorial Special Section on Communication in Automation," *IEEE Transactions on Industrial Informatics*, vol. 12, no. 5, pp. 1817–1821, 2016.

[27] L. Kay-Soon, W. N. N. Win, and E. Meng-Joo, "Wireless Sensor Networks for Industrial Environments," in *Computational Intelligence for Modelling, Control and Automation, 2005 and International Conference on Intelligent Agents, Web Technologies and Internet Commerce, International Conference on*, vol. 2, pp. 271–276, 2005.

[28] D. Sexton, M. Mahony, M. Lapinski, and J. Werb, "Radio Channel Quality in Industrial Wireless Sensor Networks," in *Sensors for Industry Conference, 2005*, pp. 88–94, 2005.

[29] F. Chen, R. German, and F. Dressler, "QoS-oriented Integrated Network Planning for Industrial Wireless Sensor Networks," in *Sensor, Mesh and Ad Hoc Communications and Networks Workshops, 2009. SECON Workshops '09. 6th Annual IEEE Communications Society Conference on*, pp. 1 –3, june 2009.

[30] G. P. Hancke, "Industrial wireless sensor networks: A selection of challenging applications," in *2012 6th European Conference on Antennas and Propagation (EUCAP)*, pp. 64–68, March 2012.

[31] F. Xia, Y.-C. Tian, Y. Li, and Y. Sun, "Wireless Sensor/Actuator Network Design for Mobile Control Applications," *Sensors (Basel, Switzerland)*, vol. 7(10), pp. 2157–2173, 2007.

[32] K. Al-Agha, M.-H. Bertin, T. Dang, A. Guitton, P. Minet, T. Val, and J.-B. Viollet, "Which Wireless Technology for Industrial Wireless Sensor Networks? The Development of OCARI Technology," *Industrial Electronics, IEEE Transactions on*, vol. 56, no. 10, pp. 4266–4278, 2009.

[33] S.-E. Yoo, P. K. Chong, D. Kim, Y. Doh, M.-L. Pham, E. Choi, and J. Huh, "Guaranteeing Real-Time Services for Industrial Wireless Sensor Networks With IEEE 802.15.4," *Industrial Electronics, IEEE Transactions on*, vol. 57, no. 11, pp. 3868–3876, 2010.

[34] P. Zand, S. Chatterjea, K. Das, and P. Havinga, "Wireless Industrial Monitoring and Control Networks: The Journey So Far and the Road Ahead," *Journal of Sensor and Actuator Networks*, vol. 1, no. 2, pp. 123–152, 2012.

[35] G. P. Hancke and B. Allen, "Ultrawideband as an Industrial Wireless Solution," *Pervasive Computing, IEEE*, vol. 5, no. 4, pp. 78–85, 2006.

[36] J.-S. Lee, Y.-W. Su, and C.-C. Shen, "A Comparative Study of Wireless Protocols: Bluetooth, UWB, ZigBee, and Wi-Fi," in *Industrial Electronics*

Society, 2007. IECON 2007. 33rd Annual Conference of the IEEE, pp. 46–51, 2007.

[37] D. Yang, Y. Xu, and M. Gidlund, "Wireless Coexistence between IEEE 802.11- and IEEE 802.15.4-Based Networks: A Survey," *Hindawi Publishing Corporation International Journal of Distributed Sensor Networks*, vol. Volume 2011, p. 17, 2011.

[38] K. Yu, F. Barac, M. Gidlund, J. Akerberg, and M. Bjorkman, "A flexible error correction scheme for IEEE 802.15.4-based industrial Wireless Sensor Networks," in *Industrial Electronics (ISIE), 2012 IEEE International Symposium on*, pp. 1172–1177, 2012.

[39] Profibus and Profinet user organization (PNO), "WSAN Air Interface Specification," *PROFIBUS and PROFINET International (PI)*, 2012.

[40] D. Brevi, D. Mazzocchi, R. Scopigno, A. Bonivento, R. Calcagno, and F. Rusina, "A Methodology for the Analysis of 802.11a Links in Industrial Environments," in *Factory Communication Systems, 2006 IEEE International Workshop on*, pp. 165 –174, 0-0 2006.

[41] Q. Wang, X. Liu, W. Chen, L. Sha, and M. Caccamo, "Building Robust Wireless LAN for Industrial Control with the DSSS-CDMA Cell Phone Network Paradigm," *Mobile Computing, IEEE Transactions on*, vol. 6, pp. 706 –719, june 2007.

[42] IEC 62591:2010, "Industrial communication networks - Wireless communication network and communication profiles - WirelessHART," *International Electrotechnical Commission*, 2010.

[43] ISA 100.11a, "Wireless systems for industrial automation: Process control and related applications," *International Society of Automation*, 2011.

[44] IEC 62601:2011, "Industrial communication networks - Fieldbus specifications - WIA-PA communication network and communication profile," *International Electrotechnical Commission*, 2011.

[45] IEEE Std 802.15.4-2006, "IEEE Standard for Information technology - Telecommunications and information exchange between systems - Local and metropolitan area networks - Specific requirements Part 15.4: Wireless Medium Access Control (MAC) and Physical Layer (PHY) Specifications for Low-Rate Wireless Personal Area Networks (WPANs)," *IEEE Computer Society*, 2006.

[46] S. Han, X. Zhu, A. K. Mok, D. Chen, and M. Nixon, "Reliable and Real-Time Communication in Industrial Wireless Mesh Networks," in *Real-Time and Embedded Technology and Applications Symposium (RTAS), 2011 17th IEEE*, pp. 3 –12, april 2011.

[47] IEC 62591:2016, "Industrial networks - Wireless communication network and communication profiles - WirelessHART," *International Electrotechnical Commission*, 2016.

[48] G. Wang, "Comparison and Evaluation of Industrial Wireless Sensor Network Standards ISA100.11a and WirelessHART," Master's thesis, Department of Signals and Systems CHALMERS UNIVERSITY OF TECHNOLOGY Gothenburg, Sweden, 2011.

[49] W. Liang, X. Zhang, Y. Xiao, F. Wang, P. Zeng, and H. Yu, "Survey and experiments of WIA-PA specification of industrial wireless network," *Wireless Communications and Mobile Computing*, vol. 11, no. 8, pp. 1197 – 1212, 2011.

[50] IEC 62601:2015, "Industrial networks - Wireless communication network and communication profiles - WIA-PA," *International Electrotechnical Commission*, 2015.

[51] IEEE Std 802.15.1-2005, "IEEE Standard for Information Technology - Telecommunications and Information Exchange Between Systems - Local and Metropolitan Area Networks - Specific Requirements. - Part 15.1: Wireless Medium Access Control (MAC) and Physical Layer (PHY) Specifications for Wireless Personal Area Networks (WPANs)," *IEEE Computer Society*, 2005.

[52] G. Scheible, D. Dzung, J. Endresen, and J. E. Frey, "Unplugged but connected - Design and implementation of a truly wireless real-time sensor/actuator interface," *IEEE Industrial Electronics Magazine*, vol. 1, pp. 25–34, Summer 2007.

[53] J. Kjellsson, A. E. Vallestad, R. Steigmann, and D. Dzung, "Integration of a Wireless I/O Interface for PROFIBUS and PROFINET for Factory Automation," *IEEE Transactions on Industrial Electronics*, vol. 56, pp. 4279–4287, Oct 2009.

[54] IEC PAS 62948:2015, "Industrial networks - Wireless communication network and communication profiles - WIA-FA," *International Electrotechnical Commission*, 2015.

[55] IEEE Std 802.11-2012, "IEEE Standard for Information technology - Telecommunications and information exchange between systems Local and metropolitan area networks - Specific requirements Part 11: Wireless LAN Medium Access Control (MAC) and Physical Layer (PHY) Specifications," *IEEE Computer Society*, 2012.

[56] Y.-H. Wei, Q. Leng, S. Han, A. K. Mok, W. Zhang, and M. Tomizuka, "RT-WiFi: Real-time high-speed communication protocol for wireless cyber-physical control applications," in *Real-Time Systems Symposium (RTSS), 2013 IEEE 34th*, pp. 140–149, IEEE, 2013.

[57] A. Willig, M. Kubisch, C. Hoene, and A. Wolisz, "Measurements of a wireless link in an industrial environment using an IEEE 802.11-compliant physical layer," *IEEE Transactions on Industrial Electronics*, vol. 49, pp. 1265–1282, Dec 2002.

[58] F. D. Pellegrini, D. Miorandi, S. Vitturi, and A. Zanella, "On the use of wireless networks at low level of factory automation systems," *IEEE Transactions on Industrial Informatics*, vol. 2, pp. 129–143, May 2006.

[59] L. L. Bello, G. A. Kaczynski, F. Sgro, and O. Mirabella, "A wireless traffic smoother for soft real-time communications over IEEE 802.11 industrial networks," in *2006 IEEE Conference on Emerging Technologies and Factory Automation*, pp. 1073–1079, Sept 2006.

[60] G. Cena, L. Seno, A. Valenzano, and C. Zunino, "On the Performance of IEEE 802.11e Wireless Infrastructures for Soft-Real-Time Industrial Applications," *IEEE Transactions on Industrial Informatics*, vol. 6, pp. 425–437, Aug 2010.

[61] S. Vitturi, L. Seno, F. Tramarin, and M. Bertocco, "On the Rate Adaptation Techniques of IEEE 802.11 Networks for Industrial Applications," *IEEE Transactions on Industrial Informatics*, vol. 9, pp. 198–208, Feb 2013.

[62] T. Adame, A. Bel, B. Bellalta, J. Barcelo, and M. Oliver, "IEEE 802.11ah: the WiFi approach for M2M communications," *IEEE Wireless Communications*, vol. 21, pp. 144–152, December 2014.

[63] E. Khorov, A. Lyakhov, A. Krotov, and A. Guschin, "A survey on IEEE 802.11 ah: An enabling networking technology for smart cities," *Computer Communications*, vol. 58, pp. 53–69, 2015.

[64] F. Tramarin, S. Vitturi, M. Luvisotto, and A. Zanella, "The IEEE 802.11n wireless LAN for real-time industrial communication," in *2015 IEEE World*

Conference on Factory Communication Systems (WFCS), pp. 1–4, May 2015.

[65] F. Tramarin, S. Vitturi, M. Luvisotto, and A. Zanella, "On the Use of IEEE 802.11n for Industrial Communications," *IEEE Transactions on Industrial Informatics*, vol. 12, pp. 1877–1886, Oct 2016.

[66] M. Sahin and H. Arslan, "System Design for Cognitive Radio Conmunications," in *Cognitive Radio Oriented Wireless Networks and Communications, 2006. 1st International Conference on*, pp. 1–5, June 2006.

[67] B. Wang and K. J. R. Liu, "Advances in cognitive radio networks: A survey," *Selected Topics in Signal Processing, IEEE Journal of*, vol. 5, pp. 5–23, Feb 2011.

[68] B. Farhang-Boroujeny and R. Kempter, "Multicarrier communication techniques for spectrum sensing and communication in cognitive radios," *Communications Magazine, IEEE*, vol. 46, pp. 80–85, April 2008.

[69] P. Wang, M. Zhao, L. Xiao, S. Zhou, and J. Wang, "Power Allocation in OFDM-Based Cognitive Radio Systems," in *Global Telecommunications Conference, 2007. GLOBECOM '07. IEEE*, pp. 4061–4065, Nov 2007.

[70] G. Bansal, J. Hossain, and V. K. Bhargava, "Optimal and Suboptimal Power Allocation Schemes for OFDM-based Cognitive Radio Systems," *Wireless Communications, IEEE Transactions on*, vol. 7, pp. 4710–4718, November 2008.

[71] H. Mahmoud, T. Yucek, and H. Arslan, "OFDM for cognitive radio: merits and challenges," *Wireless Communications, IEEE*, vol. 16, pp. 6–15, April 2009.

[72] R. Zhou, X. Li, V. Chakravarthy, C. Bullmaster, B. Wang, R. Cooper, and Z. Wu, "Software Defined Radio Implementation of SMSE Based Overlay Cognitive Radio," in *New Frontiers in Dynamic Spectrum, 2010 IEEE Symposium on*, pp. 1–2, April 2010.

[73] M. Shaat and F. Bader, "Comparison of OFDM and FBMC performance in multi-relay cognitive radio network," in *Wireless Communication Systems (ISWCS), 2012 International Symposium on*, pp. 756–760, Aug 2012.

[74] Q. Zhang, A. B. J. Kokkeler, and G. J. M. Smit, "An oversampled filter bank multicarrier system for Cognitive Radio," in *Personal, Indoor and Mobile Radio Communications, 2008. PIMRC 2008. IEEE 19th International Symposium on*, pp. 1–5, Sept 2008.

[75] H. Zhang, D. Le Ruyet, M. Terr, D. Roviras, M. Renfors, T. Ihalainen, C. Bader, M. Shaat, A. Merentitis, D. Triantafyllopoulou, M. Huchard, and A. Kuzminskiy, "Application of the FBMC physical layer in a cognitive radio scenario," tech. rep., PHYsical layer for DYnamic AccesS and cognitive radio (PHYDYAS), 2009.

[76] X. Zhang, M. Jia, L. Chen, J. Ma, and J. Qiu, "Filtered-OFDM-enabler for flexible waveform in the 5th generation cellular networks," in *Global Communications Conference (GLOBECOM), 2015 IEEE*, pp. 1–6, IEEE, 2015.

[77] A. Ijaz, L. Zhang, P. Xiao, and R. Tafazolli, *Analysis of Candidate Waveforms for 5G Cellular Systems*, ch. 1, pp. 3–25. InTech, 2016.

[78] F. Luo and C. Zhang, *Signal Processing for 5G: Algorithms and Implementations*. Wiley - IEEE, Wiley, 2016.

[79] L. Zhang, A. Ijaz, P. Xiao, A. Quddus, and R. Tafazolli, "Subband Filtered Multi-carrier Systems for Multi-service Wireless Communications," *IEEE Transactions on Wireless Communications*, vol. 16, no. 3, pp. 1893–1907, 2017.

[80] M. Agiwal, A. Roy, and N. Saxena, "Next Generation 5G Wireless Networks: A Comprehensive Survey," *IEEE Communications Surveys Tutorials*, vol. 18, pp. 1617–1655, thirdquarter 2016.

[81] M. Series, "IMT Vision - Framework and overall objectives of the future development of IMT for 2020 and beyond," tech. rep., Internation Telecommunication Union - Radiocommunication Sector (ITU-R), 2015.

[82] H. Ji, S. Park, J. Yeo, D. Kim, J. Lee, and B. Shim, "Introduction to Ultra Reliable and Low Latency Communications in 5G," 2017.

[83] O. N. Yilmaz, "Ultra-Reliable and Low-Latency 5G Communication," in *European Conference on Networks and Communications (EuCNC), 2016*, 2016.

[84] G. Cherubini, E. Eleftheriou, and S. Olcer, "Filtered multitone modulation for very high-speed digital subscriber lines," *Selected Areas in Communications, IEEE Journal on*, vol. 20, pp. 1016–1028, Jun 2002.

[85] N. Moret and A. M. Tonello, "Design of Orthogonal Filtered Multitone Modulation Systems and Comparison among Efficient Realizations," *EURASIP Journal on Advances in Signal Processing*, vol. 2010, no. 1, p. 165654, 2010.

[86] E. Gutierrez, J. Lopez-Salcedo, and G. Seco-Granados, "Systematic design of transmitter and receiver architectures for flexible filter bank multi-carrier signals," *EURASIP Journal on Advances in Signal Processing*, vol. 2014, no. 1, p. 26, 2014.

[87] R. Gerzaguet, N. Bartzoudis, L. G. Baltar, V. Berg, J.-B. Doré, D. Kténas, O. Font-Bach, X. Mestre, M. Payaró, M. Färber, *et al.*, "The 5G candidate waveform race: a comparison of complexity and performance," *EURASIP Journal on Wireless Communications and Networking*, vol. 2017, no. 1, p. 13, 2017.

[88] P. Siohan, C. Siclet, and N. Lacaille, "Analysis and design of OFDM/OQAM systems based on filterbank theory," *Signal Processing, IEEE Transactions on*, vol. 50, pp. 1170–1183, May 2002.

[89] J. Du and S. Signell, "Classic OFDM Systems and Pulse Shaping OFDM/O-QAM Systems," Tech. Rep. 07:01, KTH, Electronic, Computer and Software Systems, ECS, 2007. QC 20111026A hard copy is available in ICT/ECS archive. Electronic copy is available on www.ee.kth.se/ jinfeng.

[90] B. Farhang-Boroujeny and C. (George) Yuen, "Cosine Modulated and Offset QAM Filter Bank Multicarrier Techniques: A Continuous-Time Prospect," *EURASIP Journal on Advances in Signal Processing*, vol. 2010, no. 1, p. 165654, 2010.

[91] A. Viholainen, M. Bellanger, and M. Huchard, "Prototype filter and structure optimization," 2009.

[92] M. Bellanger, "FBMC physical layer: a primer," 2010.

[93] M. Danneberg, R. Datta, A. Festag, and G. Fettweis, "Experimental Testbed for 5G Cognitive Radio Access in 4G LTE Cellular Systems," in *IEEE Sensor Array and Multichannel Signal Processing Workshop*, 2014.

[94] N. Michailow, M. Matthe, I. S. Gaspar, A. N. Caldevilla, L. L. Mendes, A. Festag, and G. Fettweis, "Generalized Frequency Division Multiplexing for 5th Generation Cellular Networks," *Communications, IEEE Transactions on*, vol. 62, pp. 3045–3061, Sept 2014.

[95] A. Farhang, N. Marchetti, and L. E. Doyle, "Low Complexity Transceiver Design for GFDM," *CoRR*, vol. abs/1501.02940, 2015.

[96] V. Vakilian, T. Wild, F. Schaich, S. T. Brink, and J.-F. Frigon, "Universal-filtered multi-carrier technique for wireless systems beyond LTE," in *Globecom Workshops (GC Wkshps), 2013 IEEE*, pp. 223–228, Dec 2013.

[97] F. Schaich, T. Wild, and Y. Chen, "Waveform contenders for 5G - suitability for short packet and low latency transmissions," in *IEEE VTCs'14*, 2014.

[98] I. S. Gaspar and G. Wunder, "5G Cellular Communications Scenarios and System Requirements," tech. rep., 5th Generation Non-Orthogonal Waveforms for Asynchronous Signalling, 2013.

[99] P. Popovski, V. Braun, H. Mayer, P. Fertl, Z. Ren, D. Gonzales-Serrano, E. Ström, T. Svensson, H. Taoka, P. Agyapong, A. Benjebbour, G. Zimmermann, J. Meinilä, J. Ylitalo, T. Jämsä, P. Kyösti, K. Dimou, M. Fallgren, Y. Selén, B. Timus, H. Tullberg, M. Schellmann, Y. Wu, M. Schubert, D. Kang, J. Markendahl, C. Beckman, M. Uusitalo, O. Yilmaz, C. Wijting, Z. Li, P. Marsch, K. Pawlak, J. Vihriala, A. Gouraud, S. Jeux, M. Boldi, G. Dell'aera, B. Melis, H. Schotten, P. Spapis, A. Kaloxylos, and K. Chatzikokolakis, "Scenarios, requirements and KPIs for 5G mobile and wireless system," tech. rep., Mobile and wireless communications Enablers for the Twenty-twenty Information Society (METIS), 2013.

[100] X. Mestre, D. Gregoratti, M. Renfors, S. Nedic, D. Le Ruyet, D. Tsolkas, M. Haardt, J. Louveaux, P. Mge, and V. Ringset, "ICT-EMPhAtiC Final Project Report," tech. rep., Enhanced Multicarrier Techniques for Professional Ad-Hoc and Cell-Based Communications, 2015.

[101] H. Lin and P. Siohan, "FBMC/COQAM: An Enabler for Cognitive Radio," in *COCORA 2014: The Fourth International Conference on Advances in Cognitive Radio*, pp. 8097–8101, May 2014.

[102] H. Lin and P. Siohan, "An advanced multi-carrier modulation for future radio systems," in *2014 IEEE International Conference on Acoustics, Speech and Signal Processing (ICASSP)*, pp. 8097–8101, May 2014.

[103] H. Lin and P. Siohan, "Multi-carrier modulation analysis and WCP-COQAM proposal," *EURASIP Journal on Advances in Signal Processing*, vol. 2014, no. 1, 2014.

[104] A. B. Üçüncü and A. Ö. Yilmaz, "Pulse Shaping Methods for OQAM/OFDM and WCP-COQAM," *CoRR*, vol. abs/1509.00977, 2015.

[105] A. B. Üçüncü and A. Ö. Yilmaz, "Out-of-Band Radiation Comparison of GFDM, WCP-COQAM and OFDM at Equal Spectral Efficiency," *CoRR*, vol. abs/1510.01201, 2015.

[106] H. Lin and P. Siohan, *Signal Processing for 5G: Algorithms and Implementations*, ch. 8, pp. 169–187. Wiley, 2016.

[107] J. J. Benedetto, C. Heil, and D. F. Walnut, *Gabor systems and the Balian-Low Theorem*, ch. 2, pp. 85–122. Boston, MA: Birkhäuser Boston, 1998.

[108] L. Zhang, P. Xiao, A. Zafar, A. ul Quddus, and R. Tafazolli, "FBMC System: An Insight into Doubly Dispersive Channel Impact," *IEEE Transactions on Vehicular Technology*, 2016.

[109] H. Minn, V. K. Bhargava, and K. B. Letaief, "A robust timing and frequency synchronization for OFDM systems," *IEEE Transactions on Wireless Communications*, vol. 2, pp. 822–839, July 2003.

[110] I. S. Gaspar, L. L. Mendes, N. Michailow, and G. Fettweis, "A synchronization technique for Generalized Frequency Division Multiplexing," *EURASIP Journal on Advances in Signal Processing*, vol. 2014, no. 1, pp. 1–10, 2014.

[111] P. Popovski, "Ultra-reliable communication in 5G wireless systems," in *1st International Conference on 5G for Ubiquitous Connectivity*, pp. 146–151, Nov 2014.

[112] U. Vilaipornsawai and M. Jia, "Scattered-pilot channel estimation for GFDM," in *2014 IEEE Wireless Communications and Networking Conference (WCNC)*, pp. 1053–1058, April 2014.

[113] J. P. Javaudin, D. Lacroix, and A. Rouxel, "Pilot-aided channel estimation for OFDM/OQAM," in *The 57th IEEE Semiannual Vehicular Technology Conference, 2003. VTC 2003-Spring.*, vol. 3, pp. 1581–1585 vol.3, April 2003.

[114] T. Hidalgo, T. Ihalainen, A. Viholainen, and M. Renfors, "Pilot-Based Synchronization and Equalization in Filter Bank Multicarrier Communications," *EURASIP J. Adv. Signal Process*, vol. 2010, pp. 9:1–9:11, #jan# 2010.

[115] J. Bazzi, P. Weitkemper, and K. Kusume, "Power Efficient Scattered Pilot Channel Estimation for FBMC/OQAM," in *SCC 2015; 10th International ITG Conference on Systems, Communications and Coding*, pp. 1–6, Feb 2015.

[116] X. Mestre and E. Kofidis, "Pilot-based channel estimation for FBMC/OQAM systems under strong frequency selectivity," in *Acoustics, Speech and Signal Processing (ICASSP), 2016 IEEE International Conference on*, pp. 3696–3700, IEEE, 2016.

[117] A. Lizeaga, M. Mendicute, P. M. Rodríguez, and I. Val, "Evaluation of WCP-COQAM, GFDM-OQAM and FBMC-OQAM for industrial wireless

communications with Cognitive Radio," in *2017 IEEE International Workshop of Electronics, Control, Measurement, Signals and their Application to Mechatronics (ECMSM)*, May 2017.

[118] A. Lizeaga, P. M. Rodríguez, I. Val, and M. Mendicute, "Evaluation of 5G Modulation Candidates WCP-COQAM, GFDM-OQAM and FBMC-OQAM in Low-Band Highly Dispersive Wireless Channels," *Journal of Computer Networks and Communications*, 2017.